DISCOVERY AND CHARACTERIZATION OF NOVEL ANTIMICROBIALSAGAINST*MYCOBACTERIUM TUBERCULOSIS*

by

CAROLINA RODRIGUES FELIX
B.S. Universidade Federal de Pelotas, 2010
M.S. Universidade Federal de Pelotas, 2013

A dissertation submitted in partial fulfillment of the requirements
for the degree of Doctor of Philosophy
in the Division of Immunity and Pathogenesis
in the Burnett School of Biomedical Sciences
in the College of Medicine
at the University of Central Florida
Orlando, Florida

Fall Term
2017

Major Professor: Kyle H. Rohde

ABSTRACT

Tuberculosis disease is currently a global health emergency, causing the most deaths worldwide due a single infectious agent. Eradication of TB is hampered by lack of an effective vaccine and poor treatment options. During infection, host-derived cues such as hypoxia and starvation induce *Mycobacterium tuberculosis* to halt replication and become dormant, which leads to tolerance to front-line antibiotics used in the TB treatment. This dormant phenotype causes delayed clearance of *M. tuberculosis*, therefore a long treatment time is required for stable cure without relapse. Poor patient compliance increases the emergence of drug resistant strains, posing yet another challenge for the eradication of TB. There is dire need for novel compounds targeting not only drug-resistant, but also dormant bacteria so as to effectively eliminate drug-resistant strains and also shorten treatment time. This requires compounds with novel modes of action and novel drug screening approaches which focus on dormant *M. tuberculosis*. In the current work a method was optimized which induces the dormant phenotype of *M. tuberculosis* in vitro allowing large scale screening of compounds against these tolerant bacteria. The high chemical diversity of marine natural products was explored to increase the chances of finding novel compounds with novel mechanisms of action. Additionally, gold-complexed scaffolds were examined for their putative ability to inhibit topoisomerase 1, which is a highly conserved and essential protein of mycobacteria, not currently targeted in classical treatment

regimens. Several marine natural products were identified with selective bactericidal activity against dormant bacteria, emphasizing the powerful tool that was developed for drug screening. Moreover, the gold-complexes were also bactericidal against not only replicating and dormant bacilli, but also mycobacteria resistant to front-line TB drugs. Compounds characterized in this study represent a promising starting point for the development of novel TB therapeutics and discovery of new conditionally essential pathways of dormant bacteria.

For my husband, Augusto Schneider.

ACKNOWLEDGMENTS

I would like to thank my mentor Dr. Kyle H. Rohde for his patience and endless dedication throughout this process. Dr. Rohde has always provided me with excellent opportunities and guidance which ultimately led me to this achievement.

I am grateful to my committee members Dr. William Self, Dr. Otto Phanstiel and Dr. Mollie Jewett for always providing their advice and feedback.

To the entire Rohde Lab family, past and present, I am very grateful for the friendly environment they have always provided me, and for all the help they gave me professionally and personally. Thank you to my buddy Aaron Pollock for all his help in the whiB7 project! I am grateful to Rashmi Gupta, without whom much of the drug discovery in this dissertation would not have happened. To Hillary Bengtson (Hilly Bear) who was always there ready to listen and help. And finally, aspecial thanks to Sandy Geden, not only for all her help in lab life, but alsobecause she made me feel like part of her family.

I would also like to thank Dr. Pedro Eduardo Almeida da Silva for always believing in me and encouraging me in academia.

Thank you to Dr David Russell for giving me the opportunity that started this entire process, and for supporting my career development.

These past 5 years have been a very intense experience for me, and I am grateful that I found other people here to share it with. We became a family, always supporting and lifting each other up in the many ways that families do. Thank you, Philip Adams, Marisa Fuse and Ana Martini, for always understanding, for never giving up on me and carrying me through when I needed you to.

Thank you to my family Luiz, Neusa, Samuel, Luisa, Fernando, Anelize, Leonardo and Fernanda for understanding and supporting me through this difficult time away. You have all been deeply missed, but you have also made me feel brave enough to see this through to the end.

To my extended family Eloi, Eloina and Helena, thank you for always cheering for me, your support has been essential.

Finally, I would like to thank my husband, Augusto Schneider. For flying all over the place just to be with me, for never letting me give up, for guiding me to be more patient like him and for so many things, I could not have done this without him.

TABLE OF CONTENTS

LIST OF FIGURES

LIST OF TABLES

CHAPTER 1:

INTRODUCTION

This chapter was written by Carolina Rodrigues Felix. Revisions and edits from Kyle Rohde were incorporated to the final version.

There and back again: A pathogen's tale

Since its conception, human kind has been shadowed by tuberculosis (TB) disease. Molecular clock analyses of mycobacterial genomes suggest early hominids were infected with progenitors of the TB infectious agent, *Mycobacterium tuberculosis* (*Mtb*) [1-3]. Though the incidence of TB only became a problem with the onset of civilization, this mycobacterial pathogen may have been co-evolving with its human host for almost three million years.

The exponential growth of human populations which followed civilization and agriculture promoted a dramatic increase in the incidence of airborne infectious diseases such as TB [4]. High population densities coupled with poor nutrition and sanitation ignited an epidemic across Europe, now known as The Great White Plague, which would last two centuries and reach the American and African continents [5]. During this period (17^{th} to 19^{th} centuries), lack of treatment for this disease led to the inevitable death of most infected persons with mortality rates reaching up to 9000 per 100,000 in the 19^{th} century [5]. The term tuberculosis was coined by Johann Lukas Schonlein in 1839 after he and other physicians in Europe had noticed the presence of tubercle-like structures in the lungs of consumptive patients [6].

The infectious nature of the disease had been pointed out by physicians throughout the 16^{th}, 17^{th} and 18^{th} centuries, however, it was only in 1882 that Robert Koch demonstrated this disease was caused by a living organism [7].

Following this, Koch attempted to use extracts of liquid *Mtb* cultures (tuberculin) to treat the disease [8]. Though tuberculin failed as a treatment in humans, it is still used today as a diagnostic tool for TB. Even though novel diagnostic technologies have been developed, the gold standard laboratory diagnostic for TB is still comprised of smear microscopy and bacterial culture, especially in developing countries where insufficient resources hinder the implementation of novel, more expensive diagnostic tools [9].

Effective antibiotic treatment for TB only began with the discovery of streptomycin (STR) in 1943 by Waksman and Shatz. Resistance to streptomycin was observed early during clinical trials of the compound [10]. However, the later development of para-aminosalicylic acid (PAS) in 1944, and consequently isoniazid (INH) in the 1950's, allowed for combination therapy, which proved much more effective against the disease, and helped slow the appearance of resistance [11]. Though other potent compounds have since been discovered and implemented, such as rifampicin (RIF), combination therapy has remained a cornerstone of TB treatment to this day [9]. An effective treatment combined with public health measures lead to the control of TB disease in the 1970's. However, with the HIV/AIDS pandemic starting in the 1980's, the incidence of TB grew across the globe including in developed countries [12, 13]. The history of TB treatment is depicted in Figure 1.

Currently, TB is a global health emergency with 1.4 million deaths reported in 2015. More than 10 million new cases occurred in 2015 worldwide, 11% of which are HIV/TB coinfections, and 5% of which were caused by multi-drug resistant bacilli [14]. More than 70 years after the first antibiotic use against *M. tuberculosis,* the treatment is comprised of a 4-drug combination, which is taken for at least 6 months [14]. Even though the discovery of pyrazinamide (PZA) drastically shortened the treatment from 12 to 6 months [15], this delayed clearance of the pathogen remains a challenge which hampers patient compliance leading to increasing frequencies of drug-resistant mutants among infected individuals [16]. The prolonged treatment time required to cure TB is partially attributed to the metabolically quiescent (persister), drug-tolerant bacterial subpopulations present during infection [17]. This work focuses on early-stage drug discovery and development of compounds capable of effectively killing persister bacteria, which can ultimately shorten treatment time and help prevent the rise of drug resistance.

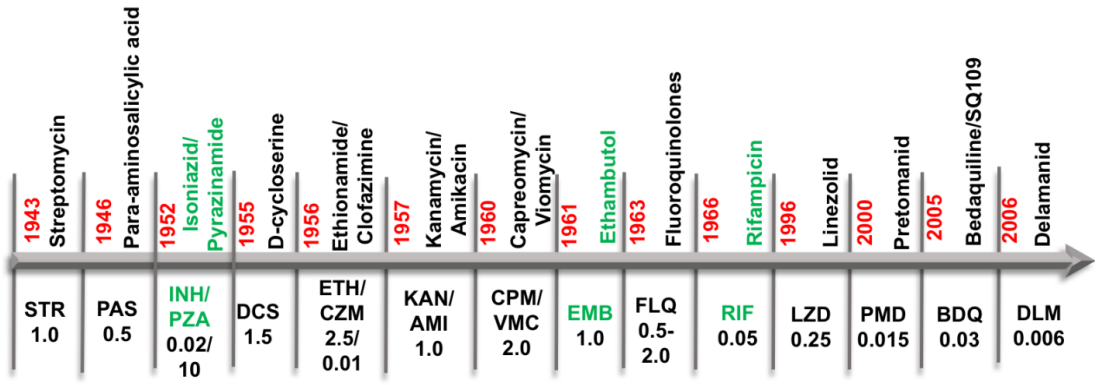

Figure 1. The history of TB treatment
Schematic view representing the year of discovery of compounds currently used in the treatment of TB. Below the horizontal arrow are the drug abbreviation and MIC *in vitro* in µg/mL. Drugs shown in green are the front-line antibiotics currently used for TB treatment.

A day in the life of *Mtb*

The bacteria which cause TB arefastidious, slow-growing bacilli capable of infecting and living within host macrophages. Even though TB is predominantly pulmonary,these pathogens are able to infect any organ or tissue in the host. At the interface between *Mtb*and the host immune system is the complex mycobacterial cell wall, which is highly lipid-rich serving as a strong permeability barrier and a modulator of the immune response. Furthermore, this organism's capability to undergo metabolic shifts during infection in response to the host environment is also a key contributor to its exceptional success as a pathogen.

The main aspects of bacterial physiology influencing host-pathogen interactions are reviewed in this section.

Granuloma formation: did you really think it was your idea?

The presence of “tubercle-like structures" in patient lungs, noted by physicians centuries ago, is a trade-mark characteristic of TB pathology. TB granulomas are host protective structures built by the immune system to contain and prevent the spread of *Mtb* to other tissues. However, this process is also modulated by *Mtb*to ensure its own survival and transmission [18, 19]. In fact, studies have shown that these structures may actually provide a sheltered environment for *Mtb*, often permissive of bacterial growth [20].

The development of granulomas usually begins with the infection of alveolar macrophages by *Mtb* carried in aerosolized droplets from an infected to a healthy host [19]. *Mtb* can be phagocytosed through several different receptors including complement receptor, dendritic cell-specific intracellular adhesion molecule (ICAM)-3-grabbingnonintegrin (DC-SIGN) and Fc receptors [21, 22]. Once the bacteria gain entry into the macrophage, continued stimulation of TLR by bioactive lipids such as, ManLAM, will lead to arrest of phagosomal maturation

[23]. *Mtb* infected phagosomes fail to acidify and fuse with lysosomal vesicles, reaching a pH of 6.4, which allows *Mtb* growth[24-26]. Macrophage activation mediated by interferon-γ can override the block on phagolysosomal fusion leading to acidification of the compartment [27]. Recently, a study has shown that *Mtb* can survive even in these acidified compartments [28].

A mature TB granuloma generally contains a necrotic core surrounded by a layer of macrophages with neutrophil infiltration, as well as lymphocytes and fibrosis on the periphery (Figure 2) [29]. Induction of granuloma occurs through the activity of mycobacterial effectors such as trehalose dimycolate (TDM) and 6KDa early secretory antigenic target (ESAT-6). The latter induces the secretion of matrix metalloproteinase-9 (MMP-9)by epithelial cells, which degrades the extracellular matrix leading to the recruitment of macrophages to the site of infection[30]. Early studies with mycobacterial cell wall extracts extensively characterized the role of TDM as a key stimulator of granuloma formation [31-35]. This lipid not only acts within the infected macrophage, but it also accumulates and is exocytosed in vesicles to be internalized by adjacent cells, thus expanding its effect to uninfected cells [36]. TDM induces the production of several pro-inflammatory cytokines such as IL-1, IL-6 and tumor necrosis factor α (TNF–α) by stimulating TLR-2 and -4, which in turn leads to recruitment of immune cells [37]. Nevertheless, it contains cyclopropane modifications, lack of which leads to an increased inflammatory response in mice. Therefore, cyclopropanation of TDM produces less inflammatory environment more

conducive with bacterial survivalin comparison to non-cyclopropanated TDM [18].Additionally, to promote its own persistence*Mtb* can delaythe recruitment of T lymphocytes which secrete interferon-γ (IFN-γ),and activate the macrophages, enhancing their antimicrobial activity[38].

As active disease progresses, early lesions evolve into caseous granulomas with a necrotic core which will eventually liquefy and break down, exuding its contents into the airways leading to TB transmission [29]. Alternatively, immunological containment of TB, which occurs in 95% of infected individuals, leads to fibrosis and calcification of the granuloma, providing a long-term niche for persistence of dormant *Mtb* during latent disease [29].

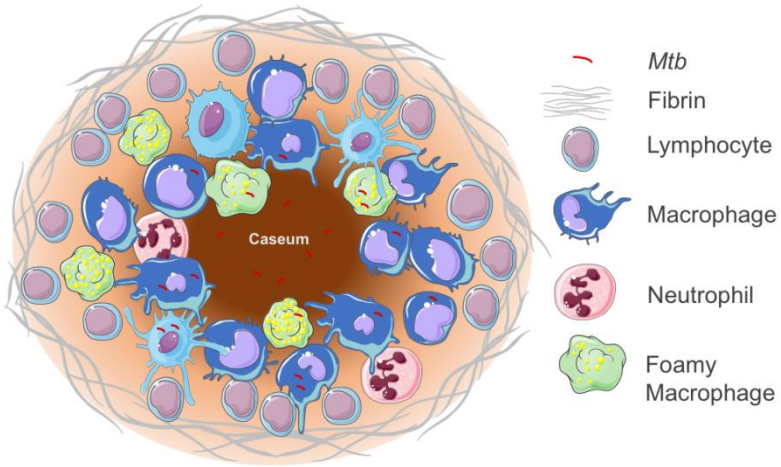

Figure 2. Schematic view of a TB granuloma
Schematic representation of a granulomatous lesion typically observed during infection, which often comprises a necrotic core where hypoxia and extracellular *Mtb* are observed. Depicted cell types are listed on the right. The figure was

assembled using elements extracted from http://smart.servier.com under the creative commons license.

When in a macrophage, embrace the phagosome

During infection, the first environment that bacilli will encounter is inside a macrophage phagosome. As discussed, this pathogen has mechanisms to prevent the full development of this compartment into a phagolysosome. However, even when these mechanisms are fully successful, the bacteria are still faced with hostile conditions including acidic pH, starvation, oxidative bursts, lytic enzymes, and hypoxia [25].

Profound transcriptional responses have been reported for *Mtb* living within a macrophage. Microarray studies demonstrated these bacteria respond to phagosomal cues such as acidic pH as early as 2 hours post-infection and continue to modulate transcription far beyond 2 days of infection, implying that survival requires constant surveillance and tweaking of cellular processes [39]. To endure the intraphagosomal environment, *Mtb* modulates core pathways, upregulating fatty acid degradation as well as DNA and cell wall repair pathways while repressing energy production and aerobic respiration [40]. Even though regulation of these pathways is similar between clinical isolates of divergent lineages, significant gene expression and phenotypic differences upon

macrophage infection were observed for different lineages [41]. This suggests each lineage may have recently evolved particular traits allowing them to thrive in specific human populations.

The hibernating bacteria

Mtb dormancy, or persistence, is a process by which the bacterium reduces its metabolic activity to enter a non-replicative state in response to host-derived signals such as hypoxia, starvation, nitrosative stress and acidic pH [42]. This capability allows the pathogen to establish chronic and latent infections notoriously difficult to clear since dormant bacteria are tolerant to antibiotics [43]. Although the persistence phenotypes associated with TB bacteria have been studied for a long time, only more recently has the research field begun to fully appreciate its impact on disease treatment and drug discovery [43-45].

The *in vivo* relevance of dormant *Mtb* has been widely characterized using not only animal models but also patient samples. Early studies reported the ability of *Mtb* to persist in murine tissue and guinea pig granulomatous lesions [46, 47]. During the same period, evidence for the presence of viable-but-non-culturable bacilli was also observed. A “vanishing phenomena” was described in murine infections with *Mtb* in which bacteria could not be re-isolated from an infected

mouse after treatment, however culturable bacteria would appear in the same mouse after a treatment-free period [44, 48]. In human patients, oxygenated cavitary lesions and caseous necrotic granulomas with extracellular bacteria residing in the hypoxic core have been detected [45, 49-51]. The hypoxic nature of granulomas in several animal models, including guinea pigs, was revealed [52], emphasizing the relevance of these models especially since one of the main signals driving *Mtb* dormancy is hypoxia [42].

To further understand the bacterial survival mechanisms during dormancy and screen for compounds active against these bacteria, several *in vitro* models of dormancy have been developed. Reduced oxygen concentrations have been successfully utilized *in vitro* to induce mycobacterial persistence. The most well-known model was developed by Wayne and collaborators. A stepwise shift down in oxygen tension *in vitro* was utilized, mimicking the disease progression from early oxygenated cavitary lesions to late stage necrotic caseous granulomas with hypoxic cores, and severe decrease in growth rate was observed coupled with increased tolerance to front-line TB drugs [53-55]. A variety of other *in vitro* models utilizing different host-mimicking signals have also been developed to dissect the physiological aspects of dormant bacteria. Bacteria maintained in stationary phase for an extended period of 100 days were tolerant to rifampicin [56]. Furthermore, growth under low oxygen tension induced bacterial stationary phase with cell wall modulation in *Mtb*[57]. Nutrient starvation alone leads to growth arrest and decline in bacterial respiratory rates as well as drug-tolerance

[58, 59]. Although the dormancy phenotypes can be observed *in vitro* under individual stress conditions, including nitric oxide [60], multiple stress models of *invitro* dormancy more closely reproduce the *in vivo* conditions faced by the pathogen. Multiple stress dormancy models include combinations of stresses thought to be relevant *in vivo* such as starvation, hypoxia, acidic pH and nitrosative stress. Deb and coworkers developed an *in vitro* method in which bacteria are cultured in 10X diluted Dubos Media at pH 5 in a hypoxia chamber. Under these conditions *Mtb* stopped replicating, became drug-tolerant, lost acid fastness, accumulated lipid droplets, and up-regulated the DosRS regulon [61]. *In vitro* models of persistence and their impact on drug discovery and development will be further discussed in section 1.4.

To maintain viability in harsh conditions, modulation of metabolic pathways is key. Understanding these pathways is therefore essential not only to discover novel drug targets, but also in the development of *in vitro* drug screening models. The accumulation of lipid bodies under stress conditions is common in prokaryotes, although triacylglycerol (TAG) and wax ester (WE) accumulation occurs in fewer taxa including actinomycetes [62]. Studies have demonstrated that *Mtb* accumulates lipid bodies in its cytosol during dormancy through the activity of TAG synthases, mainly *tgs1* [63, 64]. Notably, this phenotype has been detected in bacteria obtained from patient sputum samples, demonstrating its true biological relevance [65]. An important study by Baek and collaborators [66] showed that *Mtb* arrests growth and becomes drug-tolerant by modulating

carbon flux. Dormant cells shift away from central carbon metabolism by sequestering acetyl-CoA from the TCA cycle for the production of lipid droplets with TAG synthase (*tgs1)*. This study demonstrated that *tgs1,* similarly to *dosR,* was necessary for growth arrest, and that citrate synthase (*citA*) overexpression or *tgs1* deletion produced a high fitness cost for bacteria under hypoxic conditions and *in vivo* [66].

The fact that *Mtb* prefers to utilize fatty acids as carbon and energy source during chronic infectionswas demonstrated in the 1950's [67]. For this process bacteria upregulate a redundant array of β-oxidation and glyoxylate shunt enzymes [68, 69]. Acyl-CoA dehydrogenases are the first enzyme in the process of lipid catabolism [70]. Even though *Mtb* has more than 30 genes putatively encoding for Acyl-CoA dehydrogenases, induction of *fadE28* has been associated with virulence and intra-macrophage survival [71, 72]. The main products of β-oxidation, acyl and propionyl coenzyme A (CoA), will be assimilated through the glyoxylate shunt. The essentiality of isocitrate lyase in maintenance of persistent macrophage and mouse infections is well established, therefore representing a potential "druggable" target for eliminating dormant *Mtb*[73]. Moreover, this enzyme also has methylcitrate lyase activity, working to clear propionyl-CoA and its toxic by-products through the methylcitrate cycle, which is also essential bacterial persistence *in vivo*[73-75].

The electron transport chain is currently a recognized “Achilles’ heel” of dormant *Mtb*. The novel compound bedaquiline, available for drug-resistant (DR) TB treatment*,* is an ATP synthase inhibitor currently in clinical trial for shortening treatment time [76].During dormancy, *Mtb* needs to preserve its ATP levels within a very narrow window, 5-fold lower than in the replicating cell, in order to remain viable. Therefore, an energized membrane and ATP synthase are essential for persistence, as illustrated by their unique vulnerability to inhibitors in dormant bacteria [77]. Other enzymes involved in the respiratory chain are also essential for *Mtb* persistence, and thus may also pose interesting drug-targets. These include *cydC*, a cytochrome assembly transporter, and the synthesis pathway of menaquinone, an electron acceptor essential for reactivation [78, 79]. The type II NADH dehydrogenases (Ndh and NdhA) of *Mtb,* which oxidize NADH to reduce menaquinone in the electron transport chain,are essential for *Mtb* growth [80]*.* Furthermore,inhibition of NdhA was more toxic to dormant than replicating *Mtb*[77]*.* In light of this, NADH dehydrogenase enzymes have been recently investigated as promising targets for the development of novel anti-TB compounds [81, 82].

Molecular master minds

The response regulator DosR/DevR, coupled with the two sensor kinases DosS/DevS and DosT/DevT form a unique two component system (TCS) which drives dormancy in *Mtb* by sensing host signals and regulating transcription of dormancy survival genes [83]. This TCS was characterized concomitantly in two independent research laboratories during the late 1990's to early 2000's. An earlier genetic screen was carried out using the virulent *Mtb* strain, H37Rv, and the attenuated strain H37Ra to find differentially expressed genes in the virulent strain (*dev* genes) [84]. This lead to the discovery and characterization of *devR* as a response regulator of *Mtb,* which isco-transcribed with the histidine kinase gene *devS* [85]. At the same time, induction of the same regulator was observed in *M. bovis* BCG specifically during hypoxia-induced dormancy and not under aerated stationary phase [86-88]. The protein's essentiality for bacterial survival during *in vitro* hypoxic dormancy, also demonstrated in *M.bovis* BCG, led the authors to name it dormancy survival regulator, DosR [86] . The "Dos" nomenclature is used from this point further in this review. A significant phenotype was observed by Malhotra and collaborators [89] with a *dosR* knockout strain (Δ*dosR)* of *Mtb* in guinea pigs. Furthermore, a *dosR* deletion strain only exhibited an impaired growth phenotype in the C3HeB/FeJ mouse strain, which develops organized hypoxic granulomas, and not in the C57Bl/6

strain which does not [90]. Interestingly, the biggest difference in bacterial loads between wild type (WT) and Δ*dosR* was observed only after seven weeks of infection. Furthermore, no differences were observed between WT and Δ*dosR* during *in vitro* macrophage infections. These data suggested that the DosR regulon was essential for persistence in later stages of disease, when granulomas develop necrotic hypoxic cores, but non-essential for invasion and early survival within macrophages [89], which was consistent with the previously defined role of DosR in hypoxic dormancy.

DosR responds directly to O_2, CO and NO through the sensor kinases DosS and DosT, which contain a heme group that modulates their kinase activity; while O2 will cause oxidation of the heme protein leading to its inactivation, CO and NO can form stable complexes with the reduced proteins locking them in an active state [91-94]. Furthermore, the *dosR* regulon also responds to ascorbic acid as well as the macrophage and murine environments [40, 95, 96].The hypoxic response in *Mtb,* comprises a set of 50 genes, all induced by DosR under low oxygen concentrations or nitric oxide [60, 97]. Most of these genes contain a palindromic consensus sequence located upstream, to which DosR binding was predicted and shown experimentally for the *hspX* gene, encoding a heat shock protein. Among the DosR-induced pathways are fatty acid metabolism, alternative electron transport genes and TAG synthesis gene (*tgs1*) [98]. Furthermore, a set of more than 200 genes were induced after prolonged *Mtb*

culture in hypoxia, this broader, DosR independent transcriptional response is known as the enduring hypoxic response [99].

The highly specialized TB pathogen has evolved robust regulatory networks allowing it to rapidly adapt its own physiology in response to environmental cues, which in turn promotes its persistence in the host. Concurrently with the dormancy survival regulon, several other transcriptional regulators also play a role in bacterial adaptation to the host environment, including several sigma factors and important two component systems (TCS). The sigma factors which have the strongest and most direct impact on host adaptation and survival are SigE, F, G and H. Sigma factors E and F are essential for bacterial growth in macrophages and mice, respectively [100] . Although SigG and SigH are induced during macrophage infections, their requirement for growth in these conditions has not been demonstrated [100]. This could be due to a certain level of redundancy in the activity of these regulatory proteins.

TCS are usually comprised of a membrane-bound sensorkinase, which senses an external signal and phosphorylates a partner response regulator, which will modulate the expression of several downstream genes, to produce a phenotype [101]. Among the most noteworthy *Mtb* TCS for surviving the host environment are PhoPR, MprAB and the dormancy regulator DosRS, which has been discussed in depth in the previous section [86, 102]. MprA regulates stress response genes such as chaperone proteins; this autoregulatory system

functions in a larger transcriptional network and also regulates the expression of stress response sigma factor E and B under certain conditions [103]. This TCS is essential for maintenance of persistent infections in a murine model [104], and may modulate host cytokine production by regulating the secretion of ESAT-6 [105]. Furthermore, the phosphorylation of MprA by MprB leading to SigE induction, activates RelA expression and the stringent response, which is essential for *Mtb* survival under starvation, hypoxia [106], and in various *in vivo* models of infection [107-109]. PhoPR is an essential virulence TCS; a single nucleotide polymorphism (SNP) in the response regulator PhoP has been associated with the attenuation of the H37Ra *Mtb* strain in murine and macrophage models of infection [110]. This TCS controls the expression of more than 100 genes, though its role in virulence is attributed partly to the modulation of cell wall lipid metabolism and secretion as well as ESAT-6 secretion [111-113]. The strict regulation of this secreted protein further highlights its fundamental role in TB pathogenesis.

These regulators and their associated downstream effectors which are essential for *Mtb* virulence or *in vivo* persistence represent an untapped pool of drug targets. Inhibition of these proteins/pathways may cause death of dormant bacteria and potentially serve as a stepping stone for the development of a shorter more effective treatment for TB.

TB treatment

Ineffective drugs, with a side of less effective drugs

The standard treatment for TB comprises 4 front-line antibiotics: RIF, INH, PZA and ethambutol (EMB). The current regimen is at least 6 months long for both new and retreatment cases. Usually, in new cases of TB all 4 drugs are taken for the first 2 month of treatment (intensive phase) whereas only RIF and INH are used in the following 4 months (continuation phase) [114, 115]. Individuals previously treated for TB who relapse or are re-infected are subjected to 7 months extendable to 24 months of treatment depending on the drug-susceptibility profile of the bacteria. Also, in cases of relapse, STR is introduced in the intensive phase in combination with the 4 front-line drugs [116, 117]. Following drug-susceptibility testing, combinations of second-line drugs are used against drug-resistant strains of *Mtb* during the intensive and continuation phases of treatment [118].

Drug-resistant strains of *Mtb* are categorized according to their susceptibility profiles. Multi drug-resistant *Mtb* (MDR-TB) is resistant to RIF and INH. The inability to use standard treatment for MDR-TB can usually be compensated with fluoroquinolones (FQ) and injectable aminoglycosides (AG), although these

antibiotics cause more severe side effects, are less effective and need to be administered for up to 2 years [115]. MDR bacteria which develop additional resistance to a FQ and an AG are designated extensively drug-resistant (XDR). Very few drugs are effective against these strains leading to poor prognosis and increased treatment failure rates for XDR-TB [119, 120]. Even though the frequency of MDR-TB reaches an alarming 5% of all TB cases, the rise of XDR-TB is slowed by the fitness cost associated with XDR mutants, which hampers the transmission of these strains [14, 121].

Novel approaches in the TB treatment

Repurposed antimicrobials which increase the success rate of XDR and MDR-TB treatment have been reported in the literature. Linezolid, an oxazolidinone compound effective at treating MDR and XDR-TB patients, is currently recommended by the World Health Organization for strains resistant to at least 4 second-line drugs [116, 122, 123]. In a randomized trial with individuals failing previous therapies due to XDR-TB, culture conversion was observed for 87% of patients after 6 months treatment with linezolid added to a standard regimen for XDR-TB treatment [124]. However, severe adverse effects, such as rhabdomyolysis and optic neuropathy have been reported for this compound in

the long-term treatment required to clear *Mtb* infection [125, 126]. Other repurposed compounds such as beta-lactams in combination with clavulanate (beta lactamase inhibitor) have also been successfully used in the experimental treatment of MDR and XDR-TB patients [127].

Novel compounds recently discovered for the treatment of TB have been the subject of intensive research to achieve more effective treatment options. Bedaquiline (ATP synthase inhibitor) and delamanid (mycolic acid biosynthesis inhibitor) were recently approved for the treatment of drug-resistant TB [76, 128]. Use of delamanid with the optimized background regimen led to an almost 2-fold increase in culture conversion rates and an 8-fold decreased mortality in patients receiving the compound for 6 rather than 2 months [129-132]. Rapid culture conversion and minimal appearance of bedaquiline-resistant mutants is encouraging further use of this compound to treat susceptible *Mtb* infections with new combination therapies [133-135].

Drug Discovery and Development

The ineffectiveness of TB treatment poses a major barrier in any attempts to control the disease worldwide. Novel, more effective therapies capable of clearing the infection in shorter periods are urgently needed. New drugs should

have rapid bactericidal activity, novel mechanisms of action, higher safety and tolerability than the currently available antibiotics, as well as effectiveness against non-replicating *Mtb*. To achieve this, a compound will have to be thoroughly characterized in the long and laborious drug discovery and development pipeline. This is divided into three major stages: i) discovery, ii) preclinical development and iii) clinical development [136]. The initial stage of discovery requires intensive screening of chemical compound libraries due to the high attrition rate observed in the drug discovery pipeline. Key aspects to be considered in this stage are the choice of screening model and chemical library as these will affect the likelihood of discovering a novel scaffold and/or bacterial target. Hit-to-lead optimization of scaffolds with low toxicity will involve medicinal chemistry efforts to optimize the solubility and stability, as well as selectivity of the molecule for its bacterial target [137-139]. Once a compound has been extensively characterized mainly *in vitro,* it can advance as a lead into the pre-clinical development stage. In this second stage, defining a safe and effective dose for human testing is the main goal. Pharmacokinetics (PK) to determine absorption, distribution, metabolism and excretion (ADME) of a compound is done using animal models. Furthermore, these models are also used to assess pharmacodynamics (PD) and toxicology [140-142]. In the pre-clinical development stage a compound must meet the good laboratory practices (GLP) guidelines in order to be approved for human testing in the third and final stage, which is clinical development. Clinical Development entails a costly process

which is subdivided into three phases of clinical trials. Phase I clinical trials usually include small groups of healthy individuals to assess the safety of a drug, whereas phase II trials will require hundreds of patients in order to establish efficacy and further assess safety. To validate safety and efficacy, the drug is tested with thousands of patients in a phase III clinical trial [115, 143]. Finally, positive phase III trial results will lead to approval of a drug by health agencies for commercialization. The drug discovery and development pipeline for TB is shown in Figure 3.

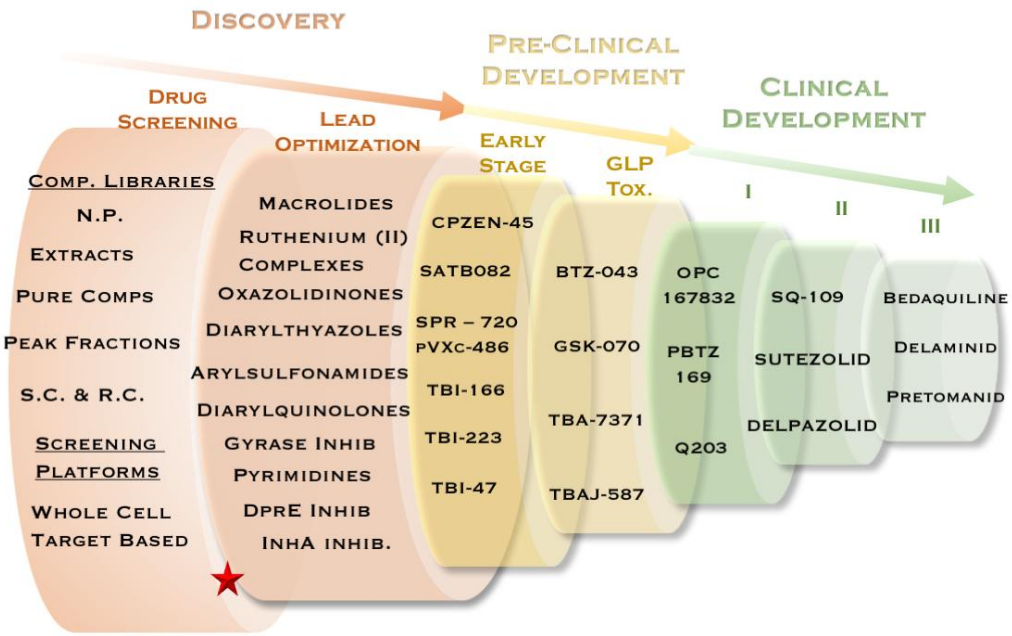

Figure 3. The TB drug discovery and development pipeline.
Schematic representation of the compounds currently being developed for the treatment of TB. The red star represents the stage in the pipeline where the current work is focused.

Just keep screening, screening, screening

Understanding mycobacterial physiology during infection has improved the drug development research field. Genomic sequencing, transcriptional profiling and genetic screens of *Mtb* mutants in these biologically relevant environments have

provided many novel essential targets to the drug-discovery pipeline [39, 40, 72, 144, 145]. Target-based assays are advantageous since hits from these screens will have a defined mechanism of action from the beginning. Nonetheless, extensive target-based screening efforts have had little success in yielding compounds able to pass through all the checkpoints in the pipeline [146]. Activity against a target*in vitro* is often translated into low potency in whole-cell assays since the mycobacterial cell wall is so impermeable[137]. Additionally, drug-modifying enzymes such as acetyltransferases, as well as efflux pumps will impact the amount of active compound reaching its target, especially during infection when many of these proteins are induced [147-149]. Optimization strategies to improve the drug's uptake are often needed before the compound can advance in the pipeline. On the other hand, the recent success of high throughput whole-cell screening is well documented with examples such as the ATP and the arabinan synthesis inhibitors bedaquiline and benzothiazinones, respectively [150, 151]. The advantages of whole-cell screening go beyond drug-uptake. Hit compounds which inhibit growth can also be used as chemical tools and reveal novel vulnerable bacterial targets. Nonetheless, whole-cell screening against *Mtb* is a multifaceted undertaking. The choice between a wide range of screening models and compound libraries will directly impact the outcome of the screen.

In vitro screening models for TB

Since *Mtb* is a slow growing, biosafety level 3 (BSL3) pathogen, researchers often use surrogate bacteria to bypass at least one of these difficulties. Surrogates include the non-pathogenic fast-growing *M. smegmatis* (*Msmeg*), the attenuated vaccine strain *M. bovis* BCG, as well as attenuated strains of *Mtb,* such as H37Ra, which are BSL2 organisms. Screening against *Msmeg* has been successful, yielding potent inhibitors of *Mtb,* including bedaquiline [150, 152], though its suitability as a surrogate remains controversial. This mycobacterium can become dormant, and activates the DosR regulator, which are key features contributing to *Mtb* virulence and persistence [153, 154]. Nonetheless, it is rapidly cleared by several different types of macrophages, including J774 murine cell line and human-derived macrophages, and it is not infectious in mice even when expressing *Mtb* genes [155, 156]. Furthermore, a study by Altaf and collaborators showed that this is the least sensitive model for identifying *Mtb* active compounds in comparison to H37Ra and BCG [157]. By screening three pure compound libraries against each mycobacteria *in vitro,* the authors demonstrated that hit scaffolds with the lowest MIC against *Mtb* were less potent against BCG and not active against *Msmeg*[157]. Aside from sensitivity of a screen, using non-virulent surrogates poses further challenges. The unique virulence traits of *Mtb* comprise a pool of excellent drug targets less likely to be discovered in surrogate screens.

Furthermore, compounds discovered this way will require an extra analysis step to confirm their activity against virulent *Mtb.*

Even though virulent *Mtb* represents the most effective choice for screening assays, the first challenge with this is finding a sensitive and robust readout that will provide reliable data. Since CFU enumeration would become an impossibly laborious and time-consuming effort for high throughput screening, alternative readouts need to be utilized. The resazurin dye is a redox indicator that becomes reduced to fluorescent resofurin due to metabolism of viable cells, thus providing a detectable fluorescent shift [158]. Resazurin assays were initially developed for drug-susceptibility testing of clinical isolates, and further optimized for screening of compound libraries [159-162]. Fluorescent reporter proteins are often chosen instead of resazurin as they do not require addition of a reagent to the screening plate before obtaining results, and are therefore more amenable to high throughput methods. Also, the expression of reporter proteins such as green fluorescent protein (GFP) and red fluorescent protein (mCherry), has been optimized in *Mtb* to provide high fluorescent signal for more sensitive assays than with resazurin [163-166]. Recently, bioluminescence has been established as a very powerful tool in which light is generated by luciferase enzymes and the ATP-dependent cleavage of their substrate. Three bioluminescent reporters were optimized for use in *Mtb,* including the *luxCDABE* operon which enables the expression of not only bacterial luciferase but also synthesis of the substrate luciferin, rendering the bacteria autoluminescent. Furthermore, this study also

demonstrated the viability of these reporter as readouts of bacterial loads in murine infection [167]. A wide range of drug screening assays has been developed with these reporters, including *in vitro* macrophage infection and dormancy assays [168-171].

The important role of the intra-macrophage life-style in modulating bacterial physiology has been extensively shown and is reviewed in section 1.2.2. Scaffolds able to inhibit the growth of intracellular rather than *in vitro* replicating *Mtb* are more likely targeting unique pathways the bacteria require to survive the harsh phagosomal environment. Furthermore, other valuable preliminary information is obtained by default when using intracellular bacteria for drug screening, including uptake by the host cell, and stability in a phagosomal compartment. Drug discovery technologies have been developed to screen for compounds active against intracellular bacteria. These have proven successful leading to the discovery of the clinical candidate drug Q203 [172-174]. In a recent study by VanderVen and coworkers [175] several inhibitors of cholesterol metabolism were discovered in a large-scale screen against *Mtb* infecting J774 macrophages. Cholesterol metabolism is key for intracellular survival of *Mtb* [176]. The importance of cholesterol metabolism for this pathogenwas even further highlighted by a study demonstrating that cholesterol analogs inhibit bacterial growth *in vitro* by obstructing the cholesterol catabolism pathway [177]. Intracellular infection methods have also been used to discover host-targeted molecules that prevent mycobacterial growth in the macrophage [178]

Historically *in vitro* drug screening utilized *Mtb* under replicating conditions in rich nutrient broth media at physiological pH and atmospheric oxygen levels. However, in recent years the field began to fully appreciate the impact of *Mtb* dormancy on disease treatment[43, 179]. An urgent need for compounds inhibiting dormancy-essential targets has led researchers to adapt and develop technologies for screening compound libraries against dormant *Mtb.* Different assays utilizing a single stress condition to induce phenotypic tolerance have been successful in identifying dormant-active compounds [180-182]. The well-known Wayne model of oxygen depletion has been utilized, for example, to discover inhibitors of ATP production in dormant *Mtb,* by using an indicator of ATP this screen directly targeted this essential pathway [183]. Single-stress models however are not mimicking the full array of host stresses. A comparison of hits obtained from the same library screened in a low oxygen assay and in a carbon starvation assay revealed very little overlap in activity [180]. Furthermore, use of individual stresses allowed the discovery of nitric oxide dependent compounds [184]. These data highlight the importance of combining several stress conditions to amplify the number of active molecules resulting from a phenotypic screen. Multi-stress models of dormancy can achieve this goal while also keeping the assays simple and amenable to high throughput screening. Two screens employing multi-stress dormancy models (hypoxia, acidic pH, starvation) have yielded small molecules from the GSK library and synthetic calanolides bactericidal against dormant Mtb[185, 186]. Cephalosporin compounds were

selectively active against persistent *Mtb* in a similar assay [184], demonstrating that compound libraries should be primarily screened against drug-tolerant bacilli as many active molecules may go undetected through a conventional assay with replicating bacteria.

Although phenotypic screens with dormant *Mtb* have proven successful, there are hurdles associated with use of non-replicating bacteria in drug screening assays. Drug screening assays usually rely on growth of uninhibited bacteria leading to a gain of signal over time. However, since dormant *Mtb* does not grow, the assays generally rely on a recovery stage, in which treated dormant samples are diluted in rich broth media and incubated in normoxic conditions for observation of outgrowth of surviving bacilli [182, 187]. For this reason, false-positive hits can occur due to inhibition of replicating bacteria by carry-over compounds during the outgrowth stage of these assays. The obvious solution to this issue is not amenable to high throughput screening as it would entail pelleting and washing out any residual compound before resuspending in rich broth for outgrowth. A novel technique was recently developed to overcome this issue which relied on placing the treated sample on media containing activated charcoal to sequester any remaining carry-over compound. This approach was rapid and useful for large-scale screens [188]. Another approach took advantage of the highly sensitive bioluminescent signal to overcome this issue. A bioluminescent strain produced enough luminescence even when not replicating to allow acceptable signal-to-background ratios without requiring outgrowth.

Nevertheless, this study utilized a streptomycin-dependent mutant *Mtb* strain which arrests replication when starved of this antibiotic [189]. Lack of host-derived stress conditions to induce a dormant phenotype may skew the results of a screen with this strain, and cause many dormant active molecules to be undetected. In the current work, we have performed phenotypic screening using a multi-stress dormancy model [61], with virulent *Mtb* and a luminescent readout, which eliminated the need for a recovery stage and allowed the discovery of dormant-selective compounds.

Pick your poison

Another important aspect of drug screening against *Mtb* is the chemical compound library that is screened. Overall, antimicrobial compounds have a unique set of physicochemical properties in comparison to other therapeutic drugs [190]. The wide chemical space covered by TB drugs poses a challenge for drug discovery. A principal component analysis was used to evaluate several physicochemical features, including lipophilicity and molecular weight, of more than 1600 marketed non-antimicrobial compounds in comparison to anti-TB drugs. This demonstrated potent anti-TB drugs, such as RIF and STR, which are natural products, on the periphery of the chemical space, whereas synthetic

drugs like fluoroquinolones are on the center, clustered with most available non-antimicrobial drugs [136]. Synthetic libraries of pure compounds are often chosen because the hits from these screens can be more easily and efficiently characterized and advanced to the next step in the drug-discovery pipeline. Nonetheless, these libraries usually do not cover the broad chemical space needed in the search for antimycobacterials, leading to high redundancy in screening results [191]. In light of these issues, there has been a shift back towards natural products recently in antimicrobial screening efforts [192, 193].

The historical success of natural products against bacterial pathogens is well established; nine out of twelve classes of antimicrobials are derived from natural products [194]. Extensive screening of natural product libraries has revealed a wide variety of *Mtb* active scaffolds [195, 196]. Examples of this include plant-derived bisbenzylisoquinoline alkaloids with MICs as low as 3 µg/mL against replicating *Mtb,* sesquiterpenes isolated from Mexican medicinal plants, which were potently active against MDR strains, as well as plant-derived apolphine alkaloids exhibiting bactericidal inhibition of mycobacterial MurE ligase [197-199].

The chemical diversity of the libraries is a reflection of the biodiversity of natural environments, and marine environments hold the highest diversity of living organisms on the planet [200]. Consequently, marine-derived scaffolds are more chemically diverse and bioactive than natural products from terrestrial environments [201]. Furthermore, marine natural products (MNP) often exhibit

exceptional potency since many have evolved to protect sedentary marine organisms from microbial parasites in a harsh environment where they rapidly become diluted [200]. The potency of marine-derived scaffolds has been comprehensively demonstrated and reviewed [202-204]. Steroidal molecules and their synthetic analogs as well as brominated metabolites from marine sponges have exhibited activity against replicating *Mtb* [205, 206]. Inhibition of dormant *Mtb* has also been demonstrated with marine natural products. Halicyclamine A is an alkaloid isolated from a marine sponge, which demonstrated equally potent activity against both replicating and dormant *Mtb* [207].Melophlins, isolated from the marine sponge *Melophlus sp.*, were also inhibitory against non-replicating *Mtb* in carbon starvation models of dormancy [208]. Often marine natural products are not synthesized by the marine invertabrate but by the symbiont microorganisms that reside on their surface. Cyanobacterial peptides, for instance, were shown to inhibit *Mtb* tyrosine phosphatases [209]. Moreover, aminolipopeptides from marine-sponge-derived fungi showed submicromolar activity against dormant *Mtb*[210]. These potent molecules isolated from marine microorganism have the advantage that the organism can often be cultured in a laboratory for scaling up the production of the bioactive scaffold [211]. Furthermore, genomic sequencing efforts have led to the discovery of microbial metabolic pathways producing these antibiotic molecules. Biosynthetic gene clusters can be engineered into bacterial reference strains for large-scale production of certain scaffolds [212].

Although the success of natural products in the search for antimicrobials has been extensively shown, there are important challenges that need to be overcome when screening natural product libraries. Scaffolds derived from natural sources often exhibit promiscuous activity, targeting multiple pathways among several different organisms [213]. Problematic broad activity of certain scaffolds is exemplified by curcumin, a potent natural product with antimicrobial, anticancer and anti-inflammatory activity. Consequently, the toxicity of this compound in murine models is also broad [214]. Additionally, natural product libraries are more difficult to work with because they are composed of compound mixtures extracted from a living organism. Therefore, a laborious, time-consuming deconvolution and dereplication process is needed to identify a pure bioactive molecule. In the current work, a marine natural products library was screened against *Mtb.* To bypass a complex deconvolution process of crude extracts, marine organism samples underwent one round of medium pressure liquid chromatography (MPLC), yielding a library of semi-pure peak fractions which facilitated the deconvolution of active mixtures.

Genomic mining to address the challenge of natural product drug discovery

As previously discussed, many challenges are associated with the use of natural product libraries for drug discovery and development. The main problem for researchers performing natural products screens is further development of hit scaffolds through medicinal chemistry and characterization of the mechanism of action [191]. Obtaining a single active molecule usually requires extensive purification of an active crude extract. Once a bioactive molecule is purified researchers have to overcome the hurdle of scaling up the production of a natural product scaffold since the organisms that synthesize these molecules, such as marine invertebrates, may be impossible to culture *in vitro* [203]. Many of these compounds often have complex structures rendering their chemical synthesis highly difficult, inefficient and expensive [196]. Innovative approaches are being used to address these issues ensuring the progression of more natural products to the next stages of drug development.

Exploring natural environments as vast sources of antimicrobials is becoming increasingly viable with the advancement of bioinformatics and genome sequencing technologies, enabling in depth analysis of sequenced genomes to reveal novel biosynthetic pathways of undiscovered natural products [215-217]. Genome analysis estimates the production of hundreds of thousands of natural products by the Streptomyces genus alone [218]; a number which drastically

increases when multiple taxa are evaluated [219]. Obtaining and characterizing these molecules is possible due to the availability of surrogates for expression of biosynthetic gene clusters and consequent production of a desired natural product [220].

Biosynthetic gene clusters usually contain genes for the biosynthesis of secondary metabolites, including polyketide, non-ribosomal peptide and terpene synthases, as well as ribosomally synthesized and post-translationally modified peptide biosynthetic genes [212]. Natural product biosynthetic gene clusters are normally very large ranging from tens to hundreds of kilobases, and have complex regulatory mechanisms which make them very difficult to express in surrogate organisms for large-scale production of desired scaffolds [221]. In order to simplify these gene clusters into more amenable tools for natural product discovery a process called refactoring is often employed. This basically consists of removing non-essential genes, non-coding DNA and the natural regulatory elements, and including well-characterized regulatory systems to control gene expression [222]. By taking the resulting DNA sequence and randomizing the gene codons, hidden regulatory elements embedded within genes are also removed [223]. This technology has allowed the discovery and production of several antibiotic molecules, including scaffolds from marine organisms such as the lipopeptide taromycin A [224-226]. Optimization of promoters for heterologous expression of gene clusters is essential not only to scale up production of an antibiotic molecule but also to allow discovery of novel

molecules in uncharacterized biosynthetic gene clusters [227]. Use of strong promoters in the spetinabilin gene cluster increased the production of this molecule by 100-fold [226]. The CRISPR-Cas9 technology has also been applied as powerful tool to regulate gene expression. By mutating the Cas9 genes to produce a catalytically inactive enzyme (dCas9) and fusing it to an activator or repressor domain it is able to regulate the expression of genes targeted by the co-transcribed sgRNA [228, 229]. This method is effective across several organisms relevant to antibiotic production [230, 231]; for instance, the production of violeicin has been controlled in yeast [232]. High throughput synthesis of DNA leads to the creation of varied biosynthetic gene clusters and consequent diversification of scaffolds through combinatorial chemistry; this, in turn allows for optimization of naturally derived molecules through medicinal chemistry [233-235].

Dissecting mechanism of action

Drug target identification in the post-genomic era

Availability of the complete *Mtb* genome sequence revolutionized the TB research field, spawning a wide range of novel technologies and facilitating drug target identification and characterization [72]. Drug discovery and development may occur via a target-to-drug or a drug-to-target approach. In the drug-to-target approach molecules active against whole-cells are used in mechanistic studies to discover the target. This approach has been most successful in the TB field, and was chosen in this study. Classically after identifying and characterizing the activity of a novel scaffold, the subsequent steps include isolation and validation of spontaneously resistant mutants. Next generation sequencing technologies enable fast and inexpensive whole-genome-sequencing [236]. Comparing genome sequences of susceptible strains with resistant mutant enables the identification of single-nucleotide-polymorphisms (SNP) that can be responsible for the resistance phenotype. Targets for several drugs currently in clinical trial phase were identified this way. For instance, *Mtb* and *M. smegmatis* bedaquiline-resistant mutants all harbored missense point mutations in *atpE* which led to the identification of ATP synthase as the drug target. This was further confirmed by

episomally expressing the mutant protein in susceptible strains leading to resistance [150].

Q203 is a potent compound currently in phase I clinical trials. To confirm its target was cytochrome bc_1 the authors not only sequenced several resistant *Mtb* mutants, but also obtained *Mtb* strains resistant to analogs of Q203 harboring mutations in the same gene. Additionally, the resistance mutation was introduced in the parental strain via homologous recombination to reproduce the resistance phenotype [172]. The use of compound analogs to isolate resistant mutants is also useful when attempts fail with the optimal compound itself, such as the MmpL3 inhibitor SQ109 [237]. A large-scale approach to identify targets for multiple compounds has been used by Ioerger and collaborators [238]. In this study, several mutants were isolated with resistance to different hits from a high throughput screen, deep sequencing of resistant mutants and recombineering were used to validate targets. Recombineering is a highly efficient gene replacement method developed by van Kessel and coworkers reliant on the mycobacteriophage recombinase enzymes which allows directed incorporation of SNP in the mycobacterial genome [239]. Several gene knockout methods for *Mtb* have been developed and are fundamental to help validate drug targets, since this can reveal secondary targets for a drug, as well as validate the essentiality of a putative target.

Even though isolation of spontaneous mutants is the most widely used method to find *Mtb* drug targets, many compounds are poorly amenable to this approach. Challenges can arise when compounds target an essential protein in which mutations produce a deadly fitness cost, or inhibit multiple targets. Pro-drugs such as INH and PZA, which need to be activated by a protein other than the target can also confound attempts to isolate the target [240]. The complex mechanism of action of PZA has been widely studied and mutated genes from at least two diverging metabolic pathways have been associated with PZA resistance [241]. The traditional target identification method becomes obsolete for compounds such as vancomycin and teixobactin, which cause bacterial death by binding to essential cell wall precursors as opposed to the biosynthetic proteins [242, 243]. Moreover, resistance to certain antibiotics, such as fluoroquinolones, can arise from efflux pump overexpression, which is also misleading in the search for a mechanism of action [244]. Alternative approaches relying on transcriptional reporters and profiles, as well as biochemical assays are therefore imperative not only to help validate and characterize targets, but also to discover a target when the standard approach fails.

Boshoff and collaborators used transcriptional profiling of treated *Mtb* to identify metabolic pathways inhibited by a very comprehensive collection of compounds [245]. This study compared 430 different transcriptional profiles exhibited by *Mtb* treated with 75 different compounds and compound combinations under varying culture conditions. Different drugs produced signature transcriptional profiles,

causing up or down regulation of gene clusters which was consistent across different drugs with similar mechanisms of action [245]. Recently, microfluidic transcriptional profiling of treated *Mtb* enabled the simplification of transcriptional responses for a drug to a single gene which robustly represented the associated gene clusters, making it more amenable to high throughput mechanistic discovery [246]. These studies represent powerful tools to predict the pathways targeted by novel compounds. The knowledge previously obtained was used in a more recent study to find inhibitors of cell wall biosynthesis [247]. In this study, the authors utilized the *iniBAC* operon promoter as a reporter of mycolic acid synthesis inhibition [247]. This was further validated for the cell wall biosynthesis inhibitor SQ109 using a proteomic approach, which also showed the overexpression of the *iniBAC* operon in *Mtb* treated with this compound [248]. Since the microarray studies by Boshoff and Murima [245, 246], novel more sensitive technologies for transcriptional profiling, such as RNAseq, have been developed. RNA-seq has been used to define the transcriptional profiles of *Mtb* under phagosomal and genotoxic stress conditions, as well as *in vivo,* and to dissect the pathogen's translational landscape by using ribosome profiling and transcriptional start site mapping [249-252]. These studies provide further insight into genes and pathways expressed during infection which may therefore constitute vulnerable targets. RNA-seq technology poses an important drug-target discovery tool that should be further explored in the TB drug-development pipeline. Additionally, use of bioluminescent reporters has become widely used in

the TB drug discovery and development field. Naran and collaborators have explored this tool in combination with reporter promoters for large-scale drug target identification [253]. The authors cloned well established *Mtb* promoters up-regulated by DNA damage and cell wall synthesis inhibition upstream of the *luxCDABE* operon to develop a gain-of-signal method for preliminarily identifying a drug's mechanism of action. This method was validated using known compounds such as INH and ciprofloxacin. Use of the methods discussed in this section provides significant information regarding the mechanism of action of novel compounds. Complementing these techniques with biochemical approaches allows identification and validation of drug targets.

Biochemical approaches to finding a target

In the case where a drug target is unknown, chemical proteomic approaches are very useful for “fishing” the protein out of a treated sample using tagged or immobilized compounds; mass spectrometry is then applied to identify the protein [254]. Wolfe and coworkers have utilized desthiobiotin-conjugated ATP to identify ATP-binding *Mtb* proteins, which would become modified with biotin in their active sites [255]. These proteins would then be digested, the biotin-labeled peptides enriched using streptavidin beads, and identified using mass

spectrometry. Powerful methods such as this can be used to detect drug targets and target competitors. An antimalarial compound was immobilized on beads and used to capture target proteins, which were then identified by liquid chromatography tandem-mass spectrometry [256]. Small-molecule protein kinase inhibitors immobilized on beads have also been extensively used to identify specific targets [257, 258]. Chemical proteomic tools are advantageous since target proteins can be identified under various *in vitro* conditions. The importance of screening *Mtb* compounds in dormancy-inducing conditions has been demonstrated in the current study. For dormancy-selective compounds, these proteomic approaches allow identification of targets specifically in the dormant *Mtb* cell.

Hit-to-lead optimization and preclinical development

There are a number of criteria that need to be considered when selecting hits from a compound library screen for optimization. As defined by the Global Health Innovative Technology Committee, hit validation for antitubercular compounds requires an MIC below 10μM, a 10-fold selectivity towards *Mtb* compared to mammalian cells and preliminary structure-activity relationship evidence. Additionally, the chemical structure of the hit scaffold should be amenable to

modification, and contain no unstable moieties [138]. Furthermore, the scaffold should be filtered for promiscuous activity using pan-assay interference (PAINS) filters [259-261]. The physicochemical properties of a hit scaffold directly impact its likelihood to advance in the drug discovery pipeline. Molecules that meet Lipinski's "Rule of Five" have a higher chance of success since the physicochemical properties of a compound directly affect its membrane permeability and ADME [262-266]. The physicochemical criteria set by Lipinski and collaborators dictate that a compounds molecular weight must be lower than 500, the lipophilicity and number of available hydrogen atoms for hydrogen bondsmust be 5 or less, and finally the molecule can have a maximum 10 groups capable of accepting hydrogen atoms in hydrogen bonds [267]. Determining the mechanism of action early on is vital for the optimization of the molecule to improve selectivity and efficacy. After a hit scaffold has gone through this process, it will be further optimized as a lead before the preclinical development stage. Lead optimization requires testing the compound to rule out liabilities. Inhibition of liver cytochrome P450 and human ion channels [268, 269], as well as microsomal stability help drive medicinal chemistry efforts [270]. Pharmacokinetic and pharmacodynamics (PK/PD) of a molecule is determined using murine models [136]. By utilizing PK/PD data in relation to MIC it is possible to calculate the area under the inhibitory curve and thus begin to calculate dosage and frequency of compound intake appropriate for efficacy studies in animal models and later in humans [271]. Time kill-kinetic profile of a

molecule has also been suggested as a powerful predictor of clinical efficacy during preclinical development [272]. The efficacy and tolerability of a lead is demonstrated in several animal models of infection during preclinical development; non-human primates are usually utilized late in this stage to define safe doses for first-in-human studies, the starting point of clinical development [139]. Compounds currently being optimized as novel leads for anti-TB treatment include diarylquinolones, cyclopeptides, ruthenium (II) complexes, spectinamides and indazoles [273].

Clinical Development

The effectiveness of novel anti-TB therapeutics in clinical trials is assessed using biomarkers, including sputum bacterial load, however, there is a shortage of reliable biomarkers to predict the outcome of TB treatment [274]. Phase I trials rely on early bactericidal activity (EBA), which is determined using sputum bacterial loads after two to five days of treatment [275]. Nonetheless, novel effective compounds such as bedaquiline display delayed bacterial clearance of sputum, which further emphasizes the need for reliable biomarkers for later stages of treatment [276].

During phase II trials, TB patients are treated for two to six months with the new therapy combined with the standardized therapy, and time to sputum conversion is evaluated in this phase of clinical development. Bactericidal activity and safety are requirements for a drug to proceed into phase III trials. Phase II trials including bedaquiline, PZA, moxifloxacin and pretomanid have demonstrated the early bactericidal activity of this combination therapy and sputum culture conversion in as little as 8 weeks [277, 278]. During phase III trials the compound will be used in novel combination regimens for six to twelve months [136]. Even though bedaquiline has been granted accelerated approval for the treatment of MDR and XDR-TB, it is currently in confirmatory phase III trials, with culture conversion being achieved in more than 70% of XDR-TB patients after three months of treatment [279]. Additionally, a phase III trial testing a novel regimen against drug sensitive (DS-TB) includes the utilization of high doses of rifapentine in the continuation phase and moxifloxacin for six months instead of isoniazid, which reduced relapse rates from 3.1% to 2.7% [280].

Difficulties in the clinical development stage stemming from unreliable biomarkers extends this phase of development, delaying the approval of novel therapies, since two-year monitoring of patients after treatment end is often required to determine relapse rates [273]. Novel strategies to overcome these difficulties, and more effectively predict treatment outcome include PET-CT scanning of patients [281], detection of bacterial DNA in urine samples, as well

as host-derived biomarkers such as the interferon-inducible blood transcriptional TB profile [282]. Moreover, a deeper understanding of the predictability of the standard biomarker, sputum bacterial load and conversion, has helped define the true efficacy of completed clinical trials [273].

In the current work the diverse chemistry provided by natural products was used in combination with a dormancy screening platform enabling us to explore the full potential of a marine natural product compound library. This study led to the discovery of several compounds active against non-replicating drug tolerant *Mtb*. Continued efforts can not only uncover further active scaffolds but also lead to the discovery of novel vulnerable targets of this important human pathogen.

M. abscessus: a growing concern

The fast-growing *M. abscessus* (*Mab*) can cause chronic lungand skin infections, affecting mainly cystic fibrosis (CF) patients [283]. These infections are extremely difficult to treat, and treatment failure rates can be as high as 50% [284]. Additionally, they are often misdiagnosed as TB by smear-microscopy which cannot differentiate between mycobacterial species. The fact that front-line TB drugs are not effective for treatment of *Mab* infections emphasizes the need for novel chemicals capable of inhibiting this mycobacterium [285].

A main theme of the current work is how the varying physiological states of *Mtb* during infection impact disease treatment and the importance of reproducing these *in vitro* to guide the drug discovery and development process. Currently very little is known regarding the different aspects of *Mab* physiology during infection, even though it is likely that these directly impact the bacterium's susceptibility to treatment. Conserved pathways essential for *Mtb* virulence and persistence, such as DosR, should be examined in depth in *Mab.* RNAseq technology can be used to dissect the *Mab* responses to dormancy inducing conditions, intracellular life and adaptation to the host. This will provide valuable information regarding genes and pathways differentially expressed by *Mab* under these conditions, which may represent druggable targets.Additionally, key stress conditions triggering the most profound responses in this pathogen may be defined. With this, novel *in vitro* models can be developed which reproduce *in vitro* the bacterium's most important physiological aspects during infection. Inducible drug resistance mechanisms can also be useful for *Mab* drug discovery, since inhibiting one of these mechanisms may restore the pathogen's sensitivity to an existing antibiotic. The *Mtb* inducible drug resistance regulator WhiB7 has recently been described in *Mab*, disruption of the gene increased the sensitivity of *Mab* to several antibiotics; the results also suggested that WhiB7 regulates known drug tolerance genes of this pathogen, such as *erm(41)*[286-288].

CHAPTER 2:

SELECTIVE KILLING OF DORMANT MYCOBACTERIUM TUBERCULOSIS BY MARINE NATURAL PRODUCTS

This chapter was written by Carolina Rodrigues Felix. Revisions and edits from Kyle Rohde were incorporated to the final version.

This chapter was previously published in Antimicrobial Agents and Chemotherapy, American Society for Microbiology. Antimicrob. Agents Chemother.61:e00743-17. https://doi.org/10 .1128/AAC.00743-17.

Rodrigues Felix C, Gupta R, Geden S, Roberts J, Winder P, Pomponi SA, Diaz MC, Reed JK, Wright AE, Rohde KH. Selective Killing of Dormant Mycobacterium tuberculosis by Marine Natural Products. Antimicrob Agents Chemother. 2017 61(8). pii: e00743-17. doi: 10.1128/AAC.00743-17.

Abstract

The dormant phenotype acquired by *Mycobacterium tuberculosis* (*Mtb)* during infection poses a major challenge in disease treatment since these bacilli are tolerant to front-line drugs. Therefore, it is imperative to find novel compounds that effectively kill dormantbacteria. By screening 4,400 marine natural product samples against dual-fluorescent *Mtb* under both replicating and non-replicating conditions we have identified compounds that are selectively active against dormant *Mtb*. This validates our strategy of screening all compounds in both assays as opposed to using the dormancy model as a secondary screen. Bioassay guided deconvolution enabled the identification of unique pharmacophores active in each screening model. To confirm the activity of samples against dormant *Mtb* we used a luciferase reporter assay and CFU enumeration. The structures of five purified active compounds were defined by NMR and mass spectrometry. We identified two lipid compounds with potent activity towards dormant and actively growing *Mtb*. One of these was commercially obtained and showed similar activity against *Mtb* in both screening models. Furthermore, puupehenone-like molecules were purified with potent and selective activity against dormant *Mtb.* In conclusion, we have identified and characterized antimycobacterial compounds from marine organisms with novel

activity profiles which appear to target *Mtb* pathways conditionally essential for dormancy survival.

Key words: dormancy, tuberculosis, marine natural products, drug screening

Introduction

Tuberculosis (TB) is one of the leading causes of death by an infectious disease worldwide. The large pool of individuals latently infected with *Mycobacteriumtuberculosis*(*Mtb)* (~2 billion) and lack of an effective vaccine hinders attempts to eradicate this disease [14]. Furthermore, a long multi-drug regimen is required to treat TB, which leads to poor patient compliance and increasing occurrence of multidrug-resistant (MDR) *Mtb* strains. A prolonged treatment is required due to dormancy induced drug-tolerance developed by *Mtb* during infection in response to conditions within the host [17, 54]. A considerable body of work has validated the causality between hypoxic granuloma environments and persistent tubercle bacilli [38, 289, 290]. Also, a recent study has demonstrated that *Mtb* becomes drug-tolerant as a consequence of stress cues it experiences while residing in activated macrophages [291]. These issues highlight a dire need for new scaffolds with novel modes of action effective against MDR and phenotypically drug-tolerant *Mtb.*

Efforts to find new effective treatment options have uncovered promising lead compounds, however only two new drugs have been approved specifically for the treatment of TB in the past four decades [115, 129-131, 134]. Recent studies have shown the value of screening compound libraries under *in vivo*-like conditions, since*Mtb* undergoes profound metabolic shifts during infection which may alter target vulnerability. Inducing *Mtb* dormancy phenotypes *in vitro* canenrich the discovery of compounds targeting novel and conditionally essential pathways [175, 180, 181, 185, 187, 188]. The Wayne model of gradual oxygen depletion is the most well-characterized *in vitro* dormancy model. However, this is difficult to translate into high throughput screening since it requires 2 sequential stages of oxygen depletion in sealed tubes [53]. An alternative multi-stress dormancy model (MSD) described by Deb*et al.* produced phenotypically dormant *Mtb* after 9 days of incubation under conditions of low oxygen, low pH, and nutrient limitation. Bacilli in this model exhibited all of the classical dormancy traits, including lipid droplet accumulation, loss of acid fastness, up-regulation of the *dosR* regulon and, most importantly, tolerance to frontline drugs [61]. In this study, we have successfully adapted this method for high throughput screening and used it to identify marine natural products (MNP) which kill dormant *Mtb.*

The search for antimycobacterials from natural sources is a historically validated approach. This is emphasized by the fact that 9 out of 12 classes of currently available antibiotics are natural product-derived scaffolds [292]. Though screening libraries of pure synthetic compounds may yield hits more efficiently,

these libraries are often redundant leading to rediscovery of similar scaffolds with known modes of action [191]. This observation has incentivized renewed efforts in recent years toward screening of the more chemically diverse natural product libraries [196]. The chemical diversity may be amplified for marine natural products due to the vast biodiversity encountered in marine environments [192]. Also, bioactive secondary metabolites produced by marine organisms to fight parasitic microorganisms are often very potent since they rapidly become diluted in the environment [200]. Many antimicrobial compounds with activity against *Mtb* have been isolated from marine organisms, though very few have moved beyond initial hit identification [196, 202].

In this study, a library of MNPs was screened using replicating and dormant conditions as our primary screening approaches. To our knowledge, this is the only large-scale screen of MNPs against *Mtb,* not only in replicating conditions, but also in the context of dormancy. This screen uncovered unique hits which would have been otherwise missed in a conventional *in vitro* screen. Use of the dormancy model as a primary screening approach was key to the discovery of fractions distinctively active against non-replicating *Mtb*. Rather than crude extracts, as is typical for natural product screens, this MNP library contained 4400 peak fractions purified by Medium Pressure Liquid Chromatography (MPLC) (~75% pure). The purity of the samples facilitated the deconvolution and isolation of active components. Five pure compounds were isolated from select hits, and their structures and activities were characterized. Four out of these 5

compounds were active against dormant *Mtb*, with2 puupehenone-class metabolites being highly selective for these phenotypically tolerant bacteria. Further investigation of dormant active hits could reveal novel druggable targets in dormant bacilli vulnerable to inhibition, ultimately leading to novel therapeutics able to reduce treatment time for tuberculosis.

Materials and methods

Marine Natural Product collection

The Marine Natural Products (MNP) library from the Harbour Branch Oceanographic Institute at Florida Atlantic University (HBOI) used in this study was generated by extraction of frozen specimens (either exhaustive extraction with ethanol or using an Accelerated solvent extractor (Dionex)). Extracts were analyzed by HPLC and appropriate chromatographic stationary phases were selected for large scale chromatography. The majority of the fractionations were conducted by medium pressure liquid chromatography on either an IscoTeledyne CombiFLASH Companion or CombiFLASH RF+ purification system. Some samples were fractionated using vacuum column chromatography. The library

was supplied in 96-well plates for assay. The MNP library was resuspended in 100% dimethyl-sulfoxide (DMSO) at 2 mg/mL. Working solutions were prepared at 100 µg/mL in 2.5% DMSO solution and screened at final concentrations of 20 µg/mL in 0.5% DMSO. Pure compounds were resuspended at 10 mg/mL in 100% DMSO. Refer to Supplemental methods and results for detailed description of source materials, purification, and identification of compounds.

Plasmid and Reporter strain construction

Plasmid pVVRG was constructed by utilizing a PCR-based FastCloning method[293] in which a 1084 bp hsp60-GFP cassette was inserted into pVV16 smyc:mCherry plasmid[294]. Vector primers pVV_FC_F (5'-TTCAGGCCTGGTATGAGTCAGC-3') and pVV_FC_R (5'-GCTGGATGATGGGGCGA-3') and insert primers hspGFP_FC_F (5'-GCTGGATGATGGGGCGAGGTGACCACAACGACGC-3') and hspGFP_FC_R (5'-GCTGACTCATACCAGGCCTGAACTATAGTTCATCCATGCCATGTGTAA-3') were used. The resulting pVVRG plasmid was confirmed by sequencing, and introducted into *Mtb* CDC1551 by electroporation. The transformants were selected on 7H10 plates supplemented with 10% oleic acid/albumin/dextrose/catalase (OADC) and kanamycin 50 µg/ml. The resulting

Mtb-RG expresses m-Cherry and GFP constitutively from the smyc promoter and hsp60 promoter, respectively.

Bacterial strains and growth conditions

Mtb CDC1551 derived strains containing reporter plasmids were used in this study (Table1). Screening assays were performed using fluorescent and luminescent reporter strains: i) The *Mtb*-RG strain harbors plasmid pVVRG, as described above; ii) The *Mtb*-Lux strain contains pMV306hsp+LuxG13 (a gift from Brian Robertson & Siouxsie Wiles - Addgene plasmid # 26161), which was constructed for constitutive expression of the entire *lux* operon [167] (Table 1). All strains were routinely cultured in Middlebrook 7H9 broth media supplemented with 0.05% Tween 80 and 10 % OADC. Either 50 μg/mL kanamycin or hygromycin was added for maintenance of the reporter plasmids. For experiments requiring a CFU readout, serially diluted bacteria were plated on quad plates containing Middlebrook 7H10 agar supplemented with 10% OADC and 100μg/mL cyclohexamide. For the dormancy screening assays, complete Dubos broth (Difco) medium was prepared according to manufacturer instructions including 10% Dubos-medium-albumin-supplement[61].

Table 1. Strains and Plasmids used in this study

Name	Description	Source
Plasmids		
pVV16-smyc:mcherry	episomal plasmid, mcherry driven by smyc promoter, HygR, KanR	This study
pVVRG	episomal plasmid expressing constitutively GFP and mCherry, HygR, KanR	This study
pMV306hsp+LuxG13	integration vector constitutively expressing the entre *lux* operon, KanR	Addgene plasmid #26161
Strains		
Mtb CDC1551	wild type *M. tuberculosis*	This study
*Mtb*CDC1551-RG	*M. tuberculosis* strain expressing mCherry and GFP	This Study
*Mtb*CDC1551-Lux	*M. tuberculosis* strain expressing the *lux* operon	This Study

MNP Library Screening

Overview of Screening Scheme

The HBOI MNP library containing 4400 peak fractions was initially screened in both primary screening assays (7H9 replicating and multi-stress dormancy) using the *Mtb*-RG fluorescent readout. All hit fractions from both screens were tested against mammalian cells to filter out cytotoxic fractions. Peak fractions were prioritized for deconvolution based on their activity against dormant *Mtb*, quantity of source sample available, and apparent chemical novelty of extract constituents. Bioactivity guided fractionation of select hits allowed the isolation of pure compounds. Finally, the compound structures were defined, and the activity of pure compounds was characterized using secondary *in vitro* replicating and dormancy assays (luminescent readout with*Mtb*-Lux) (Figure 4).

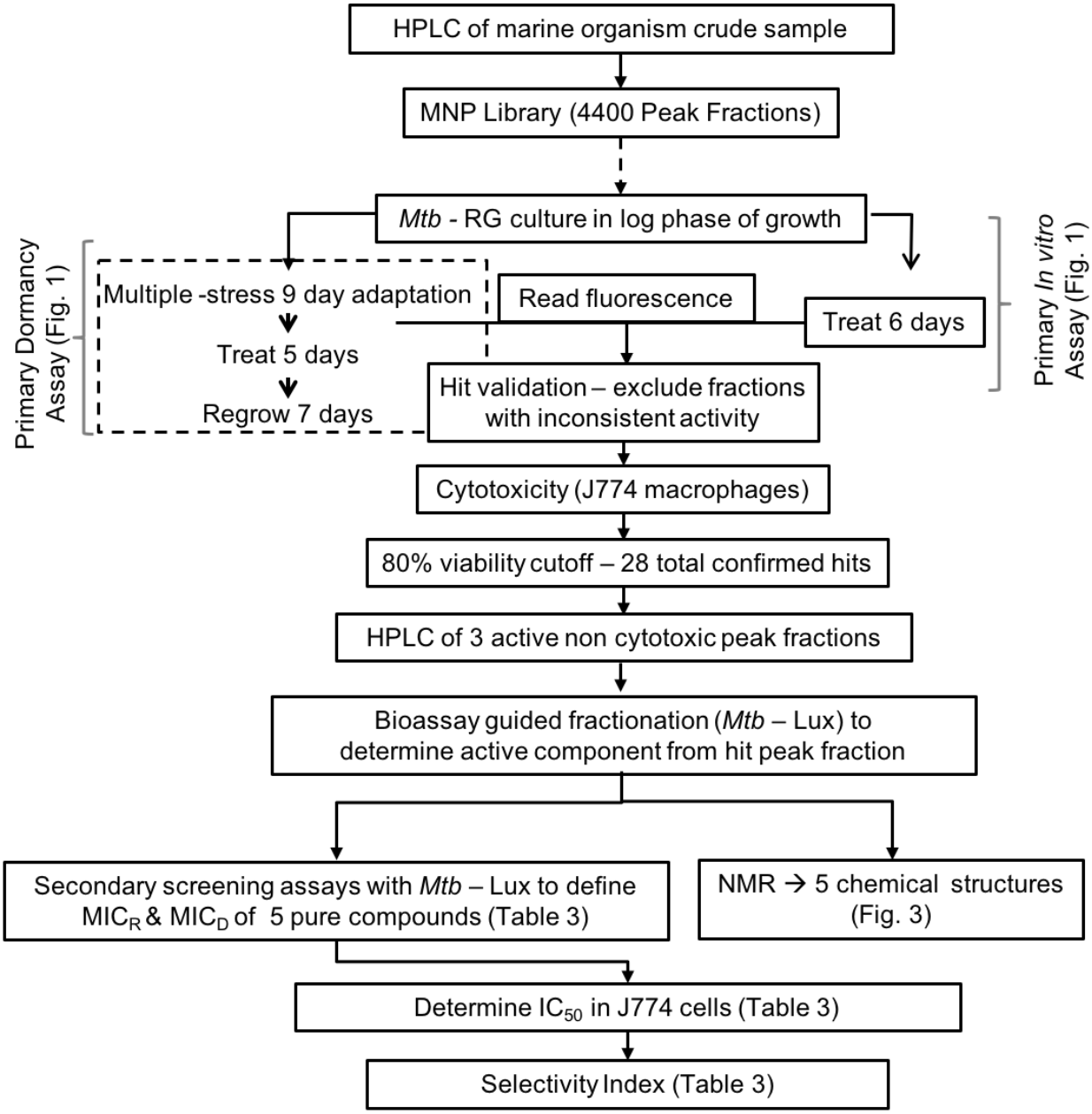

Figure 4. Schematic representation of the screening process employed in this study.
Figures and tables referred to on the work-flow contain data pertinent to that stage of the process.

Primary In vitro Screening Assay

Bacterial cultures at mid log phase were diluted in Middlebrook 7H9 OADC broth to an optical density of 0.05 at 600nm (OD_{600}). Culture and drugs were transferred to solid black 384-well plates (Corning) using a Precision robotic liquid handler (BioTeK). All 4400 peak fractions were screened at 20 μg/mL in a final volume of 30μL. GFP and mCherry fluorescence was read after a 6-day incubation at 37°C using a Synergy™ H4 plate reader (BioTek) at the wavelengths Ex480/Em528 and Ex580/Em620, respectively. Each 384-well screening plate contained three control columns: i) 0.5% DMSO; ii) 10 μM rifampicin (RIF); iii) 10 μM isoniazid (INH).

Secondary In vitro Screening Assay

Hit validation and MIC experiments were carried out using luminescence as an alternative readout. Luminescent assays with *Mtb*-Luxonly differed in the starting OD_{600} (0.01) and use of white instead of black 384-well plates.

To determine the MIC against replicating *Mtb* (MIC_R), 16-point dose response curves were carried out in triplicate using 200 μg/mL as the initial concentration in a 2-fold dilution series. The controls and serial dilutions curves were all prepared to contain a final DMSO concentration of 2%.

Primary Dormancy Screening Assay

In order to detect compounds active against dormant *Mtb* the Multi-Stress Dormancy (MSD) model was used in this study to screen the entire MNP library (4400 peak fractions) [61]. *Mtb*-RG cultures in log phase were pelleted and resuspended in MSD media (10% Complete Dubos at pH 5.0 containing 0.018% tyloxapol and no glycerol) and incubated in a hypoxia chamber (37^{o}C, 5% O_2, 10% CO_2) for nine days prior to the dormancy screening assay.

MSD adapted *Mtb*-RG were diluted in the same media to an OD_{600} of0.1 and added to 384-well plates with compounds at 20 μg/mL in 30μL final volume. Eight-point dose response curves for RIF (0.5 μM to 0.003 μM) and INH (1μM to 0.015 μM) were included in the assay as controls to confirm bacterial tolerance to front line drugs. These positive controls, as well as the 0.5% DMSO negative control, were done under both MSD and replicating conditions (Complete Dubos media, normoxic atmosphere) to compare drug susceptibilities. The plates were incubated with drugs for 5 days in the hypoxia chamber, after which 30μL of 2x 7H9 OADC buffered with 100 mM MOPS (RPI Intl.) was added for regrowth of the surviving dormant bacteria under normoxic conditions. In addition, controls were plated in duplicate on quad plates for CFU counting. Fluorescence wasread following a 7-day regrowth period using a Synergy^{TM} H4 plate reader (BioTeK). RIF and INH at 10 μM and 0.5% DMSO controls were also included in

the screening plates for Z-score calculation. Hit peak fractions were validated with a CFU readout by plating samples immediately after treatment phase.

Secondary Dormancy Assay

Mtb-Lux was used for screening of deconvoluted fractions, validation, and dose response curves. Cultures were grown and adapted in the dormancy model for 9 days as described above. Dormant cultures at OD_{600}=0.2 were treated with compounds in white 384-well plates (30 μL total volume per well). The luminescent signal was read after 2, 4 and 6 days of treatment using a Synergy™ H4 plate reader (BioTeK). MIC of compounds against dormant *Mtb* (MIC_D)was determined using the same dilution series described for the *in vitro* assay. Sixteen-point dose response curves were prepared for RIF and INH starting at 12 μM and 500 μM, respectively. These control drugs were used against dormant bacteria and replicating *Mtb*-Lux in complete Dubos media for comparison of MICs. Appropriate DMSO-free untreated controls were also included.

Cytotoxicity Counter-screening Assay

J774A.1 macrophages and HepG2 cells were cultured from a freezer stock in Dulbecco's Modified Eagle Medium (DMEM, GIBCO) supplemented with 10% heat inactivated fetal calf serum (Atlanta Biologicals), 1mM sodium pyruvate (Mediatech, Inc.), 2mM L-glutamine (Mediatech, Inc.) and 1% PenStrep (100 U/mL Penicillin, 100 μg/mL Streptomycin, GIBCO). On the day prior to performing the assay, $2.5x10^4$ cells/well were seeded in black 384-well plates in a final volume of 30 μL per well. Six hours later the compounds (20 μg/mL) and the control drugs (0.5% DMSO and 2% Triton X) were added to each well. Cell survival was determined 24 hours later based on reduction of resazurin [295].A stock solution of resazurin was prepared in water at 140 μg/mL and added to each well at a final concentration of 20 μg/mL. Fluorescence was measured following a 4-hour incubation at 37^oC by excitation at 560nm and emission at 590nm using a Synergy™ H4 plate reader (BioTeK). Fractions exhibiting greater than 20% inhibition of J774 cells were considered cytotoxic and eliminated from the study. After deconvolution of non-cytotoxic fractions, compounds isolated with lower than 20% cytotoxicity against J774 cells were used for dose response curves. To determine the IC_{50} of pure compounds, 12-point dose response curves were prepared starting at 200 μg/mL. Untreated controls for these experiments were all prepared using a final 2% DMSO solution.

Data Analysis

Z-factors and percent inhibition were calculated using the respective formulas. The letter “X” is the drug sample value; µp and µn are the averages of positive (10 □ MRIF) and negative (0.5% DMSO) controls; σp and σn are standard deviations of the same controls.

$$Z' = 1 - 3\left(\frac{\sigma p + \sigma n}{|\mu p - \mu n|}\right) \text{ AND } \%\text{Inhibition} = \left(\left(\frac{\mu n - X}{\mu n}\right) \times 100\right) \div \frac{\mu p}{100}$$

The dose response curves were analyzedusing normalized data considering the highest and lowest output values in the curve to be 100% and 0% growth respectively.A Gompertz model, and a nonlinear regression - normalized response curve fit, were used to determine MIC and IC_{50} respectively in GraphPad Prism 5 [296], considering MIC as 99% killing. The selectivity Index (SI) was calculated as IC_{50}/MIC.

Statistical analysis of the CFU results obtained for the pure compounds and control drugs was also done using GraphPad Prism 5. One-way ANOVA and Tukey’s multiple comparisons post-test were performed to compare treatment groups between each other and to respective untreated controls. Differences were considered significant when $p<0.05$.

All the data from hit validation and characterization of pure compounds is averaged from at least 2 independent experiments with SEM shown on the figures.

Results

Purification and identification of compounds

Fistularin-3 (1) and 15-methyl-9(Z)-hexadecenoic acid (2)

Biological material

Compounds **1** and **2** were isolated from a sponge identified as belonging to the Family Aplysinidae. (HBOI ID; 20-V-00-3-008) [Phylum Porifera, Class Demospongiae, Order Verongiida]. The specimen was collected at a depth of 73 m using the Johnson Sea-Link II manned submersible in Curacao off the South Coast near Boka Santa Maria [latitude 12.250225 N, longitude, 69.1500 W]. The specimen consists of two thick tubes, with epibionts over part of the surface. It has a central opening at the top of each tube. The sponge was orange alive, but turned blue-black upon exposure to air. The ethanol-preserved specimen is massive, dense, and black. The surface is microconulose, with no pits or polygonal depressions on the fragment studied. The skeleton has a sparse, dendritic fiber skeleton of thick and deformed amber fibers (250-300 um thick). The inner core of the fibers measures 100-125 um (approximately 50 %

of the fiber diameter). The skeletal organization matches *Aiolochroia* sp. with a predominant dendritic skeleton of coarse thick deformed pithed fibers, however, there are not yet any described species of *Aiolochroia* that are tubular. There is only one species, *Aiolochroia crassa*, described from shallow coral reefs; there are two species from shallow water currently being described, but these are not at all like the present specimen (M.C. Diaz, personal communication). There is a newly described *Aplysina* species from the Eastern Pacific that has a dendritic skeleton towards the surface and a mesh skeleton towards the center of the body which is like the sample in this study but full details have not yet been published. Based upon the observed differences, this specimen can only be defined at the family level, Aplysinidae [297]A voucher specimen is available for study upon contacting author AEW.

Isolation and Structure Elucidation

The sample was frozen immediately after collection and stored at -20°C until extraction. The original active peak library fraction (047.F07) was obtained by MPLC in a manner like the protocol that follows. Because < 4 mg of the fraction was available for study, additional frozen sponge was extracted and the separation repeated. The method used to obtain pure **1** and **2** is as follows: 200 g of the frozen specimen was extracted exhaustively by grinding the sample in ethanol using a blender. The extract was filtered and the tissue returned to the blender and extracted again. After concentration by

distillation under reduced pressure the dried extract was partitioned between *n*-butanol and water. The n-butanol phase was concentrated by distillation under reduced pressure to yield 3.4 g of dried residue. 0.99 g of this partition was chromatographed using a Teledyne Isco Combiflash Rf_{x4} flash chromatography system. The material was adsorbed onto approximately 1 g of C-18 bonded silica gel, dried and then placed into a loading column. The chromatography column used was a 30 g C18 Redisep Gold column. The flow rate was 35 ml/min. Solvent A: 100% water; Solvent B: CH_3CN; Solvent C: CH_3OH; Solvent D: CH_2Cl_2. The run lasted 23.9 minutes and 32.4 column volumes. The gradient was as follows: t=0 min. A:B 90:10 v/v; t= 3 min. A:B 90:10 v/v; t= 15 100% B; t=23.9 minutes 100% B. The *in vitro* active fraction eluted between 12 and 14 minutes as a large peak observed by UV at 225 nm. The dormancy active fraction eluted at 16-17 minutes and had very limited UV absorbance. The *in vitro* active fraction was further chromatographed by preparative HPLC on a Vydac C-18 Protein and Peptide column 22 x 150 mm 10 u particle size eluted with a linear gradient. Solvent A: H_2O:CH_3CN (95:5 v/v); Solvent B: CH_3CN; t=0 min A:B (90:10 v/v), t=15 min. 100% B, t=24 min. 100% B. The flow rate was 15 ml/min and detection used both Photodiode array (PDA) and MS with Electrospray ionization (ESI). The *in vitro* active compound **1** eluted at 11.1 minutes and showed mass peaks in negative ion mode consistent with multiple bromines at m/z 1109, 1111, 1113, 1115 and 1117. The dormancy active fraction was further chromatographed by preparative HPLC on a Vydac C-18 Protein and Peptide column 22 x 150 mm 10 µ particle size eluted with a linear gradient Solvent A: H_2O:CH_3CN (95:5 v/v); Solvent B: CH_3CN; t=0 min A:B (75:25 v/v), t=10 min. 100% B t=24 min. 100% B. The flow rate was 15 ml/min and detection

used both Photodiode array (PDA) and MS with Electrospray ionization (ESI). The active compound **2** eluted at 13.4 minutes and by negative ion MS detection had an apparent [M-H] of *m/z* 267.

Structure identification

Mass spectrometry and NMR data sets (^{1}H, ^{13}C, 2D-COSY, edited HSQC and 2D-HMBC) were collected and assigned to confirm the identity of both compounds. Compound **1** had NMR data corresponding to that reported for mixtures of fistularin-3 and 11-epifistularin-3 [298]. These have been reported to co-occur as inseparable mixtures in some collections of *Aplysina* sp. Compound **2** was identified as 15-methyl-9(Z)-hexadecenoic acid[299]. A series of 1D-dpfgse TOCSY experiments strongly suggested the placement of the double bond between C-9 and C-10. This was confirmed through degradative studies with osmium tetraoxide to yield 9-oxo-nonanoic acid methyl ester after cleavage of the double bond and oxidation to the aldehyde. ^{1}H NMR of **2** (methanol-d_4): 2.28 (bt (*J*=6.8) 2H, H_2-2), 2.01 (bq (*J*= 6.9) 4H, H_2-8, H_2-11), 1.57 (bp (*J*=6.9) 2H, H_2-3) 1.50 (septet (*J*=6.9) H-15), 1.31 (2H, H_2-4), 1.30 (4H, H_2-7, H_2-12).1.28 (2H, H_2-13), 1.29 (4H, H_2-5, H_2-6) 1.16 (2H H_2-14), 0.87 (d *J*=6.9, 6H, CH_3-16, CH_3-17). ^{13}C NMR (methanol-d4): 176.8 (C-1), 129.8 (2C, C-9, C-10), 39.1 (C-14), 34.0 (C-2), 30.1 (C-13), 29.8, 29.32, 29.28, 29.19, 29.4 (C-4, C-5, C-6, C-7, C-12), 28.2 C-15, 27.2 (C-8 and C-11), 25.6, (C-3), 21.8 (C-16 and C-17).

Degradation study to define the position of the cis olefin in **2**

The fatty acid **2** (1.5 mg) was treated with 1 mL 0.5N methanolic HCl for 5 hours at 50°C. The resulting methyl ester was purified by partitioning between ethyl acetate and water. HBOI.062.A11 methyl ester was dissolved in acetone then 2,6-lutidine (2.0 equiv), 4-methylmorpholine *N*-oxime (1.5 equiv), and 2% osmium tetroxide in water (0.02 equiv) were added along with additional water for a final 10:1 acetone:water concentration. The reaction was monitored by thin layer chromatography (silica gel, EtOAc:CH_3OH(19:1 v/v), detected by spraying with 1% vanillin in sulfuric acid and heating). After 2 hours the starting material **2**had been consumed. Next, Phenyliodonium Diacetate (PhI(OAc)2) (1.5 equiv) was added. After stirring for 2 hours, the reaction was quenched with saturated aqueous sodium sulfite (5 mL). The reaction products were extracted with CH_2Cl_2(3 X 5 mL), washed with saturated aqueous copper sulfate (2 X 10 mL), and concentrated under a stream of nitrogen. The product was analyzed by direct infusion mass spectrometry and ^{1}H NMR. The major ion observed for the product was observed at *m/z* 187.0 which is the predicted [$M+H^+$] for the 9-oxo-nonanoic acid methyl ester, the predicted product of the degradation reaction

3-(hexadecyloxy)propane,1,2-diol (3)

Biological Material

Compound **3** was isolated from a specimen of the soft coral *Pterogorgiacitrina* (HBOI ID 12-VI-85-1-002) [Phylum-Cnidaria, Class-Anthozoa, Order- Alcyonacea Family-Gorgoniidae]. The specimen was collected at a depth of 19.8 m by scuba off Rum Cay in the Bahamas [Latitude 23.6166 N Longitude, 74.80014 W]. A voucher specimen is available for study upon contacting author AEW.

Isolation and Structure Elucidation

The sample was frozen immediately after collection and stored at -20°C until extraction. 132 g of the soft coral was freeze-dried and then ground and extracted sequentially using a Dionex Accelerated Solvent Extractor in 3 steps (Step 1: heptane; Step 2: EtOH: EtOAc (5:1 v/v) and Step 3: CH_3OH:H_2O (5:1 v/v)) at 100 °C with 3 static cycles per step. 761 mg of the heptane extract was separated using an Isco Combiflash™ Companion. The material was adsorbed onto Celite and solvent removed for solid sample loading. A 12 g NP Rf Gold silica column was used for the separation. The

column was eluted with gradient elution as follows: Solvent A: heptane, Solvent B: EtOAc, Solvent C: CH_3OH; t=0 minutes 100% A, t= 20 minutes 100% B, t=23 minutes 100% B, t=30 minutes 100% C. The pressure was maintained at 200 psi over the course of the elution. A fraction eluting at 12 minutes (18 mg) was found to be selectively active against the dormant form of *Mtb*. NMR and MS analysis indicated that it was substantially pure. Its structure was defined by interpretation of the MS, 1D and 2D NMR data and was confirmed to be 3-(hexadecyloxy) propane-1,2 diol, **3**, by NMR and MS. ^{1}H NMR (methanol-d_4): 3.72 pentet (*J*=4.8 H-2), 3.54 dd (*J*=11.3, 4.8, H3a), 3.48 dd (*J*=11.3, 4.8, H3b), 3.45 m (H-1a), 3.44 2H t (*J*=6.9 H-4ab), 3.38 dd (*J*=10, 5.5 H-1b), 1.55 pentet (*J*=5.5 H_2-5), 1.38 m (H2-19), 1.33 m (H_2-6), 1.29 bs H_2-7to H_2-), 1.26 (H_2-20), 0.87 t (*J*=6.9, H_3-21). ^{13}C NMR (Methanol-d_4): 72.2 (CH_2 C-1), 71.6 (CH_2 C-4), 71.3 (CH_2 C-2), 63.6 (CH_2 C-3), 32.1 (CH_2 C-19), 29.8 (CH_2 C 7 to 17), 29.6 (CH_2 C-5), 29.5 (CH_2 C-18), 26.2 (CH_2 C-6), 22.8 (CH_2 C-20), 13.5 (CH_3 C-21).

15-α-methoxy-puupehediol (4), puupehedione (5)

Biological Material

Compounds **4** and **5** were isolated from a sponge identified as *Petrosia* (*Strongylophora*) n. sp. (HBOI ID; 6-IV-05-1-004) [Phylum Porifera, Class

Demospongiae, Order Haplosclerida, Family Petrosiidae]. It was collected at a depth of 176 m using the Johnson Sea-Link I manned submersible in the Bahamas off Ocean Cay, South of Bimini Island, [latitude 25.400005 N, longitude, 79.23378 W]. The specimen is vase- to mound-shaped, pinkish to yellowish in color. It has a smooth surface, is compressible and partially hollow inside, with growth layers evident when the specimen is cut transversely. It does not have a dense choanosome. It has 3 to 4 size classes of strongyle oxeas and a few small fusiform micro-oxea. There are five species of *Petrosia* (formerly *Strongylophora*) described for the Caribbean. Two shallow species: *P. (S) dendyi* from Barbados having a thin crust 2-3 mm thick [300], and *P. (S) davilai*from Cuba described as lobate, with 1 cm wide oscules (Hechtel 1969). There are two mesophotic and deep-water species from Barbados: *P.* (*S.*) *hartmani*[301]is globose in shape and stony hard in consistency, and *Petrosia stoneae*[302]is pear- to globe-shaped and stony in consistency. The final species *P.(S) devoogdae*is from deep-water Guyana [303], and is described as massive, bread crumbly in appearance, but of very different spiculation consisting mostly of fusiform oxeas in size classes, and a unique complement of microtoxa in several size classes. The present specimen is vase to mound-shaped, with ectosome layers that are unique for this species. The spicule morphology is closest to *P. (S) davilai,* with predominantly several size classes of strongyles, and a small category of fusiform micro-oxeas. The specimen studied in this work is very distinct from the other known species from the Caribbean. The specimen in this study is likely an undescribed species of *Petrosia* (*Strongylophora*) [304]. A voucher specimen is available for study upon contacting author AEW.

Isolation and Structure Elucidation

The sample was frozen immediately after collection and stored at -20C until extraction. 144 g of the specimen was extracted exhaustively by grinding the sample in ethyl acetate:ethanol (9:1 v/v) using a blender. The extract was filtered and the tissue returned to the blender and extracted with 100% ethanol and then after filtration again with 100% methanol. The extracts were combined and concentrated by distillation under reduced pressure. The dried extract was partitioned between *n*-butanol and water. 2.35 g of the organic partition was obtained after concentration by distillation under reduced pressure. A portion of the organic partition (404 mg) was chromatographed using a Teledyne Isco Combi*FLASH*™ Rf_{x4} flash chromatography system. The material was adsorbed onto approximately 1 g of C-18 bonded silica gel, dried and then placed into a loading column. The chromatography column used was a 15.5 g C18 Redisep Gold column. The flow rate was 30 ml/min. Solvent A: 100% water; Solvent B: CH_3CN; Solvent C: CH_3OH, Solvent D: CH_2Cl_2. The run lasted 15.9 minutes and 37 column volumes (CV). Gradient elution was used as follows: t=0 min. A:B 90:10 (v/v); hold for 3 CV at A:B 90:10 (v/v); linear gradient ending at 100% B at 22 CV; hold for 3 column volumes at 100% B; linear gradient to 100% C over the next 3 CV; hold at 100% C for 1 column volume; then linear gradient to 100% D over the next 7 CV. Elution was monitored by UV at 225 nM. The fraction containing puupehedione eluted as a large peak between 21 and 23 CVs (Fraction 5). The fraction containing 15-α-methoxy-puupehediol eluted as a large peak between 24 and 25 CVs (Fraction 6). 7.5 mg of

fraction 5 was further separated by preparative HPLC on a Vydac 218TP C-18 Protein and Peptide column (22mm x 150mm, 10 μ) eluted with gradient elution as follows: Solvent A: H_2O:CH_3CN 95:5 (v/v); Solvent B: CH_3CN; flow=15 ml/minute; t=0 minutes A:B 80:20 (v/v); t=10 minutes A:B 60:40 (v/v); t=16 minutes 100% B; t= 24 minutes 100% B. **5** was detected by uv at λ = 230 nm, R_t = 15.5 minutes yielding a total of 3.7 mg of 80% pure **5.** This material was further fractionated by semi-preparative HPLC (Vydac C-18 Protein and Peptide column, 10mm x 250mm) isocratic elution H_2O/CH_3CN (1:3 v/v), flow = 3 mL/min, detected by UV at λ = 230 nm, R_t = 12.5 min. A total of 1.5 mg of compound **5** (puupehedione, calculated yield is 4 x 10^{-2}% of wet weight) was obtained. 3.5 mg of fraction 6 was further purified by semi-preparative HPLC (Vydac C-18 Protein and Peptide column, 10mm x 250mm), isocratic elution H_2O/CH_3CN (1:4 v/v), flow = 3 mL/min, detected by UV at λ = 230 nm, R_t = 10.0 min. A total of 2.5 mg of **4** (15-α-methoxy-puupehediol, calculated yield is 2 x 10^{-1} % of wet weight of sponge) was obtained.Full NMR data sets (^1H, ^{13}C, 2D-COSY, edited HSQC and 2D-HMBC were collected and assigned to confirm the identity of both compounds. Comparison to the published data showed close agreement and further confirmed their identity [305, 306].

Screening MNP Against *Mtb.*

Replicating *Mtb*

The HBOI MNP library containing 4400 peak fractions was screened at 20 μg/mL in a dual-fluorescent whole cell assay for inhibition of growth of replicating *Mtb*. Initially, 114 peak fractions were deemed active based on an arbitrary threshold of 50% inhibition relative to 10 μM RIF. The close correlation between the mCherry and GFP readoutsruled out the possibility of false positives due to quenching of reporter protein fluorescence. The average Z scores and signal to background ratio among all the plates were 0.82 and 63, respectively, emphasizing the robustness of the assay. During validation of hits by repeating the primary assay, 52 hits of the initial 114 which were near the 50% cutoff had inconsistent results and therefore were not further characterized in this study. The 62 remaining *in vitro* hits were tested for cytotoxicity against J774 macrophages at screening concentration (20 μg/mL), and 26 fractions were non-cytotoxic (< 20% cytotoxic relative to DMSO controls) (Table 2 and Fig. 5).

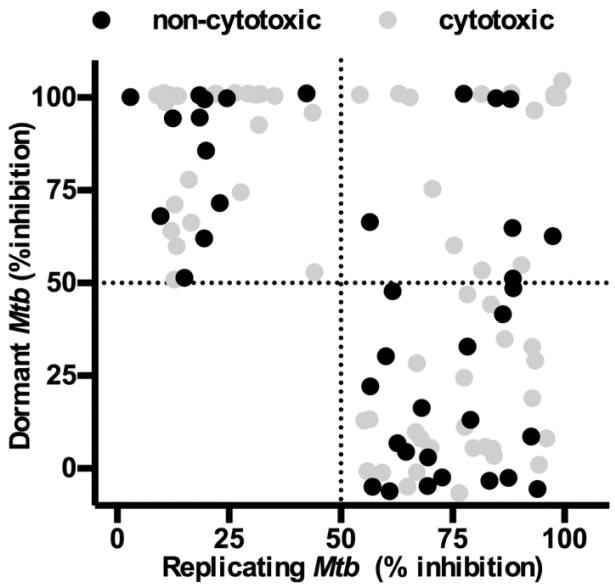

Figure 5. **Activity of peak fractions against dormant and active Mtb-RG.**
The activity of peak fractions screened at 20 μg/mL are shown. One hundred percent inhibition is defined as the inhibition observed in the presence of 12 μg/mL rifampicin. Peak fractions were considered cytotoxic when they resulted in >20% killing of J774 macrophages.

Table 2. Primary Screening Assay Results

	Z Score	S/B	Total Hits/4400	Hit Rate (%)	Non-cytotoxic hits
Primary *In vitro* Assay	0.82	63	95	2.1	26
Primary Dormancy Assay	0.81	23	35	0.77	19
Dual Active	N/A	N/A	19	0.42	7

S/B – signal to background ratio
N/A – not applicable

Dormant *Mtb*

In the primary dormancy screen, average Z scores and signal to background ratios were 0.81 and 23, respectively. Fifty-four fractions had activity above the defined threshold, 35% of which were also active against replicating *Mtb.* Further testing of dormancy active hits revealed that 19 out of 54 hit fractions were non-cytotoxic(<20% toxicity to J774), 7 of which were also active against replicating *Mtb* (Figure 5 and Table 2). All the non-cytotoxic dormancy hits (19 peak fractions) were validated by CFU without a regrowth stage in 3 independent experiments (Figure 6). Approximately 50% of the hits had activity below the threshold by CFU; these included fractions that had shown potent activity with the fluorescent readout (data not shown). This data indicated that fractions which only inhibited replicating *Mtb* were also being detected in the primary dormancy assay. The reason for this outcome could be inhibition of replicating bacilli during the regrowth stage due to carry-over drug in the wells. Furthermore, MICs for control drugs obtained with the fluorescent regrowth assay were similar between replicating and dormant *Mtb* (RIF MIC_D 0.2 μM and MIC_R 0.5 μM; INH MIC_D 0.2 μM and MIC_R 0.2 μM) (Figure 7A and B). In contrast, complete killing of dormant bacteria was not observed by CFU enumerationat any concentration of RIF or INH (Figure 7C and D). Thus, the fluorescent regrowth results significantly under-represented the tolerant phenotype observed for dormant *Mtb* in this study. To minimize this, an alternative assay was optimized for characterization of dormancy active hits which did not require a regrowth step.

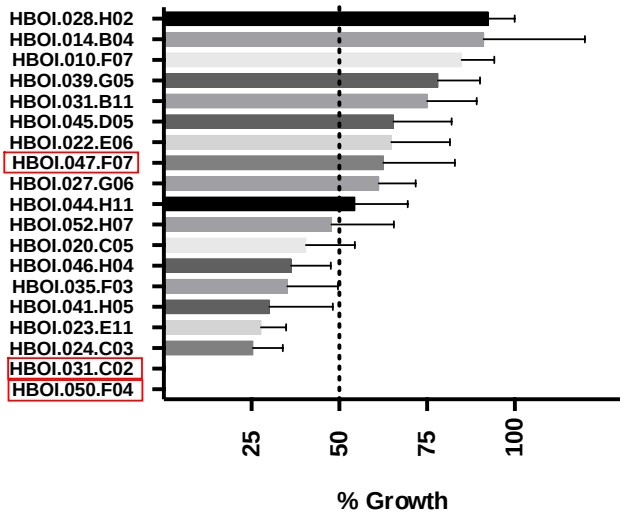

Figure 6. Validation of dormant-active peak fractions against dormant Mtb by CFU.
Cultures were adapted for 9 days in multiple-stress conditions and treated for 5 days with peak fractions at 20 μg/mL. After treatment samples were taken from each well, diluted in PBS + 0.05% Tween80 and plated on 7H10. Plates were incubated for 3 weeks at 37^{o}C for CFU counting. Dashed vertical line indicates the 50% cutoff used to call hits in the primary screens. Red boxes identify peak fractions deconvoluted in this study for the isolation of pure compounds.

Use of *Mtb*-Lux in the Dormancy Assay Eliminates the Need for aRegrowth Stage.

The secondary dormancy method was developed based on loss of luminescent signal. Dormant and replicating *Mtb*-Lux cultures were diluted to OD_{600} 0.2 and treated for 3 defined time-points (2, 4 and 6 days) before the luminescence was read. The 2-day time point was used for all further experiments since optimum signal/background ratio was observed at that time (data not shown). The MIC of INH against dormant *Mtb*-Lux (MIC_D-285μM) was >500-fold higher than replicating *Mtb*-Lux (MIC_R-0.3μM); similarly, a

>100-fold difference was shown for RIF (MIC_D-4μM; MIC_R-0.02 μM) (Figure 7E and F). Eliminating the regrowth stage by using luciferase shortened the assay by 10 days. Moreover, luminescent data closely reflected the highly drug-tolerant nature of bacteria in our dormancy model (Figure 8).

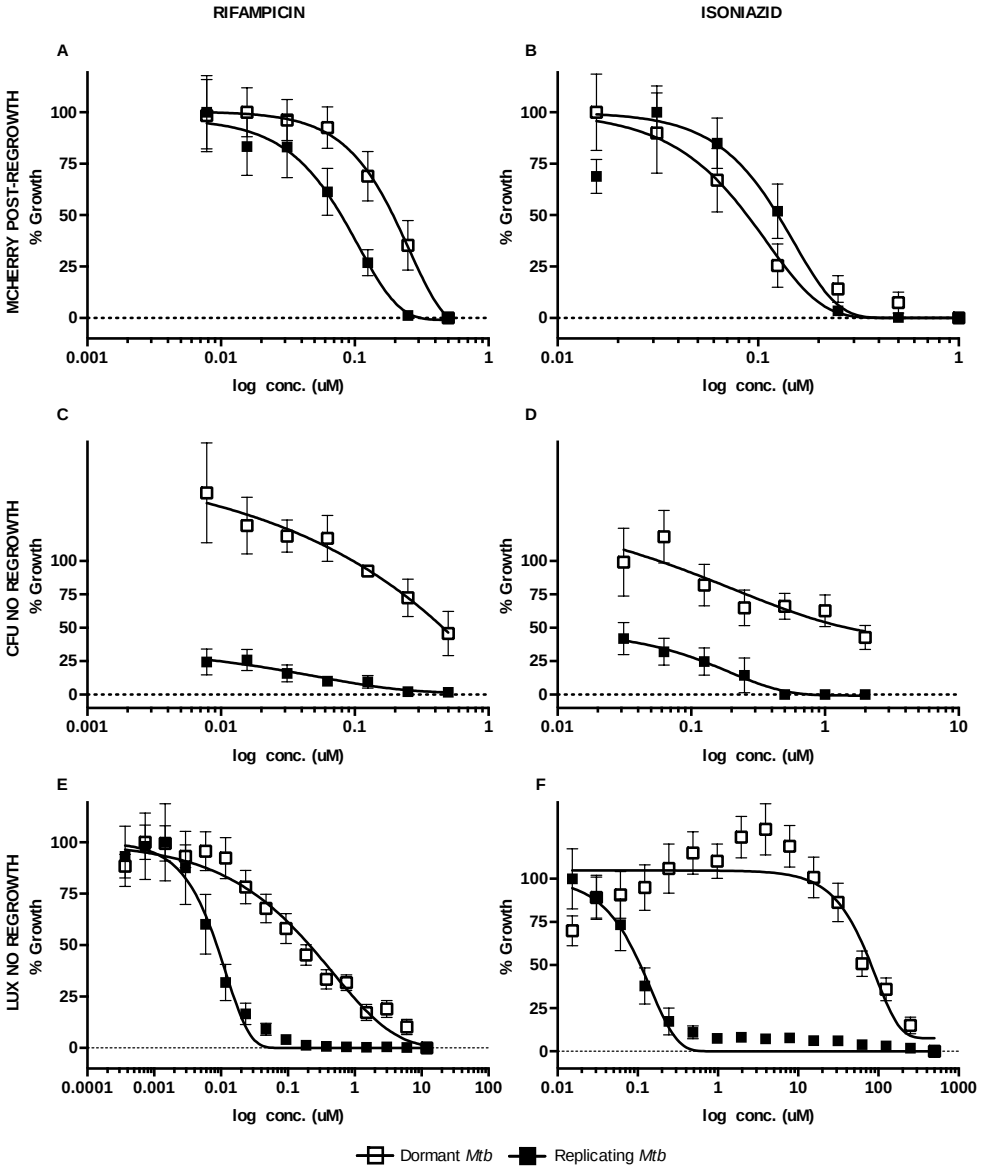

Figure 7. Optimization of MSD model screening assay.
All panels show dose-response curves for positive control drugs RIF (A,C,E) and INH (B,D, F) against replicating and dormant *Mtb* using three distinct screening assays and

readouts. **Panel A-B)** Dual Fluorescent assay - *Mtb*-RG cultureswere treated with serial dilutions of RIF and INHfor 5 days. Then,1 volume of buffered 2x 7H9 was added to each well, surviving bacilli allowed to regrow for 7 days in normoxic conditions before fluorescence was read. **Panel C-D)** CFU assay - *Mtb*-RG(replicating and dormant) was treated for 5 days with RIF and INH before serial dilution and plating for CFU counting. **Panel E-F)** Luminescent assay – *Mtb*-Lux (replicating and dormant) was treated for 2 days with RIF and INHafter which luminescence was read. Note, there is no regrowth stage for CFU and luminescence assays (Panel C-F). Open squares – dormant culture; closed squares – replicating culture in complete Dubos media.

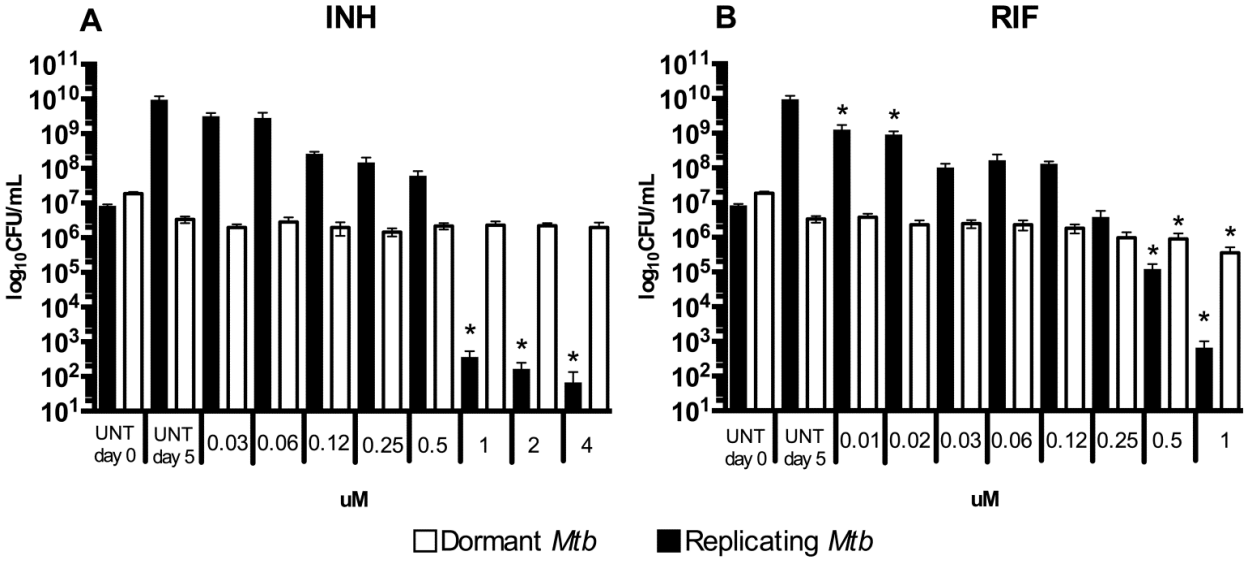

Figure 8. Validation of Mtb-lux dormancy assay by CFU.
Cultures were adapted for 9 days in multiple-stress conditions and treated for 5 days with peak fractions at 20 μg/mL. After treatment, samples were taken from each well, diluted in PBS + 0.05% Tween80 and plated on 7H10. Plates were incubated for 3 weeks at 37°C for CFU counting. Dormant (open bars) and replicating (closed bars) *Mtb*-Lux were treated for 5 days with 8 concentrations of INH (A) and RIF (B). UNT day 0 – untreated culture plated at the beginning of the assay; UNT day 5 – untreated culture plated after 5 days incubation under the same conditions as treated cultures. One-way ANOVA was used to compare treated samples with controls, and samples were considered different when p>0.05. Statistically significant differences are indicated with an asterisk. For dormant *Mtb*-Lux, the UNT day 5 control was considered a fairer comparison to treated samples since a >1logdrop was observed in CFU/mL from UNT day 0 to day 5. However, the replicating *Mtb*-Lux were compared to UNT day 0 considering those bacteria were actively growing over the 5 days of incubation, as seen in the figure.

Characterization of Pure Compound Activity

Bioactivity guided fractionation of primary hits and characterization of pure compound activities were carried out using the luminescent assay described above. Three peak fractions (047.F07, 031.C02, 050.F04), from different marine organisms,out of the 26 hits obtained were investigated, and 5 active compounds were isolated from these samples. Compound structures are shown in Figure 9, and their biological activity profiles in Table 3 as well as Figures 10 and 11.

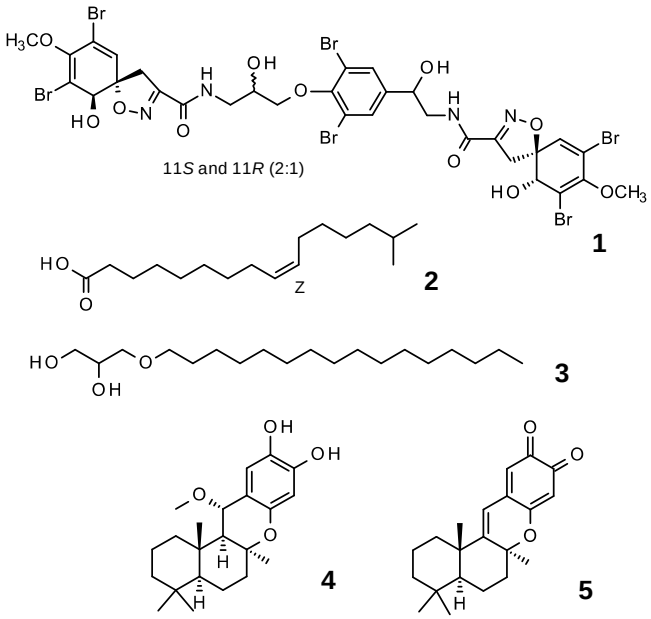

Figure 9. The structures of active molecules as defined by NMR.
Hit peak fractions had to undergo at least 2 rounds of HPLC to isolate pure active compounds.**1)** Fistularin 3/11-Epi-fistularin 3; **2)**15-Methyl-9(*Z*)-hexadecenoic acid; **3)** 3 (Hexadecyloxy)propane,1,2-diol; **4)** 15-α-Methoxypuupehenol; **5)** Puupehedione

The peak fraction (047.F07) isolated from a sponge in the Family Aplysinidae inhibited replicating *Mtb*-RGand moderately inhibited dormant *Mtb*-RG in the primary screens. The original active fraction was small and therefore additional organism was extracted and chromatographed to yield a series of 20 fractions which were tested against dormant and replicating *Mtb*-Lux to determine the active compound(s). Out of the 20 sub-fractions obtained, sub-fraction 047.F07-B8 had potent activity against replicating *Mtb*. Compound **1** was purified from this sub-fraction and was inactive against dormant *Mtb*-Lux, which is consistent with previous results obtained for the 047.F07-B8 sub-fraction (data not shown). The MIC_R (8.5 μg/mL) of **1** was determined by luminescent assays described above (Table 3 and Figure 10). The structure of **1**(determined by NMR)was found to bean inseparable mixture of fistularin 3 and 11-epi fistularin 3 [307] (Figure 9). Since antitumor activity of fistularin 3 had been previously reported [308], we tested it's cytotoxicity against HepG2 in addition to J774 cells and the IC_{50}were >200 μg/mL . Another sub-fraction (047.F07-B10) from the same Aplysinidae-derived peak fraction (047.F07) maintained potent inhibitory activity against dormant *Mtb*-Lux by luminescence and CFU readouts at 20 μg/mL (data not shown). Moreover, this sub-fraction was less inhibitory against replicating*Mtb.* The dormant-active sub-fraction was a mixture of lipids and required two rounds of preparative HPLC before defining the structure of the major bioactive component as 15-methyl-9(*Z*)-hexadecenoic acid (compound **2**, see supplemental for details) (Figure 9) [299]. The MIC_R and MIC_D for this compound were 60.8 μg/mL and 22.5μg/mL, respectively. Cytotoxicity against J774 macrophages was not observed at the highest concentration tested (200 μg/mL) yielding a SI>8.5, relative to its MIC_D(Table 3 and Figure 11A).

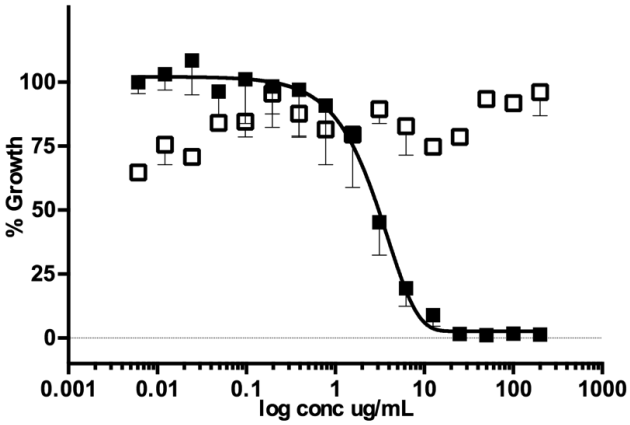

Figure 10. Dose dependent activity of Compound 1 against replicating but not dormant Mtb.
Cultures grown in either 7H9 or adapted in multi-stress conditions. Replicating*Mtb*-Lux were treated for 5 days and dormant *Mtb*-Lux for 2 days with 16 point serial dilution of compound **1** after which the luminescence was read. The drug concentrations ranged from 200 μg/mL to 0.006 μg/mL.

Peak fraction 031.C02, isolated fromthe soft coral *Pterogorgia citrina,*was active against dormant *Mtb*-RGin the primary screen and had low activity against growing bacteria. Further investigation of this peak fraction suggested it contained a single compound identified as 3-(hexadecyloxy)propane,1,2-diol(compound **3)** (Figure 9) [309, 310]. This compound was tested in the secondary luminescent assays. The MIC_R and MIC_D of **3** were 28.5 μg/mL and 7.9μg/mL, respectively, with a SI (SI_D = IC_{50}/MIC_D) of at least 31 (Table 3 and Figure 11B). Moreover, the activity of commercially acquired **3** correlated with that of the marine-derived nature product (data not shown)**.**

The *Petrosia* (*Strongylophora) sp.*-derived peak fraction (050.F04) potently inhibited dormant *Mtb*-RG in the primary screen as well as by CFU (Figure 6). Further deconvolution yielded 11 sub-fractions, 5 which maintained activity against dormant

Mtb-Lux. Further analysis of these sub-fractions suggested they contained mixtures of related hydroquinone-like structures. Compounds **4** and **5**, isolated from 050.F04, were identified as 15-α-methoxypuupehenol and puupehedione, respectively (see supplemental for details) (Figure 9) [306, 311]. We have demonstrated their potent and selective activity against dormant *Mtb* using the described luminescent assay. Table 3 and Figure 11C show that the MIC_D of **4** (0.5 μg/mL)is 21-fold lower than its MIC_R (11.3 μg/mL). Even though the SI of this compound was low when comparing IC_{50} to MIC_R, the SI was 15 in comparison to MIC_D,which highlights its potential as a scaffold targeting dormant *Mtb*. Interestingly, **5** maintained the dormant selectivity, however it was less potent in all the assays including cytotoxicity (Table 3 and Figure 11D). Compounds **4** and **5** are very similar butdiffer in the oxidation state of the ortho quinol ring and in the addition of methanol across the C-11 - C-15 double bond found in **5**(Figure 9). Thisresults in a less planar molecule than others in the puupehenone class of terpene quinones and may contribute to its activity against the dormant form of *Mtb* versus others in the class.

Table 3. Activity profile of MNP-derived pure compounds

Compound	Formula	MW	MIC_R	MIC_D	MIC_R/MIC_D	IC_{50}	SI_R	SI_D	Source
1	$C_{31}H_{30}Br_6N_4O_{11}$	1114.02	8.5	inactive	n/a	>200	>23.5	n/a	HBOI.047.F07
2	$C_{19}H_{40}O_3$	316.53	60.8	22.5	2.7	>200	>3.3	*8.5	HBOI.047.F07
3	$C_{16}H_{30}O_2$	254.41	28.5	7.9	3.6	>200	>7.0	*31.1	HBOI.031.C02
4	$C_{22}H_{32}O_4$	360.49	11.3	0.5	21.8	8	0.7	15.5	HBOI.050.F04
5	$C_{21}H_{26}O_3$	326.44	87.6	15.4	5.6	50.4	0.6	6.2	HBOI.050.F04

** MIC and IC_{50} values are in μg/mL

MIC_R – MIC against replicating *Mtb*-lux

MIC_D – MIC against dormant *Mtb*-

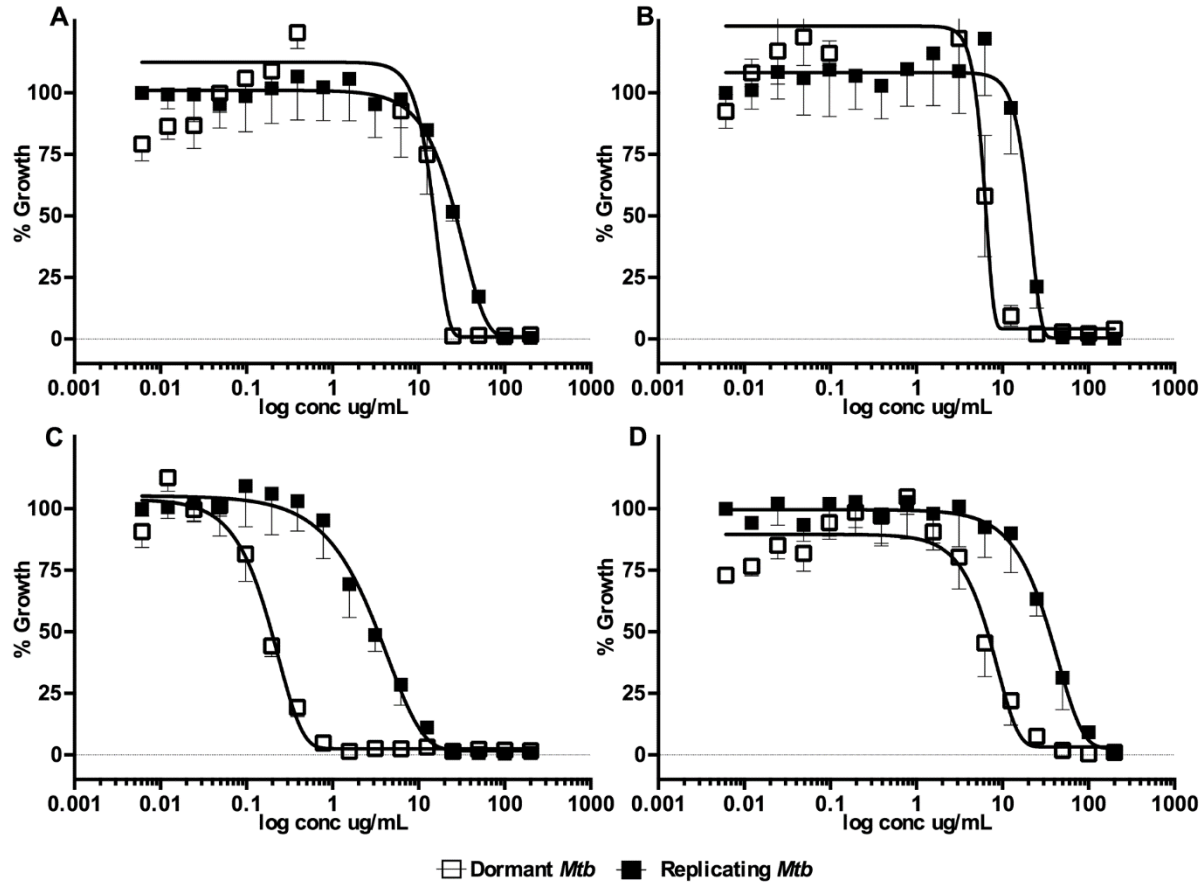

Figure 11. Dose dependent activity of select pure MNP compounds against dormant and replicating Mtb-Lux.
Cultures adapted in multiple-stress conditions for 9 days or grown in 7H9 were used in the 16-point dose response curves (200 μg/mL to 0.006 μg/mL). Dormant (open squares) and replicating (closed squares) *Mtb*-Lux were treated for 2 days with compounds **2** (A), **3** (B), **4** (C) and **5** (D) after which the luminescence was read.

Pure Compounds Show Bactericidal Activity Against *Mtb*

To investigate the mode of action of each compound, samples were taken from duplicate wells in the luminescent assays after 5 days of treatment and plated on 7H10 OADC. Four concentrations were chosen for plating (50, 12.5, 3.1 and 0.8 μg/mL) covering a broad portion of the 16-point dose-response curves. Untreated controls were plated on day 0 (inoculum) and after 5 days of incubation. A decrease in CFU/mL (<1 log) was observed after 5 days for the untreated dormant *Mtb*-Lux. Therefore, the day 5 untreated control was considered a fairer comparison with treated dormant samples. However, replicating treated bacteria were compared to day 0 controls. These data are shown in Figure 13. Compound **1** was inactive in the primary dormancy assay and showed no activity by CFU in this assay. Furthermore, it was bacteriostatic against replicating *Mtb*-Luxat all four concentrations tested (Figure 12). As expected, **2** was bactericidal against dormant but not replicating *Mtb*-Lux at 50 μg/mL (>2-fold MIC_D) given that no colonies were recovered for dormant samples treated at this concentration (Figure 13A). Though complete killing was not observed for dormant bacteria treated with **3**, a 5-log decrease in CFU/mL relative to untreated controls was noticed for dormant *Mtb*-Lux at 50 and 12 μg/mL (8 and 2-fold MIC_D, respectively). Compound **3** showed only a moderate bactericidal activity (2-log less than untreated control) against replicating *Mtb*-Luxat 50 μg/mL (Figure 13B). No colonies were recovered from dormant *Mtb*-Luxsamples treated with 50 and 12 μg/mL of compound **4**. Furthermore, a 3-log decrease in CFU/mL was observed for dormant samples treated with 3.1μg/mL (6-fold

MIC_D) relative to untreated controls, and a 1-log decrease for those treated with 0.8 μg/mL (<2-fold MIC_D). Replicating *Mtb*-Luxtreated with this same compound were only killed (2-log difference) at 50 μg/mL (5-fold MIC_R) suggesting this compound is mostly bacteriostatic against replicating *Mtb* but bactericidal against dormant *Mtb*(Figure 13C).These results validate the selectivity of **2**, **3**, **4** and **5** against dormant *Mtb* suggesting a unique mode of action in which bacterial killing by these compounds, especially **4,** is only observed for dormant but not metabolically active bacteria.

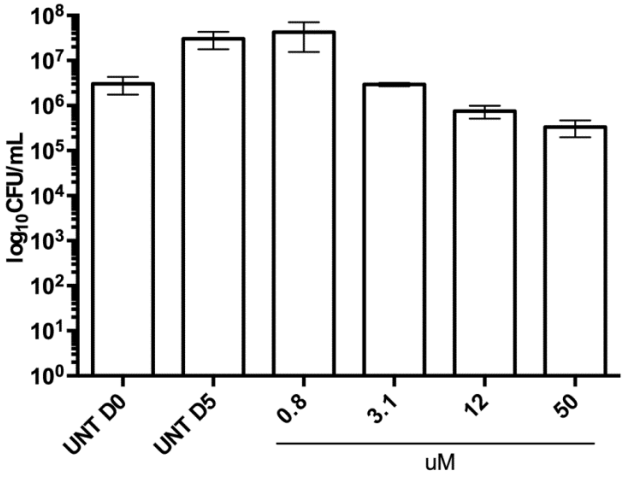

Figure 12. Bacteriostatic activity of Compound 1 against replicating Mtb validated by CFU.
Cultures grown in 7H9 were used. *Mtb*-Lux were treated for 5 days with compound **1** after which the luminescence was read. One-way ANOVA was used to compare treatment samples with controls and no statistically significant ($p<0.05$) differences were observed.

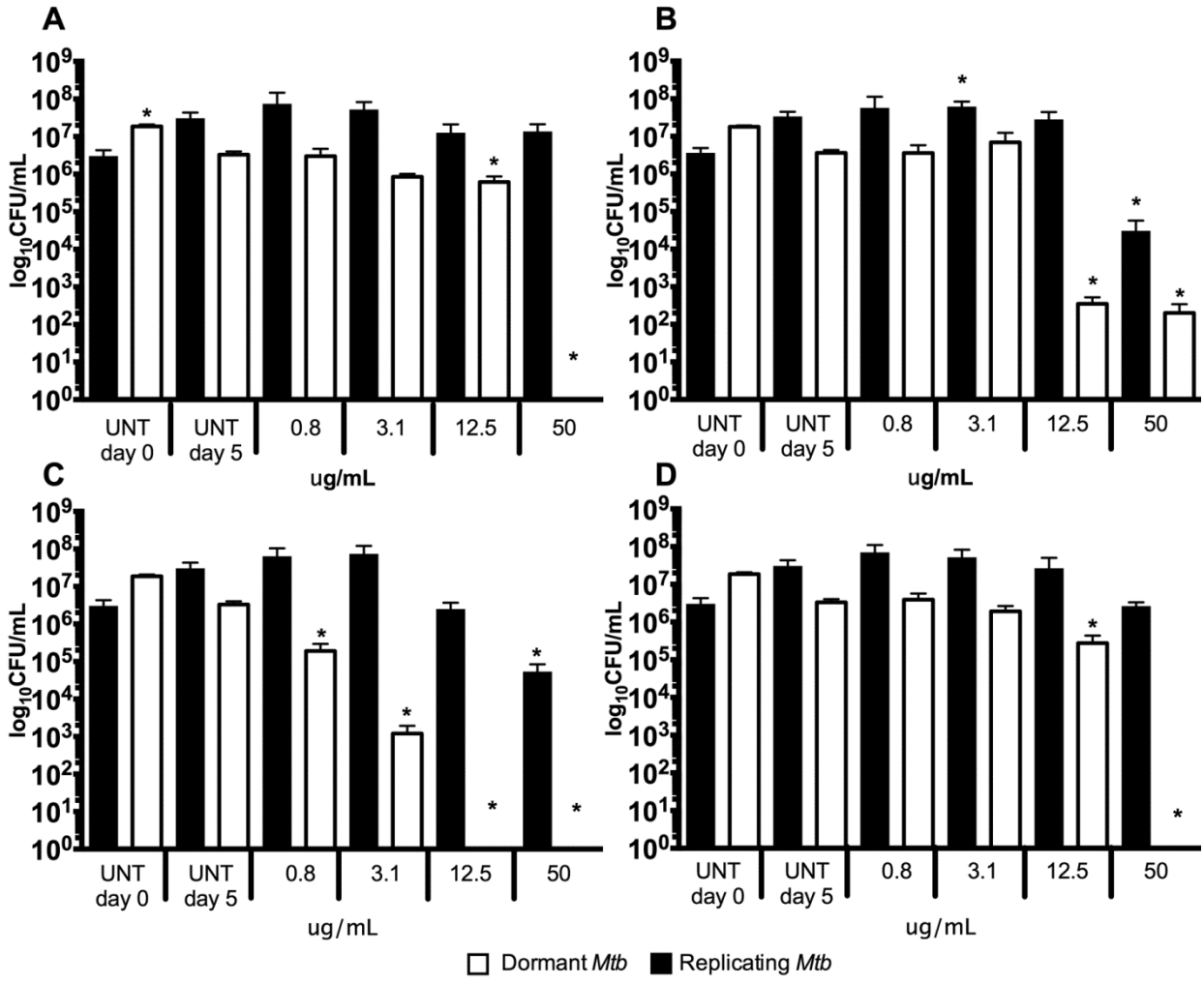

Figure 13. Activity of pure MNP compounds against dormant and replicating Mtb-Lux validated by CFU.

Dormant (open bars) and replicating (closed bars) *Mtb*-Lux were treated for 5 days with compounds **2** (A), **3** (B), **4** (C) and **5** (D) after which samples were taken for plating on 7H10 agar media. Colonies were counted after 3 week incubation. UNT day 0 – untreated culture innoculum; UNT day 5 – untreated culture plated after 5 days incubation under the same conditions as treated cultures. One-way ANOVA was used to compare data points. Asterisk denote data points which are significantly different ($p<0.05$) from the control (UNT D0 for replicating *Mtb*;UNT D5 for dormant *Mtb*).

Discussion

In the current TB treatment regimen, bactericidal drugs are effective at rapidly reducing bacterial burden in sputum [115], as evidenced bysputum culture conversion within the first 3 months of treatment [312]. Nonetheless, patients will face at least 3-4 more months of antibiotics to achieve a relapse-free cure. This severely delayed clearance of TB is thought to be due to subpopulations of dormant or persistor *Mtb* that arise during infection [17].Dormancy renders the bacteria phenotypically tolerant to front-line drugs such as RIF and INH [61, 65]. However,in contrast to its poor activity *in vitro,* pyrazinamide (PZA) provides potent sterilizing activity *in vivo* without relapse. As a result, it is credited with shortening of TB treatment from 12 to 6 months[15].Discovery of PZA's unique activity was serendipitousrather thanthrough intentional screening for compounds active against dormant bacilli[15]. Recent studies have used more focused approaches designed to uncover leadcompounds which distinctively inhibit non-replicating *Mtb*[180, 184]. With heritable resistance to PZA on the rise [313], novel molecules bactericidal against dormant *Mtb* will be important components of much needed new cocktails for shorter treatment without relapse.

Despite continuous efforts to improve TB treatment, the core drugregimen has not changed in the past 4 decades [143]. The focus on screening drugs against replicating *Mtb* in rich media has proved unsuccessful at filling the need for compounds that can

shorten treatment time. Alternatively, research into the physiology of *Mtb*during*in vivo* infection has revealed subpopulations of bacilli in distinct metabolic states and microenvironments within a single host [314]. This knowledge is being exploited to uncover essential processes critical to survival of non-replicating persistors which are vulnerable to inhibition[136]. These recent realizations in the field are also transforming the way we approach drug-discovery. Some groups are conducting chemical screens against conditionally essential targets of *Mtb*. Whole-cell screening under dormancy inducing conditions provides a more direct path to discovering novel scaffolds with bactericidal activity against phenotypically tolerant *Mtb.*Considering this, the main goal of our study was to identify compounds which could effectively kill dormant bacteria. A two-pronged approach was utilized which combined the chemical diversity of MNPs with physiologically relevant *in vitro* screening conditions.

Some dormancy screening models involve exposure of Mtb to a single environmental cue, such as starvation or hypoxia [182]. A streptomycin-dependent Mtb strain has also been employed for detecting inhibition of persistor bacteria [171]. Large-scale screens have been performed combining in vivo-like stresses to induce Mtb dormancy [184, 185, 187]. Interestingly, one study showed that using different individual stress conditions to generate non-replicating dormant Mtb yielded different hit compounds [180]. These data demonstrate the importance of combining the key stresses that trigger persistence to maximize the hits obtained in a dormant screen. Our use of a screening model which mimics several host-like conditions to induce a dormant phenotype enabled the discovery of compounds which may have otherwise gone undetected in a typical in vitro screen. In our screen, 12 out of 19 non-cytotoxic dormant hits were selectively active

against non-replicating Mtb at 20 μg/mL (Fig. 1). This unique hit list allowed us to find pure compounds bactericidal against dormant bacteria (Fig. 5). We will pursue hit-to-lead development of the scaffolds for TB treatment. Perhaps more importantly, they may serve as chemical biology tools for the discovery of new druggable targets essential for viability of dormant Mtb.

Even though our primary dormancy screen has proven effective at finding dormant active hits, we also noted false-positive hits which further validation revealed were only inhibitory against replicating bacteria (Fig. S2). We speculated this was due to the regrowth stage required for this assay during which carryover compounds could be inhibiting Mtb replication. This was evident in the discordant results for RIF and INH seen in the fluorescent readout, which showed minimal differences between replicating and dormant bacilli versus the dramatic drug tolerance of dormant Mtb measured by CFU enumeration. Similar assay artifacts have been noted by others. A previously reported solution included using activated charcoal in agar to sequester drugs from the media which may not be optimal for high-throughput screening [188]. In this study, luciferase was selected as a reporter because it is highly sensitive, ATP dependent, and more amenable to high-throughput screening. This readout provides results more rapidly since it does not require a regrowth stage or bacterial growth on agar [167]. The modified luminescent dormancy assay could rely on a loss of signal due to cell death after 2 days instead of a signal increase due to growth of uninhibited bacteria during 5 days, which is required for fluorescent assays. Due to the lack of bacterial replication under MSD conditions, by design this assay will preferentially detect bactericidal drugs. Here we describe a robust method in which luminescent Mtb CDC1551 bacteria are

exposed to 3 of the more relevant dormancy inducing conditions resulting in a severe drug-tolerance phenotype.

Screening natural products has a long and successful history of yielding effective antimicrobial compounds[292]. However, limitations of this strategy such as laborious deconvolution of complex mixtures discourages high-throughput screens. Moreover, use of host-like conditions to test natural products is rarely observed, especially in large primary screens. Due to attrition of drugs duringthe development pipeline, large-scale screening is necessary to allow prioritization of scaffolds with properties amenable to synthesis and medicinal-chemistry optimization. A few recent studies have used non-replicating *Mtb* to test small numbers of samples[207, 315]. These small-scale reports illustrate the potential of naturally-derived compounds against non-replicating *Mtb*, and highlight the need for larger scale screens of natural products under these conditions. In our study, the use ofboth replicating anddormant *Mtb* to test a library of MNPs enabled the identification of38non-cytotoxic active peak fractions, half with activity against phenotypically tolerant bacteria. Three of the hits were deconvoluted leading to the isolation and activity profiling of 5 molecules.

The chemical diversity of MNPs was evidenced in our study upon purifying multiple active compounds from single hit peak fractions. Unexpectedly, activity of the Aplysinidae-derived fraction (047.F07) against dormant and replicating *Mtb* was a consequence of 2 different scaffolds, as opposed to a single dual-active compound. Interestingly, each of the 2 compounds (**1** and **2**) had a significantly different activity profile (Table 3). Though the parent fraction (047.F07) had only moderate dormancy

activity, the dormant-active component (**2**) was more potent than previously thought, suggesting its enrichment upon deconvolution. Compound **2**was active against both replicating and dormant *Mtb,* though slightly more inhibitory towards dormant *Mtb* (2.7 fold) (Figure 11). Conversely, fistularin-3/11-epi-fistularin (**1**) was inhibitory against replicating but not dormant *Mtb.* The activity of this compound was previously described in a small screen of marine sponge extracts with a reported MIC of 7.1 μM against replicating *Mtb* H37Rv,which is similar to the findings in this study [202, 205].

An advantage of screening semi-pure peak fractions instead of crude lysates is the facilitated deconvolution of pure compounds which follows the screening process. The finding of a hit peak fraction (031.C02) containing a single compound in our library illustrated this very well. This hit fraction yielded a dormancy active lipid molecule (compound 3), known as 3-(hexadecyloxy)propane,1,2-diol. Compound **3** was almost 4-fold more inhibitory against dormant than replicating *Mtb*(Figure 11).To our knowledge this is the first report of this compound having inhibitory activity against *Mtb.* This compound and the lipid isolated from peak fraction 047.F07 are both polar lipids and could be acting as detergents. However, their cytotoxicity against J774 cells was above 200 μg/mL suggesting a specific mechanism of action for these lipids rather than detergent activity.

In this study, we isolated two terpene quinones with high selectivity against dormant *Mtb* from a sponge in the *Petrosia* (formerly *Strongylophora*) genus. Terpene quinones, including puupehenone metabolites have been extensively studied for their antimicrobial and cytotoxic properties [195, 311, 316-319]. Nonetheless, this is the first report

demonstrating that they selectively inhibit dormant drug-tolerant *Mtb*. The puupehenone derivatives identified here showed antituberculosis activity similar to that previously reported for puupehenone itself [202]. The MIC_D of 15-α-methoxypuupehenol, 0.5 μg/mL, was more than 20-fold lower than its MIC_R of 11.5 μg/mL (Figure 11 and Table 3). Furthermore, bactericidal activity was observed for this compound against dormant, but not replicating *Mtb* at only 2-fold MIC_D(Figure 13). The methanol adduct of puupehenone had been previously isolated from the sponge *Hyrtios sp* [311]. Another analog, puupehedione, was isolated from the same organism. Consistent with previous studies this compound had minor activity against replicating *Mtb* [202]. However, a 6-fold selectivity for dormant *Mtb* was still observed with puupehedione (Table 3).

Target-based studies with puupehenone metabolites have shown that they inhibit NADH oxidase activity in submitochondrial particles and human 5-lipoxigenase [320, 321]. Weinstein et al. have observed a bactericidal effect for *Mtb*'stype II NADH oxidase (NDH-2) inhibitors in a murine model [322]. Essentiality of a NDH-2 has been demonstrated in replicating bacteria [80]. But more importantly, inhibitors of NDH-2 proteins, such as thioridazine, have increased bactericidal activity towards quiescent as compared to replicating *Mtb*[77]. Considering this, we are currently investigating NADH oxidases as possible mycobacterial targets of these dormancy-selective puupehenone metabolites. Obtaining sufficient quantities of NP compounds to execute follow up studies is often a limiting factor with natural product-derived scaffolds. However, the synthesis of puupehenone and its analogs has been shown, enabling a path forward for these molecules [317, 323, 324].

Characterization of the molecular targets for these antimycobacterial MNPs with intriguingly selective activity against dormant *Mtb* will help elucidate essential mechanisms underlying the survival of dormant *Mtb* during latent infections. The use of alternate *in vitro* dormancy models to confirm the activity of compounds detected in our assay under a variety of other dormancy inducing conditions will also provide further evidence that they are likely to work *in vivo.* Animal models of persistent infection, such as the Kramnik mouse model, will further validate their unique activity profile and determine whether these compounds are capable of shortening treatment time [325, 326].

In conclusion, our findings underscore the significance of screening under *in vivo* like conditions, not only to discover novel drugs but also chemical tools to understand the physiologically relevant pathways required to initiate and sustain *Mtb* persistence.Future efforts will uncover the mode of action of compounds isolated in this study. Deconvolution of all the dormant active hit peak fractions is currently underway and will continue to provide molecules with unique activity against the tubercle bacilli under varying host-like conditions.

CHAPTER 3:

A NOVEL PLAKINAMINE ACTIVE AGAINST *MYCOBACTERIUM TUBERCULOSIS*

All results presented in this chapter were obtained by Carolina Rodrigues Felix. A first draft was written by Carolina Rodrigues Felix. Revisions and edits from Kyle Rohde were incorporated to the final version.

Abstract

Tuberculosis is the leading cause of death due to an infectious disease worldwide. This chronic infection caused by *Mycobacterium tuberculosis* is notoriously difficult to treat due to the high tolerance of the pathogen to antimicrobials. The need for compounds more effective against this pathogen has led to the discovery of a plakinamine scaffold with potent activity against *M. tuberculosis.* This prompted a further characterization of the compounds structure and activity. Plakinamine had low toxicity against J774 macrophages yielding a selectivity index (SI – IC_{50}/MIC) of 8.4. Furthermore, plakinamine was bactericidal against *M. tuberculosis* at 2-fold MIC concentrations, and exhibited moderate activity against other mycobacterial pathogens, such as *M. abscessus* and *M. avium.* In conclusion this work provides a novel promising scaffold to the TB drug discovery pipeline. Future work to determine the molecular target of this compound may reveal a pathway essential for *M.tuberculosis* survival during infection.

Introduction

Mycobacterium tuberculosis (*Mtb*),is the causative agent of the primarily pulmonary disease tuberculosis (TB). Approximately 8 million new cases of TB are diagnosed every year worldwide, and 5% of these are caused by multidrug resistant strains of *Mtb,* rendering the disease extremely difficult to control [14]. TB treatment entails a combination of 4 antibiotics taken for at least 6 months in order to achieve a relapse-free cure [115]. Considering this, there is urgent need for novel compounds more effective against this pathogen capable not only of shortening treatment time, but also of killing drug-resistant strains of *Mtb.*

Recently a large-scale screen of a marine natural products (MNP) peak fraction library containing 4400 samples yielded highly potent inhibitors of *Mtb*[327]. A laborious bioassay-guided deconvolution process is required to identify the bioactive molecule in a hit peak fraction, therefore, several hits from that screen remained to be examined in depth. A sample from the marine invertebrate *Corticium sp.* was highly active in the primary screen and was chosen for further deconvolution in this study. A novel plakinamine was discovered with potent bactericidal activity against *Mtb.* We have further characterized its activity against *Mtb* as well as other important mycobacterial pathogens, including *M. abscessus,* and two species belonging to the *M. avium* complex. The plakinamine compound was selectively active against *Mtb,* though moderate

activity was observed against the other mycobacteria tested. Investigating the mechanism of action of this compound may reveal novel druggable *Mtb* targets. The structural similarity of plakinamine and cholesterol, coupled with the essential nature of the cholesterol catabolism pathway for *Mtb* survival during infectionposes an interesting pool of putative targets for the novel structure described in this study [328].

Materials and methods

Antimicrobial Assays

Four slow-growing and 3 fast-growing mycobacterial strains (Table 4) were cultured in Middlebrook 7H9 broth media supplemented with 0.05% Tween 80, 10 % OADC and 50µg/mL kanamycin when necessary for plasmid maintenance. The previously described *Mtb*-Lux strain constitutively expressing the *luxCDABEG* operon from the episomal plasmid pMV306hsp+LuxG13, was used. All NTMs were transformed with the same plasmid to produce a stable luminescent signal. Log phase cultures of the mycobacterial strains expressing the *lux* operon were diluted to an OD600 of 0.01 and treated with serial dilutions

of plakinamine. This compounds was resuspended in 100% dimethyl-sulfoxide (DMSO) at 10 mg/mL. Sixteen-point 2-fold serial dilutions of plakinamine, starting at 200 μg/mL, were prepared in a final 2% DMSO concentration, 12 μg/mL rifampicin and 2% DMSO were used as controls. Treatments were performed in 384-well plates for 5 days at 37^{o}C for slow-growing mycobacteria and 2 days for fast-growing mycobacteria (Table 1), after which the luminescence was read using Synergy^{TM} H4 plate reader (BioTeK). Samples of *Mtb*-Lux treated with 0.8, 3.1, 12.5 and 50 μg/mL plakinamine were taken, diluted 10-fold in PBS-Tween80 and plated in 7H10 OADC. Plates were incubated for 3 weeks at 37^{o}C after which colonies were enumerated.

Cytotoxicity Assay

J774A.1 (ATCC® TIB67™) macrophages were cultured in Dulbecco's Modified Eagle Medium (DMEM, GIBCO) supplemented with 10% heat inactivated fetal calf serum (Atlanta Biologicals), 1mM sodium pyruvate (Mediatech, Inc.), 2mM L-glutamine (Mediatech, Inc.) and 1% PenStrep (100 U/mL Penicillin, 100 μg/mL Streptomycin, GIBCO). Twenty-five thousand cells/wellwere seeded overnight in black 384-well plates then treated with serial dilutions of plakinamine as described above. Tryton X and 2% DMSO were used as controls in these experiments

Data Analysis

Data were normalized to highest and lowest output values in the dose response. MIC (99% killing) and IC_{50} were calculated using a Gompertz model, and a nonlinear regression - normalized response curve fit, respectively in GraphPad Prism 5 [296]. The selectivity Index (SI) was calculated as IC_{50}/MIC.

Results

All the results reported were obtained with auto-luminescent mycobacteria expressing the *luxACDBEG* operon as previously described. Plakinamine was active against all mycobacterial strains tested, with the lowest MIC of 1.8 µg/mL observed for *Mtb* and the highest of 57 µg/mL observed for *Min*. The IC_{50} against J774 macrophages was 15.2 µg/mL, to produce a SI of 8.5 with IC_{50} compared to the *Mtb* MIC. All MIC values are listed in Table 4 and curves are shown in Figure 14. The potent inhibition of *Mtb* by plakinamine was confirmed by plating samples for CFU enumeration. These results demonstrated 90% bacterial killing by the compound at 3.1 µg/mL against *Mtb*. Furthermore, at the higher concentrations

of 12.5 and 50 µg/mL, zero colonies were observed indicating sterilization of the *Mtb* culture at those concentrations (Figure 15).

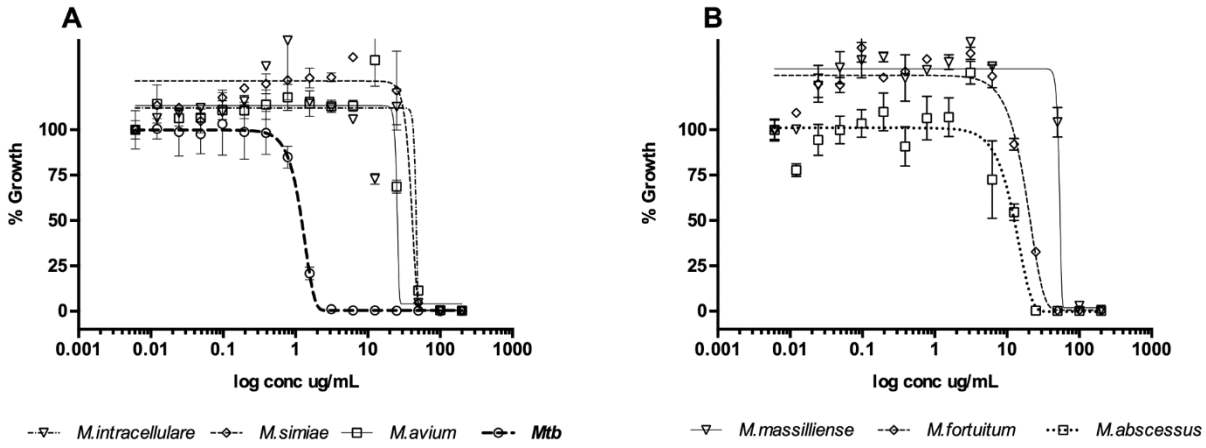

Figure 14. Activity of Plakinamine against multiple mycobacterial pathogens.
Cultures were treated with 16-point, 2-fold serial dilutions of plakinamine for 2 days (fast-growing mycobacteria – panel B) and 5 days (slow-growing mycobacteria – panel A) after which the luminescence was read. The Gompertz model was used to calculate MIC (99% killing)

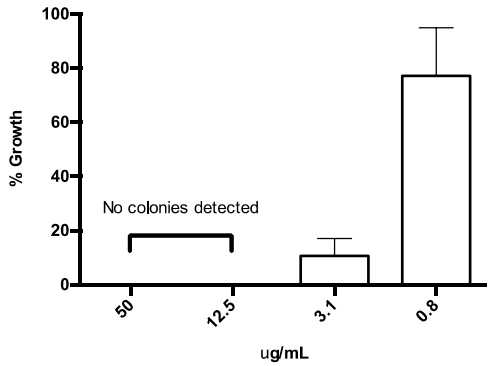

Figure 15. Bactericidal activity of plakinamine against Mtb.
Cultures treated with 50, 12.5, 3.1 and 0.8 µg/mL plakinamine were plated on 7H10 OADC and incubated for 3 weeks before CFU enumeration. The data are presented as % growth relative to average CFU/mL of the 2% DMSO controls.

Table 4. Strains used in this study and corresponding plakinamine activity

	Source	ID	MIC (µg/mL)
Plasmid			
pMV306hsp+LuxG13	Add gene	N/A	
Fast-growing mycobacteria			
M. massilliense		*Mma*	57.6
M. fortuitum		*Mfo*	32.45
M. abscessus		*Mab*	22.16
Slow-growing mycobactera			
M. tuberculosis	Rodrigues Felix et al.	*Mtb*	1.842
M. avium		*Mav*	27.28
M. intracellulare		*Min*	49.53
M. simiae		*Msi*	48.25

N/A non applicable

Discussion

The major global health threat posed by *Mtb* infections is intensified by the difficulty to treat TB disease [14]. In this study, we have identified a novel scaffold bactericidal against *Mtb,* and with low toxicity towards mammalian cells. The structural characterization of this compound revealed it to be the novel steroidal alkaloid plakinamine P. Although the activity of related scaffolds against *Mtb* has been previously reported [329], the current study is the first description of plakinamine P and its activity against *Mtb.* In our study, plakinamine P was most potent against *Mtb*, however, it was also moderately active against important opportunistic mycobacteria including *M. abscessus* and *M. avium* complex organisms. These are highly drug-tolerant pathogens known to cause chronic infections in immunocompromised individuals [285, 330]. Nevertheless, the observed selectivity of plakinamine for *Mtb* in comparison to other mycobacteriasuggests it may target pathways uniquely essential for *Mtb* survival.

The delayed clearance of *Mtb* by current front-line TB drugs is often attributed to the distinctive physiological aspects of this intracellular pathogen during infection [331]. In light of this, many TB drug discovery studies are focusing efforts on finding scaffolds capable of inhibiting *Mtb'*ssurvival pathways during infection [43, 290]. The plakinamine described in this study is structurally similar to cholesterol, with a modified side chain. Previous work has shown the essentiality

of cholesterol catabolism for the survival and persistence of *Mtb* during infection [328]. Inhibition of this pathway leads to death of intracellular *Mtb* [175]. Additionally, cholesterol analogs with undegradable side chains are capable of killing *Mtb* in culture [177]. Our data, combined with previously published work suggests that plakinamine may be causing mycobacterial death by inhibiting the cholesterol catabolism pathway. Additionally, inhibition may be owed to toxic byproducts coming from the breakdown of plakinamine via the cholesterol degradation pathway.

In conclusion, we have characterized an MNP derived scaffold with potent antimycobacterial activity. The essentiality of the putative target of plakinamine for *Mtb* survival and persistence in the host further highlights the potential of this compound in TB drug discovery. Future research will not only focus on confirming the molecular target of plakinamine, but also demonstrating its activity against *Mtb* under host-like conditions.

CHAPTER 4:

MARINE NATURAL PRODUCTS ACTIVE AGAINST *MYCOBACTERIUM TUBERCULOSIS*

All results presented in this chapter were obtained by Carolina Rodrigues Felix. A first draft was written by Carolina Rodrigues Felix. Revisions and edits from Kyle Rohde were incorporated to the final version.

Introduction

The large-scale screen of marine natural product peak fractions, described in chapter 2, yielded 149 total hit fractions. From these, 95 were active against replicating *Mtb*, 35 were active against dormant *Mtb,* and 19 were dual active peak fractions. Three peak fractions (HBOI.047.F07, HBOI.050.F04 and HBOI.031.C02) were deconvoluted initially, and 5 active compounds were purified; the activity and structures of these compounds are characterized in Chapter 2 [327]. Additionally, peak fraction HBOI.010.F07 was deconvoluted, a novel plakinamine compound was purified and its activity and structure were defined; this is described in Chapter 3. The dereplication of active peak fractions is a labor-intensive process, therefore, several hit peak fractions from this screen remain to be examined for further discovery of pure bioactive molecules. Several of the remaining active peak fractions are in different stages of bioassay guided deconvolution. This chapter describes the results obtained from the examination of these fractions, as well as the sub-fractions and compounds derived from them.

Material and Methods

Methods utilized for the discovery, and bioassay guided dereplication of the peak fractions are described in chapter 2.

Macrophage Infection Assay

This assay was developed by VanderVen and collaborators [175] and will be briefly described here. J774A.1 cells were cultured as described in chapter 2. For inoculum preparation *Mtb* CDC1551 was cultured in 7H9 OADC to log phase of growth and pelleted. The pellets were resuspended in infection media (DMEM containing 10% fetal calf serum (Atlanta Biological), 1mM sodium pyruvate (Cellgro), 2mM L-glutamine (Corning) and 1% PenStrep (100 U/mL Penicillin, 100 μg/mL Streptomycin, GIBCO)) and syringed with 28 gauge needles. The inoculum was diluted using infection media to OD_{600} 0.2. This inoculum was utilized to infect macrophages at a 5:1 multiplicity of infection (MOI). The infected cells were treated with MNP peak fractions in 384-well plates (30μL total volume – 24 μL infections media and 6 μL 5X drugs) for 5 days after which the fluorescent and luminescent signals were read.

Results

HBOI.020.C05 isolated from *Aaptos sp.*

This peak fraction initially detected in the dormancy assay provided 99.5% inhibition of dormant *Mtb*-RG, and only 19.6% inhibition of replicating *Mtb*-RG. The cytotoxicity of this peak fraction was evaluated using J774 cells, with 95% of cells remaining viable after overnight treatment with this peak fraction. Dormant treated *Mtb* cultures were plated on 7H10 OADC, and CFU were enumerated after 3 weeks incubation at 37^{o}C. The activity observed against dormant *Mtb* using the fluorescent readout was partially validated by CFU since only 60% inhibition of dormant bacteria was observed with this readout in comparison to the untreated and 10 µM controls. Nonetheless, this was still above the arbitrary 50% inhibition cutoff line used in the primary screen to analyze the data, therefore, the peak fraction was considered active against dormant bacteria, and its sub-fractions were tested in the secondary dormancy assay which utilizes a luminescent readout.

Chromatographic purification of this fraction yielded 19 sub-fractions each containing a pure compound. These sub-fractions were received in a 96-well plate (HBOI.060) and resuspended in 100% DMSO at 4 mg/mL. A 100 µg/mL

working plate was prepared, and subsequently all the sub-fractions were tested against dormant *Mtb*-Lux at 20 µg/mL since selective activity of the parent fraction was observed against dormant *Mtb* in the primary screen. Sub-fraction HBOI.060.C10 provided 90% inhibition of dormant *Mtb*-Lux. NMR analysis of this sub-fraction revealed it contained a single compound with one minor impurity. The major compound is a lipid molecule, nevertheless its structure has not been fully defined.

HBOI.022.E06 isolated from an Axinelidae marine invertebrate

This dual active sample was 87.9% and 99.6% inhibitory against replicating and dormant *Mtb*-RG in the primary screen, respectively. Also, low cytotoxicity was observed since 85.8% of J774 cells were viable after treatment with 20 µg/mL of this fraction. Nonetheless, the CFU results obtained with dormant *Mtb* treated with this fraction revealed it as a false positive hit in the primary dormancy screen, though this may also be explained by loss of activity during storage due to instability. These CFU data show only 40% inhibition of dormant bacteria treated with this peak fraction. Considering the potent inhibitory activity of this fraction against replicating bacteria, it is reasonable to assume that this peak

fraction inhibited *Mtb*-RG during the outgrowth stage required in the primary dormancy screen, thus providing a false positive result.

Even though only moderate anti-dormant activity was observed with this peak fraction upon validation, its potent activity against replicating *Mtb* and low cytotoxicity prompted further chemical separation of its components. This separation yielded 23 sub-fractions provided in 96-well plate HBOI.059, which were resuspended in 100% DMSO at 4 mg/mL, and a working plate at 100 µg/mL was prepared in 2.5% DMSO. All of these were tested against both replicating and dormant *Mtb*-Lux at 20 µg/mL in the secondary screening assays reliant on a luminescent readout. Replicating and dormant bacteria were 50% inhibited by HBOI.059.D07. Furthermore, four other sub-fractions, HBOI.059.D06, D09, D10 and E03 also exhibited modest activity against dormant *Mtb.* These fractions were collected consecutively during chromatographic separation, which suggests the sub-fractions with modest activity could contain the same compound as HBOI.059.D07 in lower concentration.

HBOI.032.H06 isolated from *Apsylinea sp.*

This peak fraction exhibited modest activity against replicating (52% inhibition) and dormant (44% inhibition) bacteria. The viability of J774 cells treated with this peak fraction was 79%. Even thoughthis fraction did not meet the maximum 20% cytotoxicity threshold defined in the original screen as the arbitrary cutoff line,further chromatography was conducted to determine if cytotoxic components could be separated from antimicrobial compounds.

Thirteen sub-fractions were obtained from the chromatographic separation of the parent peak fraction. These sub-fractions were received in 96-well plate HBOI.060, resuspended in 100% DMSO at 4 mg/mL, and a working plate was prepared at 100 µg/mL. These sub-fractions were tested at 20 µg/mL against replicating and dormant *Mtb*-Lux. Sub-fraction HBOI.060.E04 was 75% and 80% inhibitory against replicating and dormant *Mtb*-Lux, respectively. Sub-fraction HBOI.060.E05 was 80% inhibitory against replicating *Mtb*-Lux and was not active against dormant bacteria (Figure 16). This sub-fraction contains a pure compound of unknown structure. These data suggest the 2 active sub-fractions contain the same compound, although HBOI.060.E04 may contain a different compound mixed with the compound in E05 to account for its activity against dormant and replicating bacteria.

HBOI.033.C06 isolated from *Agelas clathrodes*

This fraction potently inhibited replicating *Mtb* (80%) at 20 µg/mL and did not inhibit dormant *Mtb* in the primary screening assays. The viability of J774 cells treated with this sample was 75%, which is 5% below the expected threshold of 80% designated for hits in this screen. However, 8 pure compounds were readily available after a single step of chromatographic separation of this fraction, and therefore, the activity of these was further analyzed.

Eight sub-fractions of this peak fraction were received in 96-well plate HBOI.059, resuspended in 100% DMSO at 2 mg/mL and a working plate at 100 µg/mL was prepared. All these sub-fractions were tested at 20 µg/mL against replicating *Mtb*-Lux. Interestingly, none of these 8 sub-fractions, each containing a pure compound, was active against replicating *Mtb*-Lux. Nonetheless, the parent peak fraction containing a mix of the 8 compounds retained activity comparable to that observed in the original screen. In order to confirm this result, the parent peak fraction was resubmitted to chromatographic separation and yielded 8 sub-fractions containing the same 8 pure compounds. These new sub-fractions were tested against replicating *Mtb*-Lux and the results were the same as previously observed (Figure 16).

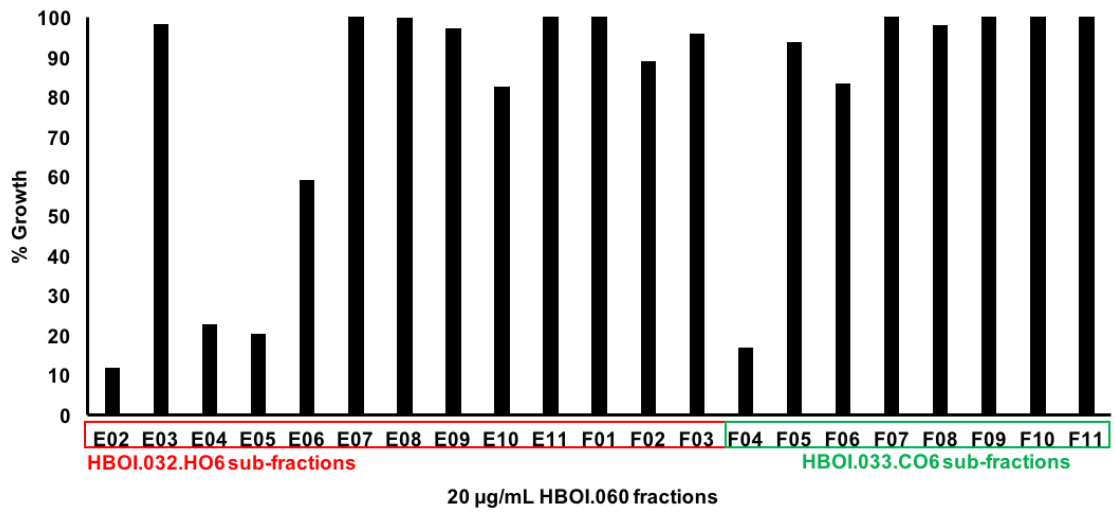

Figure 16. Activity of purified components in peak fractions HBOI.032.H06 and HBOI.033.C06.
Bacteria were cultured to log phase in 7H9 OADC, diluted to OD_{600} 0.01 in 384 well plates and treated for 5 days with compounds at 20 µg/mL. Results were obtained by reading luminescence on the 5thday. Among the sub-fractions of HBOI.033.C06 is included a new batch of the parent peak fraction (F04), to illustrate its activity relative to the activity of its sub-fractions.

HBOI.038.D11 isolated from an Axinelidae marine invertebrate

This peak fraction was originally detected in the screen against replicating *Mtb*, providing 88.6% inhibition of these bacteria. The toxicity of this fraction against J774 macrophages was extremely low, with cells treated with 20 ug/ml of fraction retaining 94.4% viability. Furthermore, a modest inhibition of dormant *Mtb*-RG (48.6%) was observed with this peak fraction in the primary screen. However, since this did not meet the 50% inhibition threshold originally applied to call hits

in the primary screen, the activity of this peak fraction against dormant *Mtb* was not tested by CFU. Furthermore, given the potent inhibition of replicating bacteria by this fraction, it is likely that the anti-dormant activity observed in the primary screen was actually due to inhibition of replicating bacteria during the outgrowth stage required for the primary dormancy assay. Nevertheless, the potent activity against replicating *Mtb* and low toxicity prompted further separation of this peak fraction.

Chromatographic separation yielded 15 sub-fractions which were initially tested against replicating *Mtb*-Lux at 20 µg/mL. Two of these sub-fractions potently inhibited (>90% inhibition) these bacteria and were further tested in dose response curves (Figure 17). These 2 sub-fractions containing semi-pure compounds of unknown structure provided dose-dependent inhibition of *Mtb*-Lux, with MIC approaching 10 µg/mL (Figure 18)

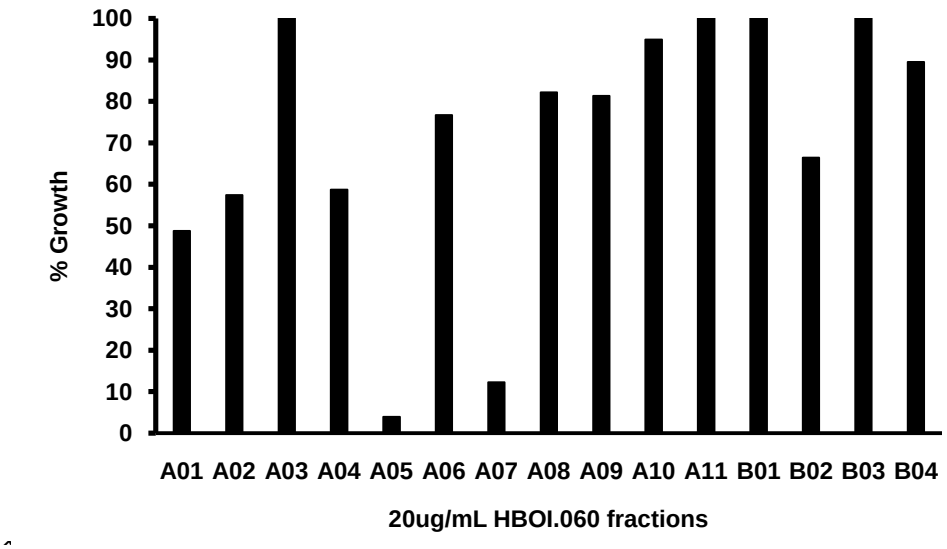

Figure 17. Purified components in peak fraction HBOI.038.D11 potently inhibit Mtb.
Bacteria were cultured to log phase in 7H9 OADC, diluted to OD_{600} 0.01 in 384 well plates and treated for 5 days with compounds at 20 µg/mL. Results were obtained by reading luminescence on the 5th day. Sub-fraction A01 is the parent peak fraction.

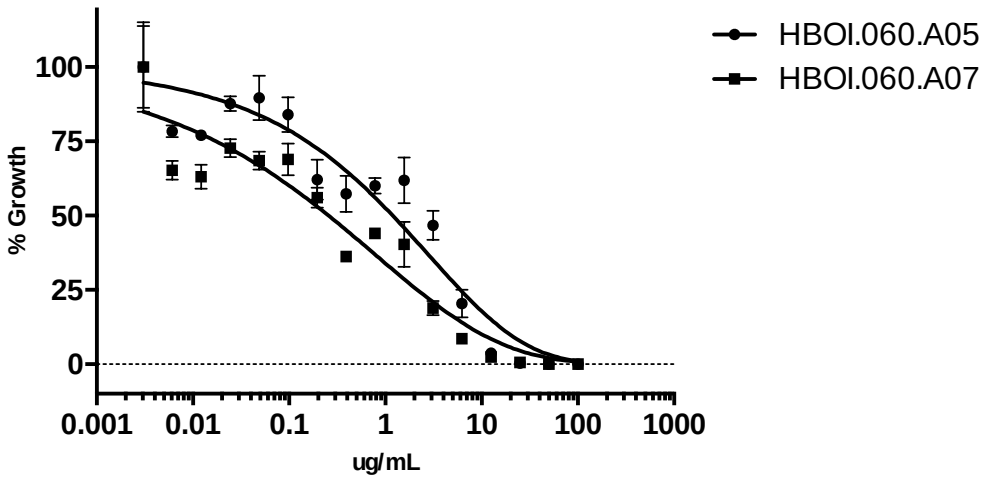

Figure 18. Dose dependent activity of semi-pure components of peak fraction HBOI.038.D11.
Bacteria were cultured to log phase in 7H9 OADC, diluted to OD_{600} 0.01 in 384 well plates and treated for 5 days with 16-point 2-fold dilution series of compounds starting at 200 µg/mL. Results were obtained by reading luminescence on the 5thday.

Activity of select hit peak fractions containing pure compounds

Two non-cytotoxic (<20% toxicity) peak fractions containing pure compounds were detected in the primary screens against *Mtb*-RG. HBOI.039.G05 was 100% inhibitory against dormant and 42.4% inhibitory against replicating *Mtb*-RG. Even though potent activity was observed with this fraction against dormant bacteria in the primary screen, this was not confirmed by CFU, only 25%

inhibitory activity was observed using that readout, suggesting HBOI.039.G05 was a false positive hit in the primary dormancy screening assay. Alternatively, this compound could be an inhibitor of reactivation, therefore regrowth would be inhibited in the presence of the compound in broth media, and not inhibited in the agar media in which the compound is absent. Nonetheless, the structure of the compound contained in this peak fraction was defined as curcumin, and a dose response curve was performed revealing the MIC to be above 100 µM. HBOI.046.D02 (Figures 19 and 20) was 89.3% inhibitory against replicating *Mtb*-RG and not inhibitory against dormant bacteria. The structure of the pure compound from this peak fraction was also defined, and a dose response curve showed the compounds MIC to also be above 100 µM (Figures 19 and 20). Given the poor potency of these compounds against *Mtb* they were no longer investigated in this study.

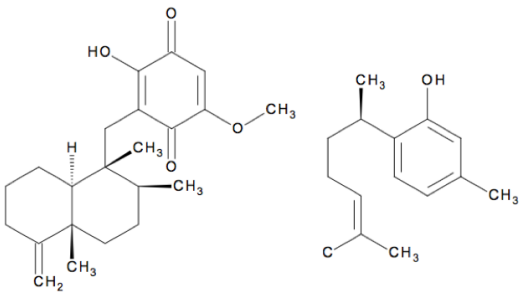

HBOI.039.G05 **HBOI.046.D02**

Figure 19. Compounds active against Mtb.
Compound structures were defined by NMR.

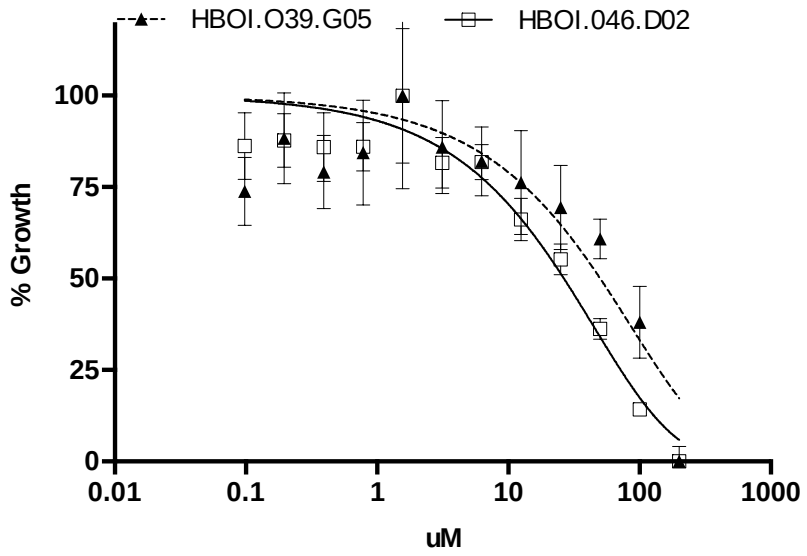

Figure 20. Dose dependent activity of two hit peak fractions containing pure compounds.
Bacteria were cultured to log phase in 7H9 OADC, diluted to OD_{600} 0.01 in 384 well plates and treated for 5 days with 12-point 2-fold dilution series of compounds starting at 200 µM. Results were obtained by reading luminescence on the 5thday.

Select hit peak fractions with activity against intracellular *Mtb.*

Two peak fractions were detected in a pilot screen of the MNP library against *Mtb* infected J774 macrophages. HBOI.001.A04, isolated from a Spongiidae marine invertebrate, was 79% inhibitory against intracellular *Mtb*-FFluc, which constitutively expresses the firefly luciferase enabling a luminescent readout upon addition of the substrate, luciferin. A single compound was present in this

peak fraction, and its structure was defined as furospinulosin 1 (Figure 21). The activity of the compound was also evaluated in the macrophage infection assay by utilizing a CFU readout, however only 40% activity was observed using this readout (Figure 22.). Furthermore, the *in vitro* activity of this compound against replicating *Mtb* was examinedwith a dose response curve. These data show that furospinulosin 1 is poorly active against replicating *Mtb in vitro* since its MIC is above 200 µM. Peak fraction HBOI.001.B03 was also detected in the pilot screen. This peak fraction, isolated from Halichondriidae, was 91% inhibitory against intracellular *Mtb*-FFluc. This activity prompted further deconvolution of the fractions by chromatography, which yielded 9 sub-fractions. Each sub-fraction, as well as the parent peak fraction, were tested at 20 µg/mL against intracellular *Mtb* using CFU as a readout Figure 22). Sub-fraction HBOI.056.009, containing a pure compound, exhibited above 75% inhibitory activity against intracellular *Mtb.* Furthermore, HBOI.056.007 contained a pure compound and its structure, determined by NMR (Figure 21), was related to the structure of HBOI.056.009. The activities of these 2 compounds was also tested against *Mtb* replicating *in vitro* using dose response curves. The MIC of both these compounds in that assay was above 200 µM (Figure 23).

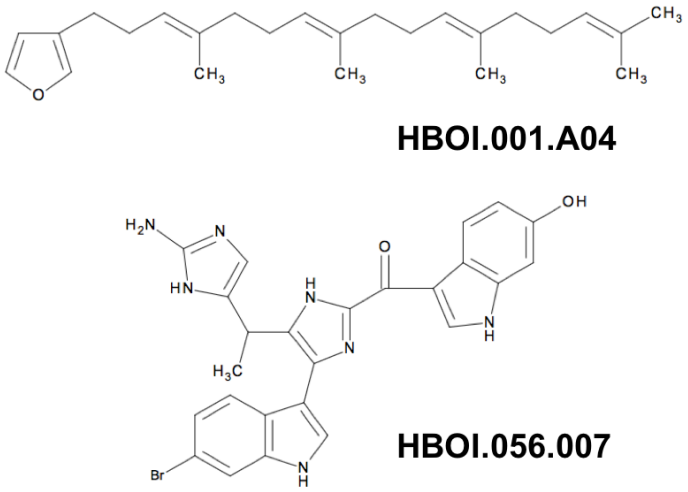

Figure 21. Compounds active against intracellular Mtb.
Compound structures were defined by NMR.

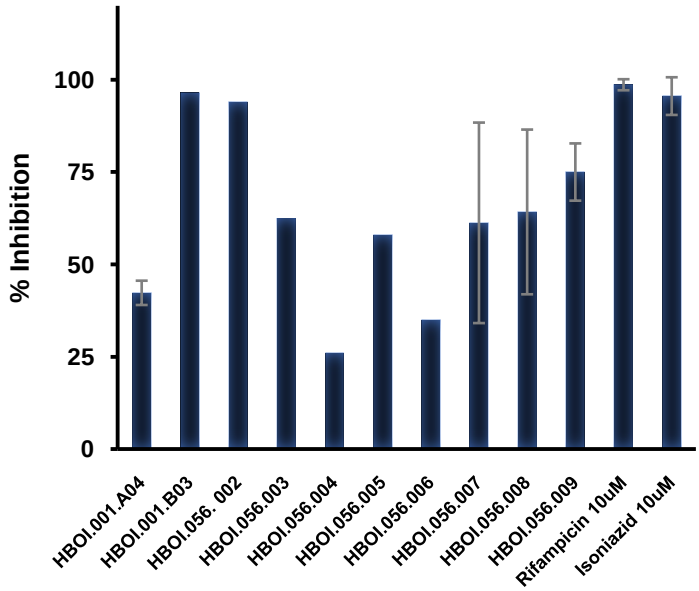

Figure 22. Activity of peak fractions against intracellular Mtb.
J774 macrophages were infected at a 5:1 and treated for 5 days with fractions at 20 µg/mL, after which infectcells were lysed and samples were taken and plated on 7H10 OADC. CFU were enumerated after 3 weeks incubation at 37^{o}C.

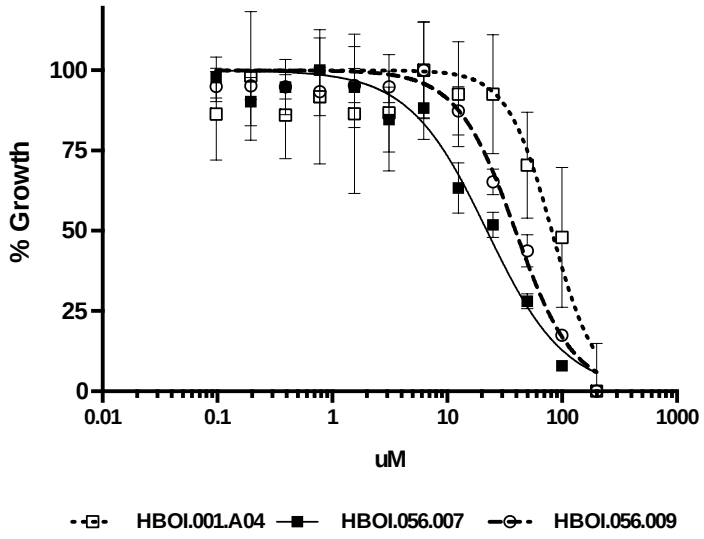

Figure 23. Peak fractions show potent activity against Mtb.
A, B - *In vitro* 12 pointdose response curves at concentrations ranging from 200uM to 0.09uM. J774 macrophages were infected over night at MOI 5:1 and treated for 6 days after which macrophages were lysed and samples were plated for CFU counting (data represents 3 independent experiments in triplicate).

Discussion

The search for antimicrobials from natural sources has led to the discovery of 9 out of 12 known classes of antibiotics [196]. This historical success, coupled withthe high levels of chemical and bioactivity redundancy observed in synthetic libraries, has led to a resurgence of natural product screens in recent years [191]. Recently we performed a large-scale screen of MNPs against replicating and dormant *Mtb*, yielding several compounds selectively active against dormant *Mtb [327].* The process of bioassay guided deconvolution of marine samples can be

laborious and time-consuming, therefore, many hits from this screen are still being examined and discovery of novel pure compounds is still underway. This chapter described the activity of select MNP peak fractions against replicating, dormant and intracellular *Mtb.*

Identification and characterization of the bioactive molecules present in a MNP mixture has many challenges. Often, individual chemical scaffolds can be readily isolated through chromatography. However, activity of the mixture is not a guarantee that one of the isolated compounds will be similarly active. Compounds with synergistic activity may appear inert when tested separately. In this study, an active peak fraction (HBOI.033.C06) was deconvoluted and individual compounds were obtained. Nonetheless, none of the isolated compounds were inhibitory against *Mtb,* suggesting that synergy between different compounds may be required for the activity observed with the parent peak fraction.

Although the structures of many compounds remain to be determined, a trend has been observed with bioactive lipid molecules. In this screen, several bioactive lipids have been identified which are selectively inhibitory against dormant *Mtb.* This trend is consistent with extensive work demonstrating the essentiality of lipid metabolism pathways for this pathogen, not only serving as virulence factors in a highly complex and impermeable cell-wall, but also as carbon and energy sources [332-335]. However, many bioactive lipids are often

inhibitory through non-specific membrane disruption, therefore, cytotoxicity needs to be extensively characterized for these molecules.

Furthermore, peak fractions selectively active against intracellular *Mtb* were discovered in a pilot screen of the MNP library, and the structures of the compounds isolated from those fractions were determined. Although the entire library was not screened in these conditions, those peak fractions were examined in depth. The fraction HBOI.001.A04 contained a single compound, furospinulosin 1. Nonetheless, its activity against intracellular *Mtb* was not confirmed when using CFU as a readout. Peak fraction HBOI.001.B03 containing several compounds was potently active in the macrophage infection assay, however, the activity of the isolated compounds was not consistent with this profile. Even though above 50% inhibition was maintained by the sub-fractions in the macrophage assay by CFU, inconsistent results were obtained for these. This could be due to variability of the assay, or instability of the compounds isolated from this peak fraction. Moreover, the poor activity of furospinulosin 1 observed by CFU could be because the compound is bacteriostatic; more detailed time-to-kill kinetics experiments would be required to confirm and further characterize this.

In conclusion, several potently active peak fractions are currently in the deconvolution process and many bioactive molecules will still be isolated. Future work will include not only isolating more pure compounds, but also determining

their structures. Furthermore, scaling up the purification process to obtain larger quantities of selected molecules will allow in depth characterization of the antimicrobial activity as well as mechanism of action. Early identification of the scaffold structure can help accelerate the characterization process, since chemical synthesis can then be utilized to produce larger quantities of active molecules; and *in silico* docking approaches can be utilized to identify putative targets. The ability to synthesize a naturally derived scaffold is a highly valuable tool for medicinal chemistry studies.

CHAPTER 5:

BIS(PYRROLIDE-IMINE) GOLD(III) MACROCYCLES AND CHELATES: REPURPOSED ANTICANCER COMPOUNDS BECOME A NOVEL CLASS OF ANTIMICROBIALS TARGETING *MYCOBACTERIUM TUBERCULOSIS* AND *MYCOBACTERIUM ABSCESSUS*

Results presented in this chapter were obtained by Carolina Rodrigues Felix and Rashmi Gupta. The chemical synthesis and characterization of compounds was performed by Matthew P. Akerman, Kate J. Akerman, Cathryn A. Slabber and Orde Q. Munro.A first draft of Results and Discussion was written by Carolina Rodrigues Felix. Introduction and Methodology were written by Rashmi Gupta. Revisions and edits from Orde Q. Munro and Kyle Rohde were incorporated to the final version.

This chapter was submitted as a manuscript to Antimicrobial Agents and Chemotherapy and is currently in review.

Abstract

Mycobacterium tuberculosis(*Mtb*) and the fast-growing *Mycobacterium abscessus* (*Mab*) are two important human pathogens causing persistent pulmonary infections that are difficult to cure and require long treatment times. The emergence of drug resistant *Mtb* strains and the high level of intrinsic resistance of *Mab* calls for novel drug scaffolds that effectively target both pathogens. In this study, we have evaluated the activity of bis(pyrrolide-imine) gold(III) macrocycles and chelates, originally designed as DNA intercalators capable of targeting human topoisomerase I and II, against *Mab* and *Mtb.* We identified a total of 5 non-cytotoxic compounds active against both mycobacterial pathogens under replicating *in vitro* conditions. We chose one of these hits, **14**, for detailed analysis due to its potent bactericidal mode of action, ease of crystallization, and ready availability (scalable synthesis). This compound exhibited activity superior to rifampicin (RIF) against phenotypically drug tolerant non-replicating bacilli in a multistress dormancy model. The clinical relevance of this compound is further demonstrated by its ability to inhibit several phylogenetically diverse *Mtb* clinical isolates. Prompted by previous data suggesting that **14** may target topoisomerase/gyrase enzymes, we demonstrated that it lacked cross-resistance with fluoroquinolones, which target the *Mtb* gyrase, as well as with the front-line drug RIF which implies a novel mechanism of action.

Drugs like compound **14** that inhibit not only replicating and dormant *Mtb* bacilli, but also *M. abscessus* represent a promising starting point for the development of novel therapeutics for infections by pathogenic mycobacteria.

Introduction

Mycobacterial pathogens are ubiquitous in human populations, causing severe chronic diseases which are notoriously difficult to treat. Among these bacteria, the most important pulmonary pathogens include *Mycobacterium tuberculosis* (*Mtb*) and *M. abscessus* (*Mab*), an emerging infectious agent in the US. *Mtb* is a slow-growing mycobacterium estimated to latently infect almost one-third of the human population, causing 8 million new cases of active tuberculosis (TB) disease worldwide every year. *Mab,* on the other hand,is a rapid growing non-tuberculous mycobacterium (NTM) which causes TB-like pulmonary infections as well as soft-tissue and wound infections [336]. It is increasingly encountered as the etiological agent of damaging pulmonary infections in patients with underlying lung conditions such as cystic fibrosis or bronchiectasis [337]. Both *Mtb* and *Mab* infections require a long multidrug treatment regimen of over 6 months [283, 338], which can lead to poor patient compliance and rising rates of drug-resistant strains. In TB, the presence of phenotypically drug tolerant sub-populations in

heterogeneous lesions in the lung further complicates the treatment of this disease [339]. For *Mab,* a high level of intrinsic resistance to many chemotherapeutic agents and the presence of genes conferring inducible resistance to clarithromycin, a cornerstone treatment for this pathogen, leads to high treatment failure rates [340, 341]. Due to similar clinical and radiographic presentations and non-definitive laboratory diagnosis based on the presence of acid-fast bacilli in sputa, *Mab* infections are often misdiagnosed and treated as TB [342]. As a result, the treatment fails because the front-line anti-TB drugs such as rifampicin (RIF), isoniazid (INH), pyrazinamide, and ethambutol are not effective against *Mab*[343, 344]. Such clinical scenarios warrant the development of powerful antimicrobial agents with dual activity against both *Mtb* and *Mab* with sufficient potency to shorten the unacceptably long duration of treatment.

Metal-containing complexes have a long history of use as chemotherapeutics. Silver and copper were used as antibacterial agents in ancient Greece [345]. The platinum-based drug cisplatin is widely used to treat genitourinary tumors [346], whereas Auranofin is a gold (I) compound licensed for rheumatoid arthritis [347, 348]. Other gold-containing compounds are used in the treatment of human diseases like asthma, cancer, HIV and malarial infections [345]. Metals, including gold, integrated into nanoparticles have proven to be potent antimicrobial agents even against multi-drug resistant bacteria [349-352]. The use of metal-based compounds against *Mtb* can be traced back to the bacteriologist Robert Koch

who discovered that gold-cyanide can cause bacteriostatic inhibition of *Mtb*[345, 353]. Since that time, very few studies have assessed the activity of metal-containing compounds against mycobacteria [354, 355].

Even though *Mab* pulmonary infections are significantly more difficult to treat than TB, most drug-discovery efforts have focused on TB due to the higher incidence of this infection worldwide. Attempts at repurposing TB drugs for use against *Mab* have had limited success [356-359]. In light of these issues, it is important to screen compounds against both pathogens simultaneously. Scaffolds thought to target essential conserved targets among mycobacteria are a promising starting point for finding dual-active compounds. With this in mind, and because repurposing anticancer drugs as potentially novel bactericidal and bacteriostatic agents [360-362] is currently relevant, especially those containing trivalent metal ions [363-365], we evaluated a small collection of 19 pyrrole-based gold(III) macrocycles [366] and chelates [367] known to target human topoisomerases.[366] Even though the mycobacterial target of these compounds has not yet been elucidated, this is the first study that has investigated the activity of novel gold(III) compounds against both *Mtb* and *Mab*. We chose whole cell phenotypic assays to test for antimicrobial activity to ensure that compounds were able penetrate the highly impermeable mycobacterial cell wall. In this study, we have identified bis(pyrrolide-imine)-based gold(III) compounds with potent activity against both mycobacterial pathogens and low toxicity to mammalian cells. Select scaffolds also demonstrated time-dependent

bactericidal activity against *Mab* and *Mtb.* Detailed analysis of the best candidate compound revealed activity against a panel of *Mtb* clinical isolates as well as non-replicating dormant bacilli. Overall these results highlight the potential of this novel class of gold complexes for hit-to-lead development, which may ultimately lead to a drug that can shorten the treatment times for these notorious mycobacterial infections.

Materials and Methods

Chemical compounds

The chemical synthesis and characterization details for the 19 bis(pyrrolide-imine) gold(III) complexes (simple chelates and macrocycles) used for antimicrobial assays in this work are reported elsewhere [366, 367]. Amikacin (AMK), ciprofloxacin (CIP), moxifloxacin (MOX), rifampicin (RIF) and isoniazid (INH) were purchased from Sigma-Aldrich and used without further purification.

Single crystals of $C_{13}H_{14}N_4ClAu$ (compound **14**) were grown by diffusion of diethylether into a methanol solution of the gold(III) complex. A suitable crystal (clear orange cube $0.1 \times 0.1 \times 0.1$ mm^3 in size) was selected and mounted on a

glass fiber with epoxy resin before centering on the goniometer of an Xcalibur2 CCD diffractometer (Oxford Diffraction) fitted with an Enhance X-ray source (3 kW ceramic X-ray tube, Mo Kα radiation, λ = 0.71703 Å). The crystal was kept at 140.15 (2) K during data collection; the intensity data were reduced using CrysAlis CCD and CrysAlis RED Version 1.171 [368]. Using Olex2 [369], the structure was solved with the ShelXS-1997 [370] structure solution program using direct methods and refined with the ShelXL-1997 [370] refinement package using least squares minimization. All hydrogen atoms were treated with the standard riding model of SHELXL and refined as isotropic contributors in the least-squares refinement process.

Crystal data for 14

Compound **14**, $C_{13}H_{14}N_4ClAu$ (M =458.70 g mol^{-1}): triclinic, space group P-1 (no. 2), a = 7.5888(4) Å, b = 9.4183(3) Å, c = 10.5118(4) Å, α = 68.707(4)°, β = 72.787(4)°, γ = 72.194(4)°, V = 651.86(5) $Å^3$, Z = 2, T = 140.15 K, μ(MoKα) = 11.479 mm^{-1}, *Dcalc* = 2.337 g/cm^3, 10708 reflections measured (7.276° ≤ 2Θ ≤ 68.306°), 4501 unique (R_{int} = 0.0173, R_{sigma} = 0.0206) which were used in all calculations. The final R_1 was 0.0163 (>2σ(I)) and wR_2 was 0.0393 (all data). The data are freely available from the Cambridge Crystallographic Database (CCDC

1567545). Tables of structural details (bond lengths, bond angles, etc. are available as Supplemental Material: Tables 7- 9).

Solution preparations

Stock solutions of amikacin (AMK), ciprofloxacin (CIP), moxifloxacin (MOX), rifampicin (RIF) and isoniazid (INH) were prepared according to the manufacturer's instructions. The gold(III) compounds were reconstituted by dissolving the powdered form in 100% DMSO to give stock solutions 10 mM in concentration. The compounds were further diluted to appropriate assay concentrations in sterile deionized water.

Bacterial strains and culture conditions

Bacterial strains: *Mtb* CDC1551 [371], 5 *Mtb* clinical isolates [372], *Mab* 390S [373], *M. smegmatis*, *M. bovis* (BCG) and *Escherichia coli* used in this study are listed in Table 5. *Mab* strains are a kind gift from Dr. Thomas Byrd of the University of New Mexico [374]. *Mtb* and *Mab* strains were cultured in

Middlebrook 7H9 supplemented with 0.05% Tween80 and 10% oleic acid/albumin/dextrose/catalase (OADC) and incubated at 37ºC and 5% CO_2 (normoxic) unless specified otherwise. Kanamycin 50 µg/mL (KAN), cycloheximide 100 µg/mL and amikacin 32 µg/mL (AMK) were added when appropriate.

Table 5. Bacterial strains and plasmids

Name	Genotype/Phenotype	Reference
Plasmids		
pVVRG	episomal plasmid, expressing mCherry and Kan^R	38
pMV306hsp+LuxG13	integrative plasmid containing the *luxCDABE* operon, Kan^R	46 (Addgene plasmid # 26161)
Strains		
CDC1551	*M. tuberculosis(Mtb*) reference strain	37
Mtb-RG	*Mtb* CDC1551 expressing pVVRG	41
Mtb-lux	*Mtb* CDC1551 expressing pMV306hsp+LuxG13	41
Mtb CI 1	*Mtb* clinical isolate 9532/03, Euroamerican lineage 2, Haarlem	38
Mtb CI 2	*Mtb* clinical isolate 2191/99, Euroamerican lineage 13, Uganda	38
Mtb CI 3	*Mtb* clinical isolate 1934/03, East Asian lineage 8, Beijing	38
Mtb CI 4	*Mtb* clinical isolate 4850/03, Indo Oceanic lineage 5, EAI	38
Mtb CI 5	*Mtb* clinical isolate 5468/02, West African 2 lineage 15, WA2	38
Mab	*M. abscessus* 390S, smooth colony phenotype	39
Mab-RG	*M. abscessus* 390S expressing pVVRG	This study
Mab-lux	*M. abscessus* 390S expressing pMV306hsp+LuxG13	This study
BCG	wild-type *M. bovis*	ATCC
BCG-*lux*	wild-type BCG expressing *luxCDABE*	This study
RIF^R-*lux*	RIF drug resistant BCG strain, *rpoB*-S531W, bioluminescent	This study
RIF^R/ FLQ^R-*lux*	RIF and FLQ resistant BCG strain, *rpoB*- S531L, *gyrA*-D94G, bioluminescent	This study

In vitro antimicrobial susceptibility assays

A total of 19 gold(III)-complexed macrocycles and simple chelates were examined for antimycobacterial activity using mCherry reporter strains of *Mtb* and *Mab* (*Mtb*-RG and *Mab*-RG) [327]. For this initial screening against *Mtb*, gold(III) complexes were added at a final concentration of 5 µM to a black solid-bottom 384-well screening plate (Corning) containing *Mtb*-RG culture in log phase of growth diluted to OD_{600} 0.05 in a final total volume of 30 µl. Negative control (0.5% DMSO) and positive control (10 µM RIF) wells were also included. The screening plate was incubated at 37ºC and 5% CO_2 for 6 days in a humidified chamber.

Evaluation of the compounds against *Mab* was carried out in a solid black 96-well plate with *Mab*-RG culture of OD_{600} 0.05. Compounds were added at 5µM in a total volume of 100 µl per well. The screening plate was incubated for 3 days. Negative (0.5% DMSO) and the positive control (32 µg/mL AMK) was also included.

Fluorescence was measured in both *Mtb* and *Mab* screening plates using a Biotek Synergy plate reader at excitation/emission wavelengths of 485/575 nm. Percent inhibition was calculated using the formula {(negative control signal -

sample signal) / negative control signal * 100}. Z-factors were calculated as described previously [375].

Minimum inhibitory concentration (MIC) assay

MICs of 5 compounds (**8**, **10**, **11**, **14**, and **15**) identified from the initial screening were determined using bioluminescent strains of *Mab* and *Mtb* [327]in solid white 384-well microtiter plates (Corning). Compounds **8**, **10** and **11** are gold(III) macrocycles, while **14** and **15** are simple gold(III) chelates. A 2-fold serial dilution series of the compounds (200-0.006 µM) was carried out in 384-well white solid bottom plates while maintaining the final 2% DMSO concentration in each dilution. Log phase cultures (OD_{600} = 0.4-0.8) of *Mab* 390S-*lux* and *Mtb*-*lux* were diluted to 0.01 before addition to the wells in a total volume of 30 µl. Untreated DMSO controls were also included. Similarly, the MIC of compound **14** was determined under dormant conditions as well using the 9-day hypoxia adapted CDC1551-*lux* culture, the details of which are described later. The plates were incubated at 37ºC, 5% CO_2 until luminescence was read at 0, 24, 48 and 72 h using a plate reader. The data expressed as percent growth was fitted by a modified Gompertz model [376]and the dose-response curve was generated using GraphPad Prism 7.0. MIC is defined as the lowest drug concentration at which more than 99% decrease in *lux* signal was observed as compared to the untreated control.

Cytotoxicity assay

Cytotoxicity was assessed on J774A.1 macrophage cell line. Macrophages were cultured in Dulbecco's Modified Eagle Medium (DMEM, GIBCO) supplemented with 10% heat inactivated fetal calf serum (Atlanta Biologicals), 1mM sodium pyruvate (CellGro), 2mM L-glutamine (CORNING) and 1% PenStrep (100 U/mL Penicillin, 100 mg/mL Streptomycin, GIBCO). Macrophages were seeded in a 384-well black transparent bottom plate (Corning) at 2.5 x 10^4 cells/well. After macrophages were allowed to adhere for 4-6 h, a two-fold dilution series of the compounds (200-0.006 µM) and controls (2% Triton X and 0.5% DMSO) were added to the wells. The plate was incubated for 24 h and then 1/10^{th} volume of resazurin dye was added. Fluorescence was measured following 4 h incubation with the dye at an excitation of 530 nm and emission at 590 nm with cell viability indicated by conversion of resazurin to fluorescent product resofurin. Viability was determined as percent growth calculated relative to the DMSO control and a dose-response curve was generated by Prism 7.0. MIC and IC_{50} values were determined from the non-linear regression fitting of the data by Prism 7.0 using the Gompertz model equation. The selectivity index (SI) is determined by the ratio of IC50/MIC.

Time-kill kinetic assay

To examine whether bacterial killing is concentration and/or time-dependent, a time-kill kinetic study was carried out with **8**, **10**, **11**, **14**, and **15**. For *Mtb,* CDC1551 cultures diluted to an OD_{600} of 0.01 in 7H9 were added to a solid-white 384-well plate containing compounds at final concentrations of 0, 1X, 4X and 8X MIC in a total volume of 30 µl. DMSO control was also included. The plate was incubated for 6 days for *Mtb*. At every time point - 0, 24, 72 and 144 h post-inoculation, an aliquot was taken, serially diluted and 50 µl plated onto 7H10 quad-plates supplemented with OADC. Colonies were counted after 3-4 weeks of incubation at 37ºC and CFU/mL was calculated. Similarly, a time-kill assay for compound **14** was performed with *Mab* 390S culture with some changes. An aliquot was taken out at time points- 0, 24, 48 and 72 h for plating. The plates were incubated for 3 days and colonies were counted after 5 days of incubation following plating.

In vitro activity of compound 14 against clinical strains

Compound **14** was also evaluated against 5 clinical strains of *Mtb* from 5 different phylogenetic lineages [372] (Table 1) at 5µM concentration in a total volume of 30 µl in black 384-well solid bottom plates. The screening plate was incubated for 5 days at 37ºC, thereafter resazurin dye was added at $1/10^{th}$ of the total volume and incubated for 24 h. Fluorescence was measured at Ex/Em 530/590 [377].

Activity of compound 14 against dormant *Mtb*

We employed a previously described multi-stress dormancy model (MSD) [61] to evaluate activity of gold complex **14** against dormant *Mtb*. Briefly, *Mtb-lux* wasgrown in multiple-stress media (10% Complete Dubos at pH 5.0 containing 0.018% tyloxapol and no glycerol) and adapted for 9 daysin a hypoxia chamber. This culture was added to the 384-well white solid bottom plates at an OD of 0.1. Gold compound **14** was added at a final concentration of 1X, 2X, 4X and 8X MIC determined under replicating conditions in a total volume of 30 µl. DMSO (0.5%), RIF and INH controls were also included. The plate was incubated under hypoxic conditions (37ºC, 10% CO_2 and 5% O_2) for 5 days and samples were serially

diluted and plated on 7H10 OADC for CFU enumeration after 3 weeks of incubation at 37^{o}C.

In parallel, we confirmed the tolerance of 9-day dormant *Mtb-lux* culture to RIF and INH by comparing it to the *Mtb-lux* culture grown under normoxic conditions (37ºC, 5% CO_2). Briefly, *Mtb-lux* grown either in multiple stress media or Complete Dubos medium supplemented with 10% Dubos-medium-albumin-supplement was added to two separate 384-well white solid bottom plates with 8-point dilutions of RIF (0.5-0.003 µM) and INH (1-0.015 µM). Negative controls (0.5% DMSO) were also included in both the plates. Plates were appropriately incubated under hypoxic and normoxic conditions for 5 days. Aliquots were diluted and plated on 7H10 OADC for CFU enumeration. We routinely observe a shift in MIC of >500-fold higher for INH and >100-fold higher for RIF of the bacilli grown under MSD conditions as compared to the normoxic culture, indicating the dormant nature of *Mtb [327]*.

BCG drug resistant strains construction

M. bovis (BCG) strains resistant to rifampicin and ciprofloxacin were obtained by selecting for spontaneous mutations in *rpoB* and gyrase genes, respectively. Briefly,BCG grown on 7H9/OADC media was plated onto 7H10 agar plates

containing either 1 µg/mL RIF or 2 µg/mL CIP. Spontaneous resistant colonies were grown, PCR amplified for *rpoB* and *gyrA* genes and sequence confirmed. The *rpoB* primers- *rpoB*_sym200_F: 5' GTCGCCGCGATCAAGGAGTT 3' and *rpoB*_sym200_R: 5' CCCTCAGGGGTTTCGATCGGG 3' and *gyrA* primers- -*gyrA.SNP.PCR-F*: 5' ATTGCCGTTCCACGGATC 3' and *gyrA.SNP.PCR*_R: 5' GGGCGATATCGACGGTCT 3' were used. A dual RIF and fluoroquinolone resistant mutant strain was generated in the RIF^R strain background by the same process. These BCG drug resistant strains- and the wild-type BCG were electroporated with plasmid pMV306hsp+LuxG13 [378]to give RIF^R-*lux*, RIF^R FLQ^R-*lux* and BCG-*lux* strains.The plasmid is a gift from Brian Robertson and Siouxsie Wiles (Addgene # 26159). Transformants were selected on 7H10 KAN plates. To confirm their drug resistant phenotype, a dose-response curve analysis for RIF (12-0.0004 µM), CIP (64-0.002 µg/mL), and gold compound **14** (200-0.006 µM) was performed with these autoluminescent BCG drug resistant strains along with the wild-type BCG control as described earlier.

Results

Gold compounds effectively inhibit replicating *Mtb* and *Mab*

Initially 19 bis(pyrrolide-imine) gold(III) compounds (macrocycles and simple chelates) were screened at a single concentration (5 μM) for 3 and 5 days against *Mab*-RGand *Mtb*-RG, respectively. Five compounds inhibited *Mtb* and four inhibited *Mab* above the defined threshold levels (>50% inhibition relative to untreated controls; data not shown). Compounds **10**, **11**, **14**, and **15** were identified as inhibitors of both mycobacterial species. One compound (**8**) inhibited only *Mtb*-RG. The chemical structures for all 5 active scaffolds are shown in Figure 1.

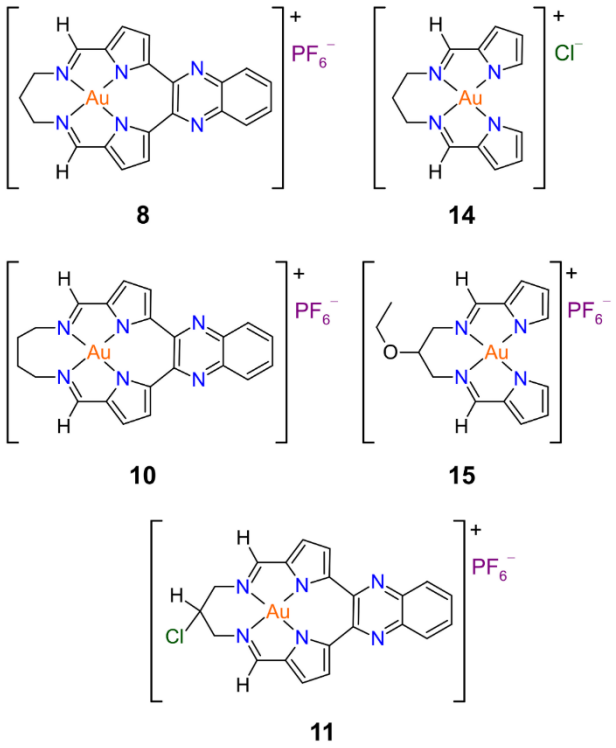

Figure 24. Structures of the bis(pyrrolide-imine) gold(III) macrocycles (8, 10, 11) and chelates (14 and 15) active against mycobacteria.
In the study by Akerman and collaborators [366], compounds 1, 3 and 5 correspond to **8, 10** and **11** in the present paper.

A luminescent readout (*Mtb*-Luxand *Mab*-Lux) was chosen for secondary assays to further characterize the activity of the hit compounds. Potency of the 5 active compounds was assessed by MIC determination (Table 6). Compound **10** had the lowest MIC (*Mtb* - 0.12 µM, *Mab* – 5.4 µM), followed by **14** (*Mtb* – 0.98 µM, *Mab* – 11.9 µM). The other 3 compounds had MIC_{Mtb} values above 1. The dose-response curves in Figure 25 showed that all dual active compounds displayed a lower potency towards *Mab* compared to *Mtb*. The cytotoxicity of these 5 active

compounds was tested against J774 macrophages with IC_{50} ranging from 42.3 µM to 108.5 µM. The SI (relative to MIC_{Mtb}) of **10** and **14** were 172 and 42, respectively. The complete antimicrobial and cytotoxicity profiles are shown in Table 2.

Table 6. Activity profiles of 5 active gold(III) complexes

	MIC		IC_{50}	SI (MIC/IC_{50})	
Compound	***Mtb***	***Mab***	**J774**	***Mtb***	***Mab***
8	2.7	849.4	48.5	17.8	0.1
10	0.1	5.4	85.8	715.2	15.8
11	4.1	91.7	108.5	26.7	1.2
14	1.0	12.0	42.3	43.2	3.5
15	4.6	13.1	48.9	10.6	3.7

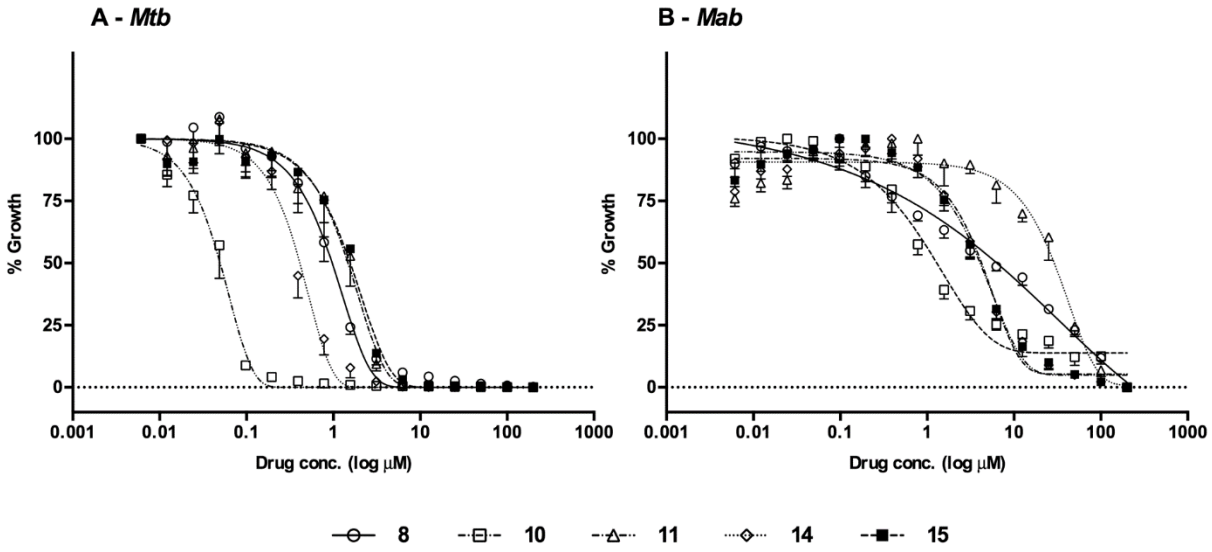

Figure 25. Dose dependent activity of bis(pyrrolide-imine) gold(III) complexes (macrocycles and simple chelates) against Mtb and Mab.
Bacterial cultures were treated for 3 (*Mab*) and 5 days (*Mtb*) after which the luminescence was read. Concentrations of compounds ranged from 200 µM to 0.006 µM in 2-fold 16-point serial dilutions. The data reflect an average of three experiments with standard deviations shown as error bars.

Gold compounds exhibit diverse modes of action

Next, we conducted time-kill kinetics experiments on the 5 active compounds to validate their activity by CFU enumeration and determine their mode of action. As seen in Figure 3A and B, the gold (III) macrocycles **8** and **10** inhibited *Mtb* by less than 1-log CFU/mL at 1, 2, 4 and 8X MIC. Concentrations of 16, 32 and 64X MIC of **10,** which had the lowest MIC, were also tested to ensure that this compound was not bactericidal even at higher concentrations. However, only moderate bacterial killing (1-log decrease relative to vehicle control) was observed at 64X MIC. Nonetheless, a >1-log decrease in CFU/mL was noted with this compound at an early time-point (24 h) which suggests that some bactericidal activity is present, and diminishes at later time-points (Figure 26C).

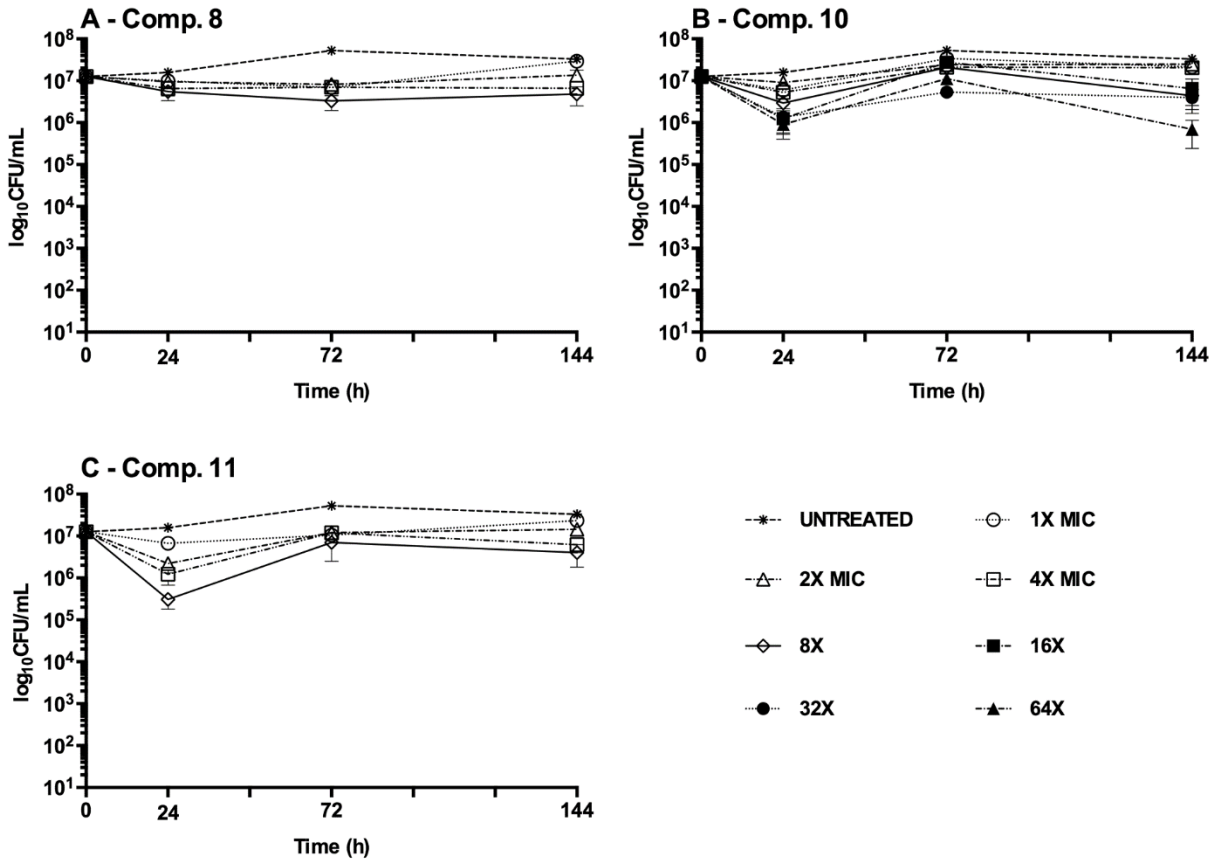

Figure 26. Bactericidal activity of bis(pyrrolide-imine) gold(III) complexes (macrocycles) against Mtb
Mtb culturewas treated with the compounds for up to 6 days. Compound concentrations ranged from 1X to 8-X MIC for **8** (A)**, 11** (C), andup to 64-XMIC for **10** (B). After each time point (0 h, 24 h, 72 h and 144 h) samples were taken from treated and untreated wells and plated for CFU/mL enumeration. The data are an average of three experiments with standard deviations shown as error bars.

Two of the bis(pyrrolide-imine) gold(III) chelates, **14** and **15,** exhibited rapid and potent bactericidal activity. A slight decrease in CFU/mL (<1 log) was observed at 24 h upon treatment with 1 and 2X MIC of **14** and **15** followed by recovery to vehicle control levels at the later time-points (Figure 27). However, treatment with concentrations at 4- and 8X of MIC resulted in ~2-4-log decreases in CFU within

24 h. Though both **14** and **15** displayed bactericidal activity, **14** was more potent based on the magnitude of the decrease in CFU/mL. Additionally, the facile and inexpensive chemical synthesis for **14** provided high yields, enabling detailed characterization of this compound. Because the patent reports only brief details on the structure of **14**, and the three-dimensional atomic coordinates are not available to the scientific community [367], we have elected to report more fully the structure of **14** here (see below) because of its significance as a novel metal-organic bactericide.

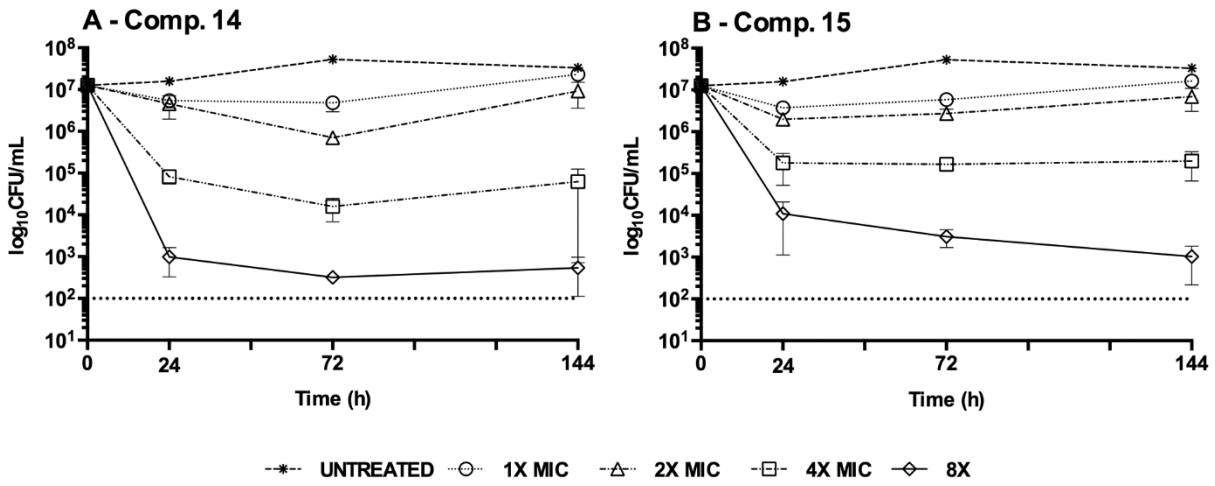

Figure 27. Bactericidal activity of bis(pyrrolide-imine) gold(III) complexes (simple chelates) against Mtb.
Mtb culturewas treated with the compounds for up to 6 days with concentrations ranging from 1X to 8-X MIC for **14** (A), **15** (B). After each time point (0 h, 24 h, 72 h and 144 h) samples were plated from treated and untreated wells and CFU/mL was enumerated. The data are an average of three experiments with standard deviations shown as error bars.

Given the potent bactericidal activity of **14** against *Mtb*, we sought to determine if the mode of action was similar against *Mab.* The mode of action of **14** was evaluated against *Mab* at 1, 2, 4 and 8X MIC (Figure 28). Since *Mab* is a fast-growing mycobacterium, the experiment was carried out for 72 h instead of 144 h, and data were collected every 24 h. Similar to our observations with *Mtb*, both 4- and 8X MIC yielded significant reductions in CFU. While we did see a 1-log rebound in CFU at later time-points with 4X MIC treatment, 8X MIC resulted in a

4-log decrease by 48 h with apparent sterilization of the culture by 72 h. These data demonstrate the potent bactericidal activity of **14** against *Mab*.

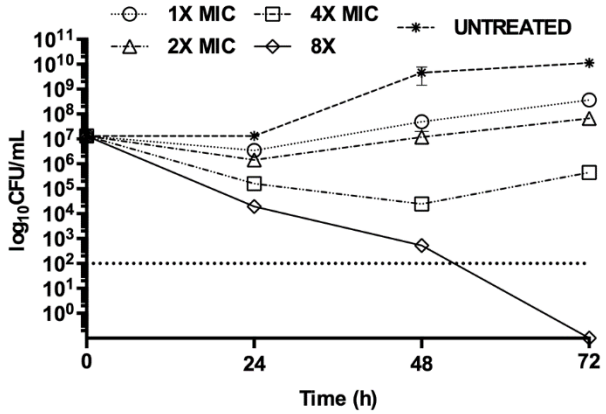

Figure 28. Bactericidal activity of bis(pyrrolide-imine) gold(III) complex 14 (simple chelate) against Mab.
Mab 390S culturewas treated with compounds for up to 3 days. Compound concentrations ranged from MIC to 8-X MIC. After each time point (0 h, 24 h, 48 h and 72 h) samples were platedfrom treated and untreated wells and CFU/mL was calculated.

Compound 14 shows no cross-resistance with rifampicin and fluoroquinolones

Compound **14** was further characterized in this study considering its potent bactericidal activity profile against both *Mtb* and *Mab*. Gold(III) macrocyles with similar scaffolds have been shown to target mammalian topoisomerases [366]. Since fluoroquinolones (FLQ) target *Mtb* gyrase, a bacterial type II topoisomerase enzyme [379], we sought to determine if FLQ^R mycobacteria

would be cross resistant to **14**. Additionally, cross-resistance with RIF was investigated due the high incidence of RIF^R*Mtb* strains in the clinic [380]. MICs of ciprofloxacin (CIP), moxifloxacin (MOX) and RIF were determined using two bioluminescent drug-resistant BCG strains: (i) a RIF^R & FLQ^R strain (*gyrA mutation:* D94Gand *rpoB* mutation:S531L); and (ii) a RIF^R strain (*rpoB* mutation, S531W), both in addition to the parent wild-type BCG-*lux* strain. The MIC of CIP and MOX against FLQ^R/RIF^R was 64- and 128-fold higher than against the wild-type BCG-*lux*, respectively. The RIF^R and FLQ^R/RIF^R strains of BCG were completely resistant to RIF, as 100% survival was observed for these strains at all tested concentrations (data not shown). When **14** was tested against these strains all the MICs were equal to BCG WT suggesting that there is no cross-resistance to **14** in FLQ^R and RIF^R strains of BCG (Figure 29).

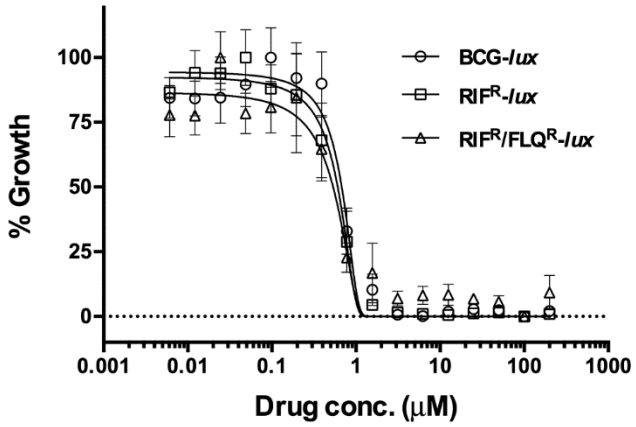

Figure 29. Sensitivity of drug resistant M. bovis BCG to compound 14. Wild-type (BCG-*lux,* open circle), a RIF resistant strain with *rpoB* mutation (RIF^R-*lux*, open square), a RIF and FLQ resistant mutant strain containing mutations in *gyrA* and *rpoB* (RIF^R/FLQ^R-*lux*, open triangle) were treated with compound **14** (200 to 0.006 μM) for 5 days after which luminescence was read. The data are an average of three experiments with standard deviations shown as error bars.

Compound 14 is active against clinical isolates and dormant *Mtb*

To further establish the potential clinical utility of this compound, the activity of **14** was tested against a panel of 5 clinical isolates of *Mtb* from different phylogenetic lineages (Table 5). As seen in Figure 30, at 5 μM **14** was similarly active against all 5 *Mtb* clinical isolates and *Mtb* CDC1551.

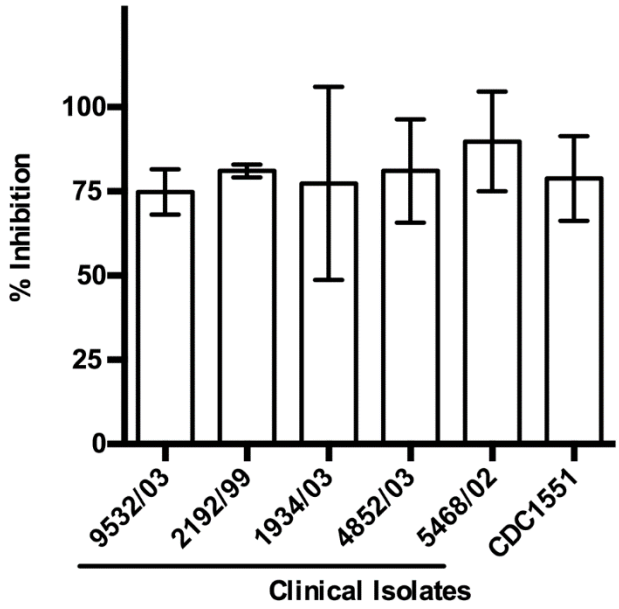

Figure 30. Activity of compound 14 against clinical isolates of Mtb.
Five clinical isolates of *Mtb* from different phylogenetic lineages and the reference strain CDC1551 were treated with 5 μM of compound **14** for 5 days. Percent inhibition values are an average from three independent experiments where error bars represent the standard deviation.

Next, we assessed the ability of **14** to kill dormant Mtb, which are phenotypically tolerant to front-line TB drugs, severely delaying bacterial clearance during treatment [43]. We used an *in vitro* multistress dormancy model that yields bacilli exhibiting phenotypes associated with dormancy *in vivo*: altered acid fast staining, accumulation of lipid droplets, upregulation of the DosR regulon, and tolerance to front-line antibiotics [61]. Cultures of *Mtb-lux* are pre-adapted in a combination of dormancy-inducing conditions (acidic pH, hypoxia and nutrient starvation) before addition of compounds. We observed a >1-log decrease in

CFU/mL upon treatment with 4X MIC of **14** for 5 days as compared to the vehicle controls (day 5), indicating that **14** is able to kill phenotypically tolerant *Mtb* (Figure 31). Treated samples were compared to controls on day 5 since a reduction in viability of dormant bacteria was observed between day 0 and day 5 of the experiment, consistent with previously reported data [327]. A less significant decrease in CFU/mL (0.5 log) was observed at 8X MIC than 4X; this could be due to lowered solubility of the compound under acidic pH. In contrast to compound **14**, we have shown that RIF at 4X MIC does not kill dormant bacilli [327]; this highlights the potential of **14** in a more clinically relevant context.

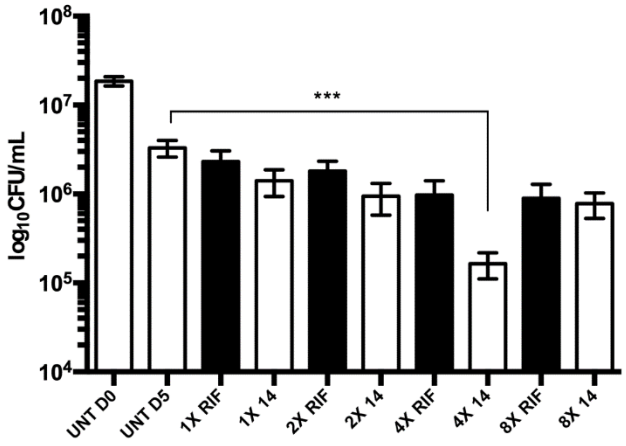

Figure 31. Activity of compound 14 against dormant Mtb.
Cultures of *Mtb* adapted for 9 days in multiple stress conditions were treated for 5 days with **14** (open bars) and RIF (closed bars) at 1, 2, 4 and 8-X MIC. The data are an average of three experiments with standard error shown. (*** $p < 0.0005$).

X-ray structure of compound 14

Because of the significant potential of **14** as a novel metal-organic bactericidal agent, the X-ray structure of the compound is essential to gaining a deeper understanding of its three-dimensional stereochemistry at atomic resolution. The information will be pivotal to future *in silico* and experimental studies aimed at delineating the protein and/or DNA targets of the compound. The X-ray structure of **14** is shown in Figure 32. The Au(III) ion has the expected square planar geometry for a d^8 metal ion. The $Au–N_{(imine)}$ and $Au–N_{(pyrrole)}$ bond distances are chemically and structurally unique, averaging 2.017(4) and 1.998(6) Å, respectively. The $N_{(pyrrole)}–Au–N_{(imine)}$ bond angles within the pyrrolide-imine chelate rings average 80.8(1)°, while the intrachelate bond angle, N2–Au–N3, which measures 95.97(8)°, is significantly more acute than the exo-chelate bond angle (N1–Au–N4, 102.53(9)°). The metrical parameters for the *cis* bond angles involving the gold(III) ion therefore deviate from the ideal square planar geometry values (90°). The *trans* $N_{(pyrrole)}–Au–N_{(imine)}$ bond angles are, however, closer to the ideal value of 180°, averaging 175.9(9)°.

The conformation of the propyl-bridged bis(pyrrolide-imine) ligand in **14** is nonplanar as evidenced by slight tipping of the pyrrole ring containing N4 below the 15-atom mean plane defined by the Au(III) ion and two chelating pyrrolide-imine groups. The maximum atomic displacement relative to this plane is –18 pm

for the pyrrole β-carbon atom C12, while the Au(III) ion is displaced +7 pm above this plane. The conformation of the central 6-membered chelate ring (Au–N2–C6–C7–C8–N3) is a distinct half-chair with the azimuthal methylene group (C7) of the propyl chain located above the three chelate rings and Au(III) ion. Notably, the chloride counterion forms a significant short contact (Au···Cl) to the Au(III) ion, which measures 3.1831(8) Å, and suggests an electrostatic interaction for the ion pair in the solid state. The two complex cations form a π-stacked dimer with crystallographically imposed inversion symmetry. The interplanar spacing of this π-stacked dimer measures 3.2575(1) Å and the shortest nonbonded contact (3.146(4) Å) occurs between a pyrrole β-C atom (C13) of one ligand and the imine carbon atom (C5′) of the partner ligand. The gold(III) ions are separated by a distance of 4.1636(4) Å in the dimer and the Au^{3+} ion of one complex cation is stacked atop a pyrrole nitrogen atom (N4′) of the partner cation in the pair; the Au···N4′ distance measures 3.434(3) Å.

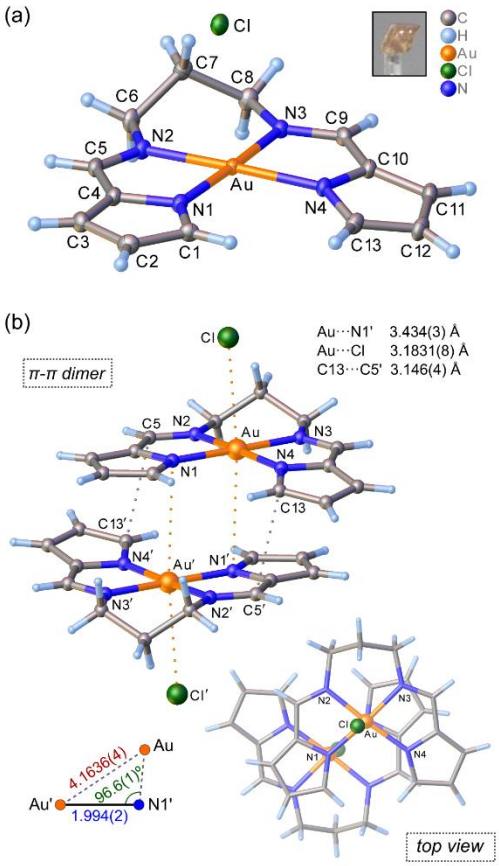

Figure 32. Low-temperature X-ray structure of compound 14.
(a) Thermal ellipsoid diagram of the molecular structure (50% probability ellipsoids for non-H atoms) showing the conformation of the complex Au(III) cation and the location of the closest chloride ion in the asymmetric unit. The crystallographic atomic numbering scheme is indicated. Selected bond distances (Å): Au–N1, 1.994(2); Au–N2, 2.014(2); Au–N3, 2.020(2); Au–N4, 2.002(2). (b) View of the closely interacting ion pair between adjacent molecules (related by inversion symmetry) in the crystal lattice. The cations are π–stacked in a laterally-offset manner. Key short contacts (in Å) for the symmetry-unique interactions are shown along with the Au···Au′ distance. The interplanar spacing measures 3.2575(1) Å.

Table 7. Crystal data and structure refinement for Compound 14.

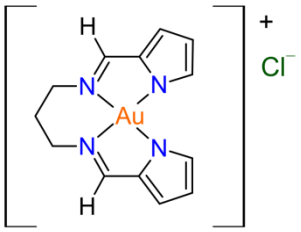

14

Identification code	AuL1Cl
Empirical formula	$C_{13}H_{14}AuClN_4$
Formula weight	458.70
Temperature/K	140.15
Crystal system	triclinic
Space group	P-1
a/Å	7.5888(4)
b/Å	9.4183(3)
c/Å	10.5118(4)
α/°	68.707(4)
β/°	72.787(4)
γ/°	72.194(4)
Volume/Å^3	651.86(5)
Z	2
ρ_{calc}g/cm^3	2.337
μ/mm^{-1}	11.479
F(000)	432.0
Crystal size/mm^3	0.1 × 0.1 × 0.1
Radiation	MoKα (λ = 0.71073)
2Θ range for data collection/°	7.276 to 68.306
Index ranges	-11 ≤ h ≤ 11, -14 ≤ k ≤ 13, -15 ≤ l ≤ 15
Reflections collected	10708
Independent reflections	4501 [R_{int} = 0.0173, R_{sigma} = 0.0206]
Data/restraints/parameters	4501/0/172
Goodness-of-fit on F^2	1.020
Final R indexes [I>=2σ (I)]	R_1 = 0.0163, wR_2 = 0.0390
Final R indexes [all data]	R_1 = 0.0187, wR_2 = 0.0393
Largest diff. peak/hole / e Å^{-3}	1.67/-1.87

Table 8. Fractional Atomic Coordinates (×104) and Equivalent Isotropic Displacement Parameters (Å2×103) for AuL1Cl. Ueq is defined as 1/3 of of the trace of the orthogonalised UIJ tensor.

Atom	*X*	*y*	*z*	U(eq)
C1	6461(3)	9847(3)	6009(2)	16.6(4)
C2	5947(3)	8973(3)	7401(2)	19.2(4)
C3	7240(3)	7536(3)	7622(2)	18.1(4)
C4	8521(3)	7562(3)	6357(2)	15.4(4)
C5	10157(3)	6530(2)	5864(2)	15.3(4)
C6	12726(3)	6086(3)	3917(2)	17.6(4)
C7	12737(3)	6339(3)	2406(2)	17.3(4)
C8	13136(3)	7909(3)	1432(2)	18.1(4)
C9	11258(3)	10546(3)	693(2)	16.3(4)
C10	9747(3)	11744(3)	1050(2)	16.0(4)
C11	9153(3)	13345(3)	412(2)	19.2(4)
C12	7711(3)	13911(3)	1405(3)	21.4(4)
C13	7457(3)	12655(3)	2611(3)	18.1(4)
N1	8025(3)	8990(2)	5381(2)	13.9(3)
N2	10984(3)	7013(2)	4560(2)	14.7(3)
N3	11553(3)	9214(2)	1654.8(19)	13.9(3)
N4	8689(3)	11340(2)	2393(2)	14.9(3)
Cl	2602.1(7)	2663.4(6)	7187.1(6)	17.46(9)
Au	9726.7(2)	9162.3(2)	3503.7(2)	11.56(3)

Table 9. Anisotropic Displacement Parameters (Å2×103) for AuL1Cl. The Anisotropic displacement factor exponent takes the form: -2π2[h2a*2U11+2hka*b*U12+…].

Atom	U_{11}	U_{22}	U_{33}	U_{23}	U_{13}	U_{12}
C1	14.6(9)	17.2(10)	17.6(10)	-7.7(8)	-2.0(8)	-1.4(7)
C2	16.7(9)	21.6(11)	18.9(10)	-8.4(9)	1.0(8)	-5.5(8)
C3	19.9(10)	18.1(10)	14.5(9)	-2.2(8)	-2.2(8)	-6.5(8)
C4	16.9(9)	13.6(9)	14.0(9)	-2.0(7)	-2.7(7)	-4.4(7)
C5	16.1(9)	12.3(9)	15.8(9)	-1.1(8)	-5.8(8)	-2.4(7)
C6	11.7(8)	14.1(9)	20.1(10)	-1.7(8)	-2.4(8)	1.5(7)
C7	15.3(9)	14.2(9)	18.8(10)	-5.9(8)	0.5(8)	-1.2(7)
C8	12.9(9)	17.7(10)	19.2(10)	-4.8(8)	0.7(8)	-1.7(7)
C9	19.1(10)	16.7(9)	12.6(9)	-1.7(8)	-2.1(8)	-7.6(8)
C10	19(1)	13.1(9)	14.7(9)	-1.0(8)	-4.8(8)	-4.3(7)
C11	22.1(10)	15.2(10)	17.6(10)	0.9(8)	-6.6(8)	-5.3(8)
C12	20.2(10)	11.9(9)	28.0(12)	-0.2(9)	-8.8(9)	-1.0(8)
C13	15.9(9)	13.7(9)	22.4(11)	-3.7(8)	-3.8(8)	-2.0(7)
N1	12.3(7)	11.9(8)	16.0(8)	-2.4(7)	-3.1(6)	-2.3(6)
N2	12.3(7)	12.0(7)	17.3(8)	-3.1(7)	-3.7(7)	-0.2(6)
N3	12.8(7)	13.6(8)	13.8(8)	-3.0(7)	-2.7(6)	-2.3(6)
N4	16.0(8)	11.3(8)	15.5(8)	-1.1(7)	-4.7(7)	-2.8(6)
Cl	15.1(2)	14.9(2)	19.5(2)	-2.69(19)	-4.17(18)	-1.85(17)
Au	11.26(4)	10.09(4)	11.79(4)	-1.76(3)	-2.40(3)	-2.09(2)

Table 10. Bond Lengths for AuL1Cl.

Atom	Atom	Length/Å	Atom	Atom	Length/Å
C1	C2	1.399(3)	C9	C10	1.411(3)
C1	N1	1.354(3)	C9	N3	1.299(3)
C2	C3	1.393(3)	C10	C11	1.399(3)
C3	C4	1.392(3)	C10	N4	1.381(3)
C4	C5	1.415(3)	C11	C12	1.393(4)
C4	N1	1.386(3)	C12	C13	1.396(3)
C5	N2	1.300(3)	C13	N4	1.353(3)
C6	C7	1.515(3)	N1	Au	1.9941(19)
C6	N2	1.470(3)	N2	Au	2.0139(18)
C7	C8	1.523(3)	N3	Au	2.0196(18)
C8	N3	1.466(3)	N4	Au	2.0022(18)

Table 11. Bond Angles for AuL1Cl.

Atom	Atom	Atom	Angle/˚	Atom	Atom	Atom	Angle/˚
N1	C1	C2	108.7(2)	C1	N1	Au	139.02(16)
C3	C2	C1	107.8(2)	C4	N1	Au	112.85(14)
C4	C3	C2	106.6(2)	C5	N2	C6	122.86(18)
C3	C4	C5	136.1(2)	C5	N2	Au	114.57(14)
N1	C4	C3	108.81(19)	C6	N2	Au	122.54(14)
N1	C4	C5	115.05(19)	C8	N3	Au	123.50(14)
N2	C5	C4	116.90(19)	C9	N3	C8	122.67(19)
N2	C6	C7	110.87(18)	C9	N3	Au	113.74(15)
C6	C7	C8	113.49(19)	C10	N4	Au	112.24(14)
N3	C8	C7	112.06(18)	C13	N4	C10	107.63(18)
N3	C9	C10	117.6(2)	C13	N4	Au	138.83(17)
C11	C10	C9	134.8(2)	N1	Au	N2	80.59(7)
N4	C10	C9	115.43(19)	N1	Au	N3	176.54(7)
N4	C10	C11	109.3(2)	N1	Au	N4	102.53(8)
C12	C11	C10	106.1(2)	N2	Au	N3	95.98(7)
C11	C12	C13	107.8(2)	N4	Au	N2	175.26(7)
N4	C13	C12	109.2(2)	N4	Au	N3	80.87(8)
C1	N1	C4	108.11(19)				

Table 12. Hydrogen Atom Coordinates (Å×104) and Isotropic Displacement Parameters (Å2×103) for AuL1Cl.

Atom	*X*	*y*	*z*	U(eq)
H1	5818	10873	5575	20
H2	4903	9299	8076	23
H3	7247	6703	8470	22
H5	10629	5531	6457	18
H6A	12823	4964	4441	21
H6B	13837	6392	3965	21
H7A	11493	6263	2346	21
H7B	13710	5494	2086	21
H8A	14286	8056	1586	22
H8B	13386	7910	452	22
H9	12033	10708	-219	20
H11	9634	13929	-510	23
H12	7023	14964	1283	26
H13	6562	12714	3451	22

Discussion

Pulmonary diseases caused by *Mtb* and opportunistic NTM pathogens like *Mab* represent a significant burden on global health. They pose a major challenge to clinicians because of the lack of effective therapeutic options capable of clearing these infections. In addition to unacceptably long treatment regimens and poor cure rates, drug-resistant strains are increasingly encountered. To address this crisis, novel antibiotics against mycobacteria are urgently needed which meet a rigorous set of criteria including potent and rapid bactericidal activity, high

selectivity for bacteria versus mammalian cells, and a novel mechanism of action that precludes cross-resistance with existing antibiotics. Dual activity against *Mtb* and *Mab*, an uncommon trait among existing TB drugs, would allow broader clinical usage against these related mycobacterial pathogens. Knowledge of the target of a novel drug candidate can be critical for medicinal chemistry optimization of lead compounds. In this study, we have used whole-cell assays to assess the potential of repurposing a novel series of bis(pyrrolide-imine) gold(III) macrocycle inhibitors of human topoisomerase I [366] from anticancer candidates into therapeutics targeting *Mtb* and *Mab.* We identified multiple gold(III) compounds that potently inhibited both *Mtb* and *Mab*by two distinct modes of action that argue for further hit-to-lead development of this unique class of compounds. This work builds on the historical success of metal complexes against bacterial infections [381] along with the recent discoveries that metallodrugs originally investigated as anticancer agents are faring well as repurposed antibacterial agents [363, 365].

Pulmonary infections caused by NTM such as *Mab* are frequently misdiagnosed as MDR-TB due to nonspecific detection of acid-fast bacilli in sputum specimens and lack of susceptibility to front-line TB drugs [342]. Although effective multidrug cocktails for drug-susceptible *Mtb* exist, treatment options for *Mab* infections are limited to macrolides and intravenous aminoglycosides combined with a beta-lactam antibiotic (i.e. imipenem) [285]. Clinically used drugs such as amikacin and clarithromycin are very ineffective against *Mab*, considering poor *in*

vitro bactericidal activity even at 32 and 64-fold MIC [382]. Likely as a result, the relapse rates after treatment are alarmingly high [284, 383]. In this study, our panel of compounds contained both gold(III) macrocycles as well as smaller gold(III) chelates. Two of the macrocycles, **8** and **11**, showed potent inhibition of *Mtb* but not *Mab* with MIC_{Mtb} of 2.72 and 4.06 μM respectively compared to MIC_{Mab} of ~850 μM and ~90. Interestingly, compound **10**, which is structurally very similar to **8** and **11,** exhibited the lowest MIC against both *Mtb* and *Mab* (MIC_{Mtb} =0.12 μM, MIC_{Mab} =5.44 μM). We also discovered two dual active gold(III) chelates, **14** and **15,** that were able to inhibit both mycobacterial species. The lower potency of these compounds against *Mab* in comparison to *Mtb* could be due to a higher affinity for the target in *Mtb* or alternatively could arise from differences in cell wall permeability or efflux mechanisms between these two pathogens. Novel classes of antibiotics with potent activity against both *Mtb* and *Mab* like these gold(III)-based compoundscould make a significant impact on the treatment of these diseases.

Analysis of the kinetics of bacterial killing by time-kill curves revealed distinct profiles for gold(III) macrocycles (compounds **8, 10, 11**) and gold(III) chelates (compounds **14** and **15**). Despite the fact that **10** had the lowest MIC_{Mtb} (0.12 μM), the macrocycles were almost completely bacteriostatic against *Mtb*. It is worth noting that the lack of cidal activity would not exclude them from clinical utility because bacteriostatic drugs such as ethambutol [384] are key

components of front-line regimens for TB and other mycobacterial diseases. We did observe a transient decrease in viable CFU (<1 log) at the higher concentrations of **10** and **11** at the 24hr time point. This could be attributed to activation of inducible drug resistance mechanisms by *Mtb* or perhaps to instability of these compounds. In contrast to the gold(III) macrocycles, the smaller "one-sided" metal chelates **14** and **15** led to a rapid bactericidal effect on *Mtb*, with 2-4 log decreases in viable CFU at only 4X and 8X MIC. We noted similar bactericidal activity for **14** towards *Mab*. Such compounds with a potent, cidal mode of action may help shorten treatment times and prevent the appearance of drug-resistant mutants over the course of treatment. It is worth nothing that complete sterilization of *Mtb* was not achieved with **14** under the conditions tested. This kinetic profile could be due to the presence of a small minority of persistor bacilli in the population, which are phenotypically tolerant to antimicrobials [43]. Alternatively, this could be attributed to instability of the molecule or activation of inducible drug resistance mechanisms.

The feasibility of repurposing these gold(III) compounds, originally designed as anticancer agents, was validated by the high level of selectivity we found in their whole cell activity against *Mtb* versus mammalian cells. Selectivity indices (IC_{50}/MIC) ranging from 10, which is generally acceptable for early stage screening hits, to as high as 43 (**14**) and 715 (**10**), indicate a high degree of specificity for bacterial targets. This can serve as a good indicator of low toxicity and potential safety for *in vivo* usage. The scalable synthesis of **14** made it

possible to also test this compound in a model of drug tolerant, non-replicating *Mtb* dormancy. The ability of this compound to kill dormant *Mtb* better than the front-line drug RIF (Figure 31) may translate into an enhanced ability to eliminate dormant persistor populations of *Mtb* within granulomas and other reservoirs of infection.

The different bioactivity profiles observed for **10** and **14**, which could potentially reflect two distinct targets or mechanisms of action, may be partially rationalized based on the chemical properties of each molecule. The Au(III) ion from **10** cannot be lost since it is very tightly bound within the macrocycle and particularly stable under cellular reducing conditions (i.e., mM concentrations of glutathione, GSH) [366]. On the other hand, *slow* reductive demetallation of **14** by GSH has been observed (k_2 = 0.0463(2) M^{-1} s^{-1} in pH 7 phosphate buffer, 37 °C; unpublished data [385]). From the UV-vis spectral data, this demetallation reaction leads to the formation of the free protonated bis(pyrrole-imine) ligand and release of the gold(III) ion (probably as the Au^{+} ion), either of which could account for the potent bactericidal activity of **14** as compared to **10.** Investigating the role of the bis(pyrrolide-imine) ligand in shaping the activity of **14** will help clarify the compound's mechanism of action. It is noteworthy that a bio-distribution study [386] with ^{198}Au-labelled **14** in Sprague Dawley rats showed that the intravenously injected compound accumulated in the lungs (the resident time in the lungs had a half-life > 24 h). This could be significant for the development of this class of metallodrugs, which are aimed specifically at

targeting bacterial infections in the lungs. Clearly, further work will be required to fully delineate how the structures of the gold(III) compounds affect their interactions with biomolecules. Perhaps more importantly, future studies will need to focus on verifying the target(s) and mechanism of action of these repurposed metallodrug candidates in mycobacteria.

We initially reported detailed characterization of this series of bis(pyrrolide-imine) gold(III) macrocycles and chelates as inhibitors of human topoisomerases by a novel mechanism [366]. *In vitro* enzyme assays with human topoisomerases show that **10** is a catalytic inhibitor of topoisomerase I [366], whereas **14** acts as a topoisomerase II poison at low doses and a catalytic inhibitor of the enzyme at high doses [367, 385]. However, in comparison to their potent selective activity against mycobacterial cells reported in this study, their activity against the human enzyme and human cancer cell lines was relatively poor. Our future studies will be guided by the hypothesis that their antibacterial activity is also due to inhibition of this class of enzymes, albeit with a higher affinity for the mycobacterial homologs. DNA topoisomerases, which provide the essential function of modulating DNA topology [387], are ubiquitous and generally conserved among living organisms [388]. These enzymes have been widely studied in mycobacterial species and their essentiality and "druggability" is well established [389-391]. Gyrase (type II topoisomerase) inhibitors such as fluoroquinolones have become well-established tools for combating *Mab* and drug-resistant *Mtb*, and evidence suggests they could shorten TB treatment

duration in combination therapy [115, 283, 392]. The clinical usage of fluoroquinolones also proves that inhibitors of bacterial topoisomerases can be selective and safe. Although topoisomerase I inhibitors are not yet in clinical use for treatment of mycobacterial infections, recent screening studies have identified promising small-molecule inhibitors targeting this enzyme in *Mtb*[393, 394]. Novel classes of antimicrobials that act on these extensively validated targets would provide much needed tools for the treatment of *Mtb* and *Mab* infections.

We do have some insight into the potential mechanism of action of the current antibacterial gold(III) compounds. The X-ray structural data for **14** (Figure 32) and **10**[366] reveal that the bis(pyrrolide-imine) chelates in the two classes of compounds have similar structures around the Au(III) ion with bond distances and angles that are within 1% of each other for the two compounds. Further, the cations in **10** and **14** are both capable of forming well-defined noncovalent π-π stacking interactions. Importantly, the ability of the Au(III) ion to interact electrostatically with electron-rich donors such as the carbonyl oxygen atom of thymine in dsDNA was found to be pivotal in the mechanism of action of **10** (specifically its ability to bind DNA at the same 5′-TA-3′ site targeted by human topoisomerase I) [366]. Clearly, **14** may have the ability to bind DNA in a similar way to **10** and a relatively high binding constant, $K_A = 2.1(2) \times 10^5\ M^{-1}$ (pH 7.0 phosphate buffer, 37°C), has indeed been determined for the reaction between **14** and calf thymus DNA [367]. The exact mechanism whereby **14** binds DNA,

however, has not been delineated and is part of an on-going investigation. It is important to note that the Au(III) ion is chelated by a tetradentate ligand in **14**. This means that any covalent interaction with a protein residue such as His or Cys would need to displace a pyrrole ring nitrogen from the coordination sphere of the Au(III) ion. This is not likely (though not impossible) on thermodynamic grounds because pyrrolide anions are powerful σ-donors to metal cations. Until further data emerge, the possibility that **14** interacts with topoisomerases and DNA purely through noncovalent interactions (e.g., electrostatics, London forces, and non-classical H-bonding) must be considered when *in silico* or experimental QSAR (quantitative structure activity relationship) studies commence.

Identifying drug targets and elucidating mechanisms of action will be crucial for the continued hit-to-lead development of bis(pyrrolide-imine) gold(III) macrocycles and chelates as antimycobacterial agents. We will exploit a variety of methods, including *in vitro* enzyme assays using *Mtb* gyrase and topoisomerase 1 and genetic approaches such as whole genome sequencing of spontaneous resistant mutants, to test our working hypothesis. Importantly, the lack of cross-resistance between **14** and fluoroquinolones indicates that clinically relevant gyrase mutations that abrogate binding of fluoroquinolones would not affect the sensitivity to this class of gold(III)-based compounds. Knowledge regarding the target and mechanism of action will facilitate optimization of these scaffolds to increase their selectivity for the mycobacterial enzyme through structure-activity relationship (SAR) studies. We are also keenly interested in

determining which aspects of the current chemical scaffolds drive bactericidal versus bacteriostatic activity. The rapid, cidal activity and ability to kill dormant bacilli bodes well, but the *in vivo* efficacy of these compounds remains to be tested. Although ADME (adsorption, distribution, metabolism, excretion) and PK/PD (pharmacokinetic/pharmacodynamics) properties for this series are not yet known, preliminary work on **10** shows this compound was well-tolerated in female athymic nude mice at a maximum threshold of 400 mg/kg/dose [366]. This is encouraging for future work with active compounds in this class using *in vivo* models of *Mtb* and *Mab* infection.

In conclusion, we have shown that pyrrole-based gold(III) chelates and macrocyles (originally designed to inhibit human topoisomerases, but subsequently found to have inherently low *in vivo* cytotoxicity in the NCI's hollow fiber assay [366]) exhibit potent, selective bactericidal activity against dormant and drug resistant *Mtb* as well as *Mab.* These repurposed metal-organic compounds clearly warrantfurther investigation as a novel class of antibacterial agents that are potentially suitable for entry into the mycobacterial drug pipeline.

CHAPTER 6:

CONCLUSION

This chapter was written by Carolina Rodrigues Felix. Revisions and edits from Kyle Rohde were incorporated to the final version.

Overview of the scope and impact of this work

Since the scope of this work focuses mainly on the discovery and characterization of molecules active against *Mtb*, a legacy of novel scaffolds remains to be further purified and characterized. Much effort remains for the hit-to-lead optimization of prioritized compounds towards the further stages of the drug development pipeline. Additionally, many molecules can be used as chemical tools which provide insight into untapped vulnerable targets and pathways of mycobacteria. This chapter will therefore focus mainly on the future work that can be done with this knowledge base to develop scaffolds into lead compounds and better understand the most vulnerable mycobacterialpathways during infection.

Even though *Mtb* is a well known pathogen, researched for more than a century now, knowledge gaps still remain which hamper the TB treatment success rates and efforts to eradicate this ancient disease. A considerable portion of the drug screening efforts for TB still rely on *in vitro* based screening methods with replicating bacteria, even though several anti-TB compounds which are bactericidal and highly effective against replicating bacteria are already available in the clinic [136]. On the other hand, dormant *Mtb* are tolerant to these and many other antimicrobials, only being affected by very few compounds including pyrazinamide [43]. Considering the high attrition rate in the drug discovery and

development pipeline, more compounds active against dormant*Mtb* should be introduced in the pipeline as this may increase the number of compounds that will progress to the clinical development phase. Therefore, screening efforts should focus on finding compounds active against these dormant bacteria. In this work, we have developed a novel method to screen compound libraries against dormant*Mtb.* This has proven effective, enabling the discovery of scaffolds selectively active against dormant bacteria [327] (Chapter 2). This further emphasized the value of screening libraries primarily against dormant *Mtb*, especially considering many compounds would have gone undetected in a classical screening assay.

Future Directions

The discovery of natural product scaffolds active against *Mtb* provided a significant base from which to derive novel chemistry for the TB drug discovery and development pipeline. Continued deconvolution of hits and structure elucidation will is expected to yield additional pharmacophores for TB drug development and/or target identification. Several molecules discovered in this study are amenable to synthetic chemistry, including the puupehenone-like scaffolds with potent activity against dormant *Mtb* [327] (Chapter 2). This

provides an important stepping stone for further characterization and optimization of these scaffolds. Synthesis of analogs of active molecules will allow the bioassay guided optimization of compounds to reduce toxicity, improve solubility, while maintaining target affinity and mycobacterial cell permeability. Scaling up the synthesis will be imperative for testing these compounds *in vivo* and dissecting their mechanism of action.

Additionally, the activity of these molecules can be evaluated against other mycobacterial pathogens. Even though most NTMs are environmental bacteria, select species, such as *M. abscessus* are opportunistic, highly drug-tolerant causing severe chronic infections in immunocompromised individuals [285]. There is a dire need for more effective treatment options. To achieve this, the gaps in knowledge pertaining to the pathogenesis of NTMs will have to be addressed; and better drug discovery and development technologies urgently need to be established for these infectious agents.

A conserved mycobacterial target to kill two pathogens with one drug

Conserved targets in TB drug discovery can be very useful for identification of molecules which inhibit not only *Mtb* but also other pathogenic mycobacteria. Although clinically utilized second-line drugs for TB (fluoroquinolones) target

mycobacterial type 2 topoisomerases (gyrase), recent studies have demonstrated the potential of the mycobacterial type 1 topoisomerases as drug targets [391, 393-395]. In light of this and the highly conserved nature of topoisomerase I among different realms of life [388], we used compounds known to inhibit human topoisomerase I by a novel mechanism, but with poor activity against cancer cells, as antimycobacterials in whole-cell screening assays (Chapter 5). The target in mycobacteria remains to be confirmed, however the availability of purified mycobacterial topoisomerase I facilitates the validation of gold (III) macrocycle activity against these pathogens. An assay reliant on gel electrophoresis of plasmid DNA incubated with the purified enzyme plus or minus the inhibitor will definitively answer the question whether these compounds inhibit the mycobacterial enzyme, but not whether this is the target of the compound in the bacterial cell [393]. Additional approaches, including isolation of spontaneously resistant mutants and overexpression of the target are underway to confirm the target and address the possibility of off-target activity. Although the same *in vitro* enzyme activity assay can be performed with the purified mycobacterial gyrase, our study suggests this is not the target based on a lack of cross-resistance with fluoroquinolone-resistant *M.bovis* BCG (Chapter 5). Nonetheless, gold(III) macrocycles may bind different portions of *gyrA* and *gyrB*than fluoroquinolones, and should not be discarded as putative targets.

The gold (III) macrocycles described in chapter 5 had 2 distinct chemical scaffolds. In the bactericidal scaffolds, the gold (III) was unstable, and the

compound was vulnerable to demetalation by glutathione, becoming a bis-pyrrole scaffold. The bacteriostatic scaffolds had additional rings which rendered the gold(III) highly stable. Future work will be done using the bis-pyrrole compound derived from the demetalation of the gold (III) macrocycle. The gold (III) macrocycles emits fluorescence at a different wave length than the derived bis-pyrrole compounds. This chemical property of the compounds will allow us to determine if the demetallation is in fact occurring in the mycobacterial cell, by measuring the fluorescence of treated and untreated *Mtb* cultures. Determining the MIC and mode of action of the bis-pyrrole scaffold will reveal whether the observed bactericidal activityis due to the compound or the released gold (III). Use of the bis-pyrrole molecule will help determine if the gold (III) macrocycle is working as a pro-drug. In that case, mutants resistant to the precursor gold (III) macrocycles may harbor mutations on different genes than mutants resistant to the bis-pyrrole scaffold. Additionally, we will synthesize the macrocycles using different metals to verify whether the activity is gold-dependent.

Validating compound activity against the respiratory chain

Preliminary knowledge of a drug's target is very useful as it can direct biochemical efforts to confirm the target early-on, facilitating medicinal chemistry.

In the current study puupehenone-like molecules were identified with potent selective activity against dormant *Mtb* [327] (Chapter 2). The puupehenone compound has been shown to target mitochondrial NADH dehydrogenase [320]. The *Mtb* respiratory chain contains a type II NADH dehydrogenase which is essential for bacterial survival *in vitro,* and has been postulated as excellent novel drug targets for *Mtb* [80, 82, 322]*.* The respiratory chain is highly vulnerable in dormant *Mtb*, and therefore compounds inhibiting this pathway may be more potent against dormant than replicating bacteria [77]. Considering these data, we hypothesize that puupehenone scaffolds inhibit the NADH dehydrogenases of *Mtb*. To test this hypothesis, several biochemical approaches should be initially applied which would provide preliminary evidence of its viability. Menaquinone is the substrate reduced by NADH dehydrogenase when NADH becomes oxidized [77]. This substrate is commercially available and has been used to block the activity of compounds targeting the respiratory chain [396]. By including menaquinone in cultures treated with puupehenone we can evaluate whether this causes the bacteria to tolerate the active scaffold. If tolerance is observed this could indicate that puupehenone scaffold bind the dehydrogenase enzymes. Additionally, ascorbic acid is an electron donor interacting directly with cytochrome b, which is further downstream on the respiratory chain than NADH dehydrogenase [77]. If this cofactor causes increasingtolerance to the puupehenone scaffolds, this can be attributed to rescue of the electron transport chain by excess cofactor. Obtaining the expected results in these experiments

could allow target validation without extensive genome sequencing efforts. Spontaneously resistant mutants isolated could be initially tested for mutations specifically in the type II NADH dehydrogenase-encoding genes of *Mtb* (*ndh, ndhA*) [80]. Furthermore, overexpressing these enzymes should also lead to increased MIC of puupehenone-derived scaffolds. The synthesis of puupehenone analogs has been previously reported, and will facilitate future medicinal chemistry efforts to optimize this scaffold for use in TB treatment [317, 323, 324].

Targeting cholesterol metabolism for TB drug development

The cholesterol metabolism pathway in *Mtb* is essential during infection and has been investigated as a potential pool of drug targets that would inhibit bacterial growth during infection [176, 328]. The screen of marine natural products yielded a potent inhibitor of replicating *Mtb* denominated plakinamine P, which displays a structure markedly similar to cholesterol with a unique side chain. Recently a study by Frank and coworkers demonstrated that cholesterol analogs with non-degradable side chains can potently inhibit *Mtb in vitro,* and that the activity was specific to the cholesterol degradation pathway[177]. Taken together, these findings led to the hypothesis that bacterial death caused by Plakinamine P was

due to inhibition of the cholesterol degradation pathway. A previous study has demonstrated that *Mtb* will preferentially utilize cholesterol as a carbon source during macrophage infection and in a mouse model [40]. Even though inhibition of cholesterol degradation when it is the only carbon source causes cell death, addition of alternative carbon sources rescues the bacterium's ability to grow [175]. Since plakinamine P was bactericidal even in the presence of alternative carbon sources and absence of cholesterol, it is likely that death occurs from toxicity of a byproduct of plakinamine P degradation by the cholesterol degradation enzymes, as opposed to inhibition of a cholesterol degradation enzyme. To evaluate this, cholesterol can be included in the bacterial cultures treated with plakinamine P in an attempt to rescue bacterial growth by using cholesterol as a competitor of the compound. Additionally, the *cyp125* genes encodes the first enzyme in the cholesterol degradation pathway of *Mtb* [397, 398]. *Cyp125* deletion strains are unable to degrade cholesterol or grow with cholesterol as the single carbon source, and would therefore most likely be resistant to plakinamine P. Deletion of enzymes downstream in the pathway cause similar phenotypes [175]. In the case that cell death is due to a toxic byproduct of plakinamine P degradation, using these deletion strains would help pinpoint where in the pathway a toxic byproduct is being produced. The proposed "Trojan Horse" mechanism of action poses an interesting solution to the issue of drug resistant mutants. In this case the compound is not binding to the enzyme and causing inhibition of its activity, but instead serving as a substrate for the

enzyme. Therefore, mutations that cause resistance to the compound would also most likely abrogate the enzyme's activity and, in this case, have a severe biological cost for *Mtb.*

New insights on *Mtb* pathogenesis *in vivo*:impact on drug development

The approach used in this study relies on *in vitro* methods for discovery and, afterwards on *in vivo* methods for drug development. Thus, there are many hurdles that a newly discovered compound has to overcome before *in vivo* efficacy can be proven. Importantly it will require chemical properties amenable to pharmacological applications in order to be safe and reach the site of infection.

Exploring *in vivo* models for TB drug development

The use of animal models to define a compound's activity is essential in the drug development process. The infection route plays an important role and usually the most biologically relevant for TB, aerosol inhalation, is ideal. Additionally, the delivery system used for the compound also needs to be carefully considered. Classically, oral delivery is used for TB drugs, however, issues facing this include

poor PK/PD parameters and toxicity. Novel approaches using aerosolized drug delivery have shown promising outcomes with murine models in *Mtb* infection [399]. One of the most important aspects is the choice of which model to use since even different mouse strains will elicit varied responses to *Mtb* infection.

Mice are the most inexpensive, well characterized organism in the field, and the majority of commercial reagents and processes are available primarily for the mouse model. Furthermore, a wide range of well-defined mouse strains and transgenic mice exists to fulfill most research purposes. For these reasons, most preclinical TB drug development relies on mouse models of infection. BALB/c and C57BL/6 mice are the usual choice for determining safety and early bactericidal activity [400]. These mouse strains form predominantly cellular lesions, underestimating the array of granulomatous lesions observed in humans, most of which include necrotic cores surrounded by fibrosis [289, 401]. C3HeB/FeJ mice (Kramnik model) form caseous necrotic granulomas, which occasionally become cavitary, reproducing key traits of the human TB lesions, including a hypoxic core [325, 326, 402]. The diverging pathological progression of TB in different mouse models has a profound impact on drug efficacy. Kramnik are less responsive to treatment with TB drugs in comparison to BALB/c, including PZA and metronidazole [403]. Furthermore, increased relapse rates were observed in Kramnik compared to BALB/c mice after 12 weeks of standard treatment, or with a regimen where rifapentine replaced RIF [404]. The repurposed leprosy drug clofazamine (CFZ) also exhibits lower efficacy in

Kramnik mice relative to BALB/c. *In vitro,* this compound was active against non-replicating *Mtb* [396]. However, this was shown using the SS18b mutant strain of *Mtb,* in which non-replicating persistence is achieved in a streptomycin-dependent manner, without exposing the bacteria to any host-like stress [171]. The failure of CFZ to eliminate bacteria residing within the hypoxic granulomas of the Kramnik mouse is consistent with evidence that its bactericidal activity requires an aerobic environment [402, 405]. These data highlight not only the utility of murine models such as C3HeB/FeJ for TB drug-development, but also the importance of using "real-life" dormancy-inducing conditions *in vitro* for drug-discovery. Moreover, since this mouse model exhibits a more "human-like" disease progression it would be an ideal platform for further development of the compounds discovered in this study, as it would more likely emphasize the potent anti-dormant activity observed with select compounds.

Heterogeneity of TB disease: overcoming a new barrier

In the past 10 years the TB drug development research community has become increasingly aware of the highly heterogeneous nature of this disease. The wide spectrum of *Mtb* dormancy poses a major challenge for treatment efforts since the bacterium will respond differently to antimicrobials depending on is metabolic

state. These varying states of *Mtb* physiology are promoted by the highly dynamic and heterogeneous nature of granulomatous lesions containing these bacteria. The complex variability of granuloma lesions within a single host poses yet another hurdle for drug development since it will directly impact a compound's diffusion and accumulation at the site of infection [139]. FDG-PET/CT scans have revealed that between human patients the spectrum of granuloma lesions is similar, however dramatic variability is observed in size and density of lesions within a single patient; a trait which was reproducible in a non-human primate model of infection [406].

The assumption that all dormant bacteria are the same is becoming less and less valid as the field begins to fully appreciate how physiologically heterogeneous the bacterial subpopulations in a lung can be and the profound impact of this on treatment efficacy and outcome [289]. Heterogeneous screening approaches in the field may therefore be an essential component of the discovery pipeline. At the same time, there may be a benefit from dissecting pathways with conserved essentiality among the entire *Mtb* dormancy spectrum. For instance, the DosR regulator could be used as a drug target since it is the molecular driving force of *Mtb* dormancy [83] (discussed in depth in Chapter 1). This regulator has been targeted in a previous study which identified inhibitors of DosR-DNA binding [407]. Recently, a study utilized a fluorescent DosRST reporter strain for whole-cell high throughput screening [408]. This study revealed molecules which not only inhibited this signaling pathway, but also reduced bacterial survival under

non-replicating conditions [408]. These results emphasized the usefulness of this transcriptional regulator in the search for compounds that specifically kill dormant *Mtb*. Inhibitors of this regulator are also more likely to be non-toxic since this is a unique bacterial protein. Since DosR regulates multiple physiological aspects of dormancy, such inhibitors would also more likely be active against dormant bacteria from diverse *in vitro* models. Whether activity across several dormancy models is a better predictor of *in vivo* efficacy remains to be examined.

Granulomas often serve as a barrier protecting the bacterial population from inhibitory molecules, since these structures become decreasingly vascularized as necrosis and caseation takes place. Although granulomas are different within a host, most mature lesions exhibit a necrotic core and a fibrotic rim, which severely hampers the diffusion of compounds to the core site of infection [289]. MALDI-MRM-MS imaging has enabled the examination of drug distribution within a granuloma *in vivo*[409]. Compounds such as moxifloxacin achieve concentrations as high or higher in rabbit granulomas as in serum [410]. However, front line drugs including RIF, INH and PZA fail to diffuse into cellular granulomas achieving concentrations much lower than in blood plasma [411]. Failure of front line compounds to diffuse in granulomas has been associated with poor treatment outcomes owing to temporal windows of monotherapy occurring as a consequence of poor drug diffusion in granulomas [412]. Recently, PET CT technology has revealed striking evidence that live *Mtb* still remain in the lungs of patients presumed to be cured of the disease [413]. These issues

emphasize the dire need not only for novel anti-TB drugs, but also new technologies in the drug discovery and development field which can improve and accelerate this process.

These recent realizations in the field are revolutionizing the discovery and development of anti-TB compounds. In this work, the variable bacterial physiology during infection and its impact on treatment was addressed, and many compounds were discovered with the potential to inhibit highly drug-tolerant *Mtb.* In the future, an ideal drug regimen will be comprised of drugs that complement each other not only in their ability to diffuse through the diverse lesions occurring in a host lung, but also in the ability to inhibit *Mtb* in all of its varying physiological states during infection.

REFERENCES

1. Boritsch, E.C. and R. Brosch, *Evolution of Mycobacterium tuberculosis: New Insights into Pathogenicity and Drug Resistance.* Microbiol Spectr, 2016. **4**(5).
2. Brites, D. and S. Gagneux, *Co-evolution of Mycobacterium tuberculosis and Homo sapiens.* Immunol Rev, 2015. **264**(1): p. 6-24.
3. Gutierrez, M.C., et al., *Ancient origin and gene mosaicism of the progenitor of Mycobacterium tuberculosis.* PLoS Pathog, 2005. **1**(1): p. e5.
4. Pease, A.C., *Some remarks on the diagnosis and treatment of tuberculosis in antiquity.* Isis, 1940. **31**: p. 13.
5. Bates, J.H. and W.W. Stead, *The history of tuberculosis as a global epidemic.* Med Clin North Am, 1993. **77**(6): p. 1205-17.
6. Herzog, H., *History of tuberculosis.* Respiration, 1998. **65**(1): p. 5-15.
7. Koch, R., *Weitere Mittheilungen über das Tuberkulin.* Dt. Med. Wochenschr., 1891. **17**: p. 3.
8. Koch, R., *Classics in infectious diseases. The etiology of tuberculosis: Robert Koch. Berlin, Germany 1882.* Rev Infect Dis, 1982. **4**(6): p. 1270-4.
9. Dheda, K., C.E. Barry, 3rd, and G. Maartens, *Tuberculosis.* Lancet, 2016. **387**(10024): p. 1211-26.
10. Schatz A., W.S., *Effect of streptomycin and other antibiotic substances upon Mycobacterium tuberculosis and related organisms.* Proc Soc Expt Biol and Med, 1944. **55**: p. 4.
11. Lehmann, J., *Twenty Years Afterward Historical Notes on the Discovery of the Antituberculosis Effect of Paraaminosalicylic Acid (Pas) and the First Clinical Trials.* Am Rev Respir Dis, 1964. **90**: p. 953-6.
12. Brudney, K. and J. Dobkin, *Resurgent tuberculosis in New York City. Human immunodeficiency virus, homelessness, and the decline of tuberculosis control programs.* Am Rev Respir Dis, 1991. **144**(4): p. 745-9.
13. Pawlowski, A., et al., *Tuberculosis and HIV co-infection.* PLoS Pathog, 2012. **8**(2): p. e1002464.
14. Organization, W.H., *Global tuberculosis report*. 2016.
15. Zhang, Y. and D. Mitchison, *The curious characteristics of pyrazinamide: a review.* Int J Tuberc Lung Dis, 2003. **7**(1): p. 6-21.

16. Almeida Da Silva, P.E. and J.C. Palomino, *Molecular basis and mechanisms of drug resistance in Mycobacterium tuberculosis: classical and new drugs.* J Antimicrob Chemother, 2011. **66**(7): p. 1417-30.

17. Gengenbacher, M. and S.H.E. Kaufmann, *Mycobacterium tuberculosis: success through dormancy.* Fems Microbiology Reviews, 2012. **36**(3): p. 514-532.

18. Russell, D.G., *Who puts the tubercle in tuberculosis?* Nat Rev Microbiol, 2007. **5**(1): p. 39-47.

19. Ramakrishnan, L., *Revisiting the role of the granuloma in tuberculosis.* Nat Rev Immunol, 2012. **12**(5): p. 352-66.

20. Silva Miranda, M., et al., *The tuberculous granuloma: an unsuccessful host defence mechanism providing a safety shelter for the bacteria?* Clin Dev Immunol, 2012. **2012**: p. 139127.

21. Ernst, J.D., *Macrophage receptors for Mycobacterium tuberculosis.* Infect Immun, 1998. **66**(4): p. 1277-81.

22. Cambi, A., M. Koopman, and C.G. Figdor, *How C-type lectins detect pathogens.* Cell Microbiol, 2005. **7**(4): p. 481-8.

23. Vergne, I., M. Gilleron, and J. Nigou, *Manipulation of the endocytic pathway and phagocyte functions by Mycobacterium tuberculosis lipoarabinomannan.* Front Cell Infect Microbiol, 2014. **4**: p. 187.

24. Mwandumba, H.C., et al., *Mycobacterium tuberculosis resides in nonacidified vacuoles in endocytically competent alveolar macrophages from patients with tuberculosis and HIV infection.* J Immunol, 2004. **172**(7): p. 4592-8.

25. Russell, D.G., et al., *The macrophage marches on its phagosome: dynamic assays of phagosome function.* Nat Rev Immunol, 2009. **9**(8): p. 594-600.

26. Deretic, V., et al., *Mycobacterium tuberculosis inhibition of phagolysosome biogenesis and autophagy as a host defence mechanism.* Cell Microbiol, 2006. **8**(5): p. 719-27.

27. Nunes-Alves, C., et al., *In search of a new paradigm for protective immunity to TB.* Nat Rev Microbiol, 2014. **12**(4): p. 289-99.

28. Levitte, S., et al., *Mycobacterial Acid Tolerance Enables Phagolysosomal Survival and Establishment of Tuberculous Infection In Vivo.* Cell Host Microbe, 2016. **20**(2): p. 250-8.

29. Martin, C.J., A.F. Carey, and S.M. Fortune, *A bug's life in the granuloma.* Semin Immunopathol, 2016. **38**(2): p. 213-20.

30. Volkman, H.E., et al., *Tuberculous granuloma induction via interaction of a bacterial secreted protein with host epithelium.* Science, 2010. **327**(5964): p. 466-9.

31. McLaughlin, C.A., et al., *Moieties of mycobacterial mycolates required for inducing granulomatous reactions.* Cell Immunol, 1978. **38**(1): p. 14-24.

32. Meyer, T.J., E. Ribi, and I. Azuma, *Biologically active components from mycobacterial cell walls. V. Granuloma formation in mouse lungs and guinea pig skin.* Cell Immunol, 1975. **16**(1): p. 11-24.

33. Moore, V.L., Q.N. Myrvik, and M. Kato, *Role of cord factor (trehalose-6,6'-dimycolate) in allergic granuloma formation in rabbits.* Infect Immun, 1972. **6**(1): p. 5-8.

34. Bekierkunst, A., *Acute granulomatous response produced in mice by trehalose-6,6-dimycolate.* J Bacteriol, 1968. **96**(4): p. 958-61.

35. White, R.G., et al., *Correlation of Adjuvant Activity and Chemical Structure of Wax D Fractions of Mycobacteria.* Immunology, 1964. **7**: p. 158-71.

36. Beatty, W.L., et al., *Trafficking and release of mycobacterial lipids from infected macrophages.* Traffic, 2000. **1**(3): p. 235-47.

37. Geisel, R.E., et al., *In vivo activity of released cell wall lipids of Mycobacterium bovis bacillus Calmette-Guerin is due principally to trehalose mycolates.* J Immunol, 2005. **174**(8): p. 5007-15.

38. Shaler, C.R., et al., *Within the Enemy's Camp: contribution of the granuloma to the dissemination, persistence and transmission of Mycobacterium tuberculosis.* Front Immunol, 2013. **4**: p. 30.

39. Rohde, K.H., R.B. Abramovitch, and D.G. Russell, *Mycobacterium tuberculosis invasion of macrophages: Linking bacterial gene expression to environmental cues.* Cell Host & Microbe, 2007. **2**(5): p. 352-364.

40. Schnappinger, D., et al., *Transcriptional Adaptation of Mycobacterium tuberculosis within Macrophages: Insights into the Phagosomal Environment.* J Exp Med, 2003. **198**(5): p. 693-704.

41. Homolka, S., et al., *Functional Genetic Diversity among Mycobacterium tuberculosis Complex Clinical Isolates: Delineation of Conserved Core and Lineage-Specific Transcriptomes during Intracellular Survival.* Plos Pathogens, 2010. **6**(7).

42. Lipworth, S., et al., *Defining dormancy in mycobacterial disease.* Tuberculosis (Edinb), 2016. **99**: p. 131-42.

43. Gold, B. and C. Nathan, *Targeting Phenotypically Tolerant Mycobacterium tuberculosis.* Microbiol Spectr, 2017. **5**(1).

44. McCune, R.M., et al., *Microbial persistence. I. The capacity of tubercle bacilli to survive sterilization in mouse tissues.* J Exp Med, 1966. **123**(3): p. 445-68.

45. Sever, J.L. and G.P. Youmans, *The relation of oxygen tension to virulence of tubercle bacilli and to acquired resistance in tuberculosis.* J Infect Dis, 1957. **101**(2): p. 193-202.

46. Steenken, W.J., *The persistence of tubercle bacilli in caseous lesions in the experimental animal (guinea pig).* Am Rev Respirat Disease 1961. **83**.

47. Rees, R.J. and P.D. Hart, *Analysis of the host-parasite equilibrium in chronic murine tuberculosis by total and viable bacillary counts.* Br J Exp Pathol, 1961. **42**: p. 83-8.

48. McCune, R.M., F.M. Feldmann, and W. McDermott, *Microbial persistence. II. Characteristics of the sterile state of tubercle bacilli.* J Exp Med, 1966. **123**(3): p. 469-86.

49. Fenhalls, G., et al., *Localisation of mycobacterial DNA and mRNA in human tuberculous granulomas.* J Microbiol Methods, 2002. **51**(2): p. 197-208.

50. Im, J.G., et al., *Pulmonary tuberculosis: CT findings--early active disease and sequential change with antituberculous therapy.* Radiology, 1993. **186**(3): p. 653-60.

51. Loring, W.E. and H.M. Vandiviere, *The treated pulmonary lesion and its tubercle bacillus. I. Pathology and pathogenesis.* Am J Med Sci, 1956. **232**(1): p. 20-9.

52. Via, L.E., et al., *Tuberculous granulomas are hypoxic in guinea pigs, rabbits, and nonhuman primates.* Infect Immun, 2008. **76**(6): p. 2333-40.

53. Wayne, L.G. and L.G. Hayes, *An in vitro model for sequential study of shiftdown of Mycobacterium tuberculosis through two stages of nonreplicating persistence.* Infect Immun, 1996. **64**(6): p. 2062-9.

54. Wayne, L.G. and C.D. Sohaskey, *Nonreplicating persistence of mycobacterium tuberculosis.* Annu Rev Microbiol, 2001. **55**: p. 139-63.

55. Wayne, L.G., *In Vitro Model of Hypoxically Induced Nonreplicating Persistence of Mycobacterium tuberculosis.* Methods Mol Med, 2001. **54**: p. 247-69.

56. Hu, Y., A.R. Coates, and D.A. Mitchison, *Sterilising action of pyrazinamide in models of dormant and rifampicin-tolerant Mycobacterium tuberculosis.* Int J Tuberc Lung Dis, 2006. **10**(3): p. 317-22.

57. Cunningham, A.F. and C.L. Spreadbury, *Mycobacterial stationary phase induced by low oxygen tension: cell wall thickening and localization of the 16-kilodalton alpha-crystallin homolog.* J Bacteriol, 1998. **180**(4): p. 801-8.

58. Betts, J.C., et al., *Evaluation of a nutrient starvation model of Mycobacterium tuberculosis persistence by gene and protein expression profiling.* Mol Microbiol, 2002. **43**(3): p. 717-31.

59. James, B.W., A. Williams, and P.D. Marsh, *The physiology and pathogenicity of Mycobacterium tuberculosis grown under controlled conditions in a defined medium.* J Appl Microbiol, 2000. **88**(4): p. 669-77.

60. Voskuil, M.I., et al., *Inhibition of respiration by nitric oxide induces a Mycobacterium tuberculosis dormancy program.* J Exp Med, 2003. **198**(5): p. 705-13.

61. Deb, C., et al., *A Novel In Vitro Multiple-Stress Dormancy Model for Mycobacterium tuberculosis Generates a Lipid-Loaded, Drug-Tolerant, Dormant Pathogen.* Plos One, 2009. **4**(6).

62. Waltermann, M. and A. Steinbuchel, *Neutral lipid bodies in prokaryotes: recent insights into structure, formation, and relationship to eukaryotic lipid depots.* J Bacteriol, 2005. **187**(11): p. 3607-19.

63. Daniel, J., et al., *Induction of a novel class of diacylglycerol acyltransferases and triacylglycerol accumulation in Mycobacterium tuberculosis as it goes into a dormancy-like state in culture.* J Bacteriol, 2004. **186**(15): p. 5017-30.

64. Sirakova, T.D., et al., *Identification of a diacylglycerol acyltransferase gene involved in accumulation of triacylglycerol in Mycobacterium tuberculosis under stress.* Microbiology, 2006. **152**(Pt 9): p. 2717-25.

65. Garton, N.J., et al., *Cytological and transcript analyses reveal fat and lazy persister-like bacilli in tuberculous sputum.* Plos Medicine, 2008. **5**(4): p. 634-645.

66. Baek, S.H., A.H. Li, and C.M. Sassetti, *Metabolic Regulation of Mycobacterial Growth and Antibiotic Sensitivity.* Plos Biology, 2011. **9**(5).

67. Bloch, H. and W. Segal, *Biochemical differentiation of Mycobacterium tuberculosis grown in vivo and in vitro.* J Bacteriol, 1956. **72**(2): p. 132-41.

68. Dubnau, E., et al., *responses of mycobacterium tuberculosis to growth in the mouse lung.* Infect Immun, 2005. **73**(6): p. 3754-7.

69. Timm, J., et al., *Differential expression of iron-, carbon-, and oxygen-responsive mycobacterial genes in the lungs of chronically infected mice and tuberculosis patients.* Proc Natl Acad Sci U S A, 2003. **100**(24): p. 14321-6.

70. Munoz-Elias, E.J. and J.D. McKinney, *Carbon metabolism of intracellular bacteria.* Cell Microbiol, 2006. **8**(1): p. 10-22.

71. Lam, T.H., et al., *Differential fadE28 expression associated with phenotypic virulence of Mycobacterium tuberculosis.* Microb Pathog, 2008. **45**(1): p. 12-7.

72. Cole, S.T., et al., *Deciphering the biology of Mycobacterium tuberculosis from the complete genome sequence.* Nature, 1998. **393**(6685): p. 537-44.

73. McKinney, J.D., et al., *Persistence of Mycobacterium tuberculosis in macrophages and mice requires the glyoxylate shunt enzyme isocitrate lyase.* Nature, 2000. **406**(6797): p. 735-8.

74. Gould, T.A., et al., *Dual role of isocitrate lyase 1 in the glyoxylate and methylcitrate cycles in Mycobacterium tuberculosis.* Mol Microbiol, 2006. **61**(4): p. 940-7.

75. Munoz-Elias, E.J., et al., *Role of the methylcitrate cycle in Mycobacterium tuberculosis metabolism, intracellular growth, and virulence.* Mol Microbiol, 2006. **60**(5): p. 1109-22.

76. Cox, E. and K. Laessig, *FDA approval of bedaquiline--the benefit-risk balance for drug-resistant tuberculosis.* N Engl J Med, 2014. **371**(8): p. 689-91.

77. Rao, S.P.S., et al., *The protonmotive force is required for maintaining ATP homeostasis and viability of hypoxic, nonreplicating Mycobacterium tuberculosis.* Proceedings of the National Academy of Sciences of the United States of America, 2008. **105**(33): p. 11945-11950.

78. Dhiman, R.K., et al., *Menaquinone synthesis is critical for maintaining mycobacterial viability during exponential growth and recovery from non-replicating persistence.* Mol Microbiol, 2009. **72**(1): p. 85-97.

79. Dhar, N. and J.D. McKinney, *Mycobacterium tuberculosis persistence mutants identified by screening in isoniazid-treated mice.* Proc Natl Acad Sci U S A, 2010. **107**(27): p. 12275-80.

80. Awasthy, D., et al., *Roles of the two type II NADH dehydrogenases in the survival of Mycobacterium tuberculosis in vitro.* Gene, 2014. **550**(1): p. 110-6.

81. Weinstein, E.A., et al., *Inhibitors of type II NADH:menaquinone oxidoreductase represent a class of antitubercular drugs.* Proc Natl Acad Sci U S A, 2005. **102**(12): p. 4548-53.

82. Sellamuthu, S., et al., *Type-II NADH Dehydrogenase (NDH-2): a promising therapeutic target for antitubercular and antibacterial drug discovery.* Expert Opin Ther Targets, 2017. **21**(6): p. 559-570.

83. Boon, C. and T. Dick, *How Mycobacterium tuberculosis goes to sleep: the dormancy survival regulator DosR a decade later.* Future Microbiol, 2012. **7**(4): p. 513-8.

84. Kinger, A.K. and J.S. Tyagi, *Identification and cloning of genes differentially expressed in the virulent strain of Mycobacterium tuberculosis.* Gene, 1993. **131**(1): p. 113-7.

85. Dasgupta, N., et al., *Characterization of a two-component system, devR-devS, of Mycobacterium tuberculosis.* Tuber Lung Dis, 2000. **80**(3): p. 141-59.

86. Boon, C. and T. Dick, *Mycobacterium bovis BCG response regulator essential for hypoxic dormancy.* J Bacteriol, 2002. **184**(24): p. 6760-7.

87. Boon, C., et al., *Proteins of Mycobacterium bovis BCG induced in the Wayne dormancy model.* J Bacteriol, 2001. **183**(8): p. 2672-6.

88. Lim, A., et al., *Oxygen depletion-induced dormancy in Mycobacterium bovis BCG.* J Bacteriol, 1999. **181**(7): p. 2252-6.

89. Malhotra, V., et al., *Disruption of response regulator gene, devR, leads to attenuation in virulence of Mycobacterium tuberculosis.* FEMS Microbiol Lett, 2004. **231**(2): p. 237-45.

90. Gautam, U.S., et al., *DosS Is required for the complete virulence of mycobacterium tuberculosis in mice with classical granulomatous lesions.* Am J Respir Cell Mol Biol, 2015. **52**(6): p. 708-16.

91. Kumar, A., et al., *Mycobacterium tuberculosis DosS is a redox sensor and DosT is a hypoxia sensor.* Proc Natl Acad Sci U S A, 2007. **104**(28): p. 11568-73.

92. Kumar, A., et al., *Heme oxygenase-1-derived carbon monoxide induces the Mycobacterium tuberculosis dormancy regulon.* J Biol Chem, 2008. **283**(26): p. 18032-9.

93. Sardiwal, S., et al., *A GAF domain in the hypoxia/NO-inducible Mycobacterium tuberculosis DosS protein binds haem.* J Mol Biol, 2005. **353**(5): p. 929-36.

94. Ioanoviciu, A., et al., *DevS, a heme-containing two-component oxygen sensor of Mycobacterium tuberculosis.* Biochemistry, 2007. **46**(14): p. 4250-60.

95. Taneja, N.K., et al., *Mycobacterium tuberculosis transcriptional adaptation, growth arrest and dormancy phenotype development is triggered by vitamin C.* PLoS One, 2010. **5**(5): p. e10860.

96. Shi, L., et al., *Expression of Th1-mediated immunity in mouse lungs induces a Mycobacterium tuberculosis transcription pattern characteristic*

of nonreplicating persistence. Proc Natl Acad Sci U S A, 2003. **100**(1): p. 241-6.

97. Sherman, D.R., et al., *Regulation of the Mycobacterium tuberculosis hypoxic response gene encoding alpha -crystallin.* Proc Natl Acad Sci U S A, 2001. **98**(13): p. 7534-9.

98. Park, H.D., et al., *Rv3133c/dosR is a transcription factor that mediates the hypoxic response of Mycobacterium tuberculosis.* Mol Microbiol, 2003. **48**(3): p. 833-43.

99. Rustad, T.R., et al., *The enduring hypoxic response of Mycobacterium tuberculosis.* PLoS One, 2008. **3**(1): p. e1502.

100. Manganelli, R., *Sigma Factors: Key Molecules in Mycobacterium tuberculosis Physiology and Virulence.* Microbiol Spectr, 2014. **2**(1): p. MGM2-0007-2013.

101. Capra, E.J. and M.T. Laub, *Evolution of two-component signal transduction systems.* Annu Rev Microbiol, 2012. **66**: p. 325-47.

102. Parish, T., *Two-Component Regulatory Systems of Mycobacteria.* Microbiol Spectr, 2014. **2**(1): p. MGM2-0010-2013.

103. He, H., et al., *MprAB is a stress-responsive two-component system that directly regulates expression of sigma factors SigB and SigE in Mycobacterium tuberculosis.* J Bacteriol, 2006. **188**(6): p. 2134-43.

104. Zahrt, T.C. and V. Deretic, *Mycobacterium tuberculosis signal transduction system required for persistent infections.* Proc Natl Acad Sci U S A, 2001. **98**(22): p. 12706-11.

105. Pang, X., et al., *MprAB regulates the espA operon in Mycobacterium tuberculosis and modulates ESX-1 function and host cytokine response.* J Bacteriol, 2013. **195**(1): p. 66-75.

106. Primm, T.P., et al., *The stringent response of Mycobacterium tuberculosis is required for long-term survival.* J Bacteriol, 2000. **182**(17): p. 4889-98.

107. Dahl, J.L., et al., *The role of RelMtb-mediated adaptation to stationary phase in long-term persistence of Mycobacterium tuberculosis in mice.* Proc Natl Acad Sci U S A, 2003. **100**(17): p. 10026-31.

108. Klinkenberg, L.G., et al., *The stringent response is required for full virulence of Mycobacterium tuberculosis in guinea pigs.* J Infect Dis, 2010. **202**(9): p. 1397-404.

109. Dutta, N.K. and P.C. Karakousis, *Latent tuberculosis infection: myths, models, and molecular mechanisms.* Microbiol Mol Biol Rev, 2014. **78**(3): p. 343-71.

110. Ryndak, M., S. Wang, and I. Smith, *PhoP, a key player in Mycobacterium tuberculosis virulence.* Trends Microbiol, 2008. **16**(11): p. 528-34.

111. Walters, S.B., et al., *The Mycobacterium tuberculosis PhoPR two-component system regulates genes essential for virulence and complex lipid biosynthesis.* Mol Microbiol, 2006. **60**(2): p. 312-30.

112. Gupta, S., A. Sinha, and D. Sarkar, *Transcriptional autoregulation by Mycobacterium tuberculosis PhoP involves recognition of novel direct repeat sequences in the regulatory region of the promoter.* FEBS Lett, 2006. **580**(22): p. 5328-38.

113. Frigui, W., et al., *Control of M. tuberculosis ESAT-6 secretion and specific T cell recognition by PhoP.* PLoS Pathog, 2008. **4**(2): p. e33.

114. WHO, *The treatment of tuberculosis guidelines*. 2010: Geneva.

115. D'Ambrosio, L., et al., *New anti-tuberculosis drugs and regimens: 2015 update.* ERJ Open Res, 2015. **1**(1).

116. in *Companion Handbook to the WHO Guidelines for the Programmatic Management of Drug-Resistant Tuberculosis*. 2014: Geneva.

117. in *Guidelines for the Programmatic Management of Drug-Resistant Tuberculosis: 2011 Update*. 2011: Geneva.

118. Falzon, D., et al., *World Health Organization treatment guidelines for drug-resistant tuberculosis, 2016 update.* Eur Respir J, 2017. **49**(3).

119. Pietersen, E., et al., *Long-term outcomes of patients with extensively drug-resistant tuberculosis in South Africa: a cohort study.* Lancet, 2014. **383**(9924): p. 1230-9.

120. Kim, D.H., et al., *Treatment outcomes and long-term survival in patients with extensively drug-resistant tuberculosis.* Am J Respir Crit Care Med, 2008. **178**(10): p. 1075-82.

121. Gagneux, S., et al., *The competitive cost of antibiotic resistance in Mycobacterium tuberculosis.* Science, 2006. **312**(5782): p. 1944-6.

122. Cox, H. and N. Ford, *Linezolid for the treatment of complicated drug-resistant tuberculosis: a systematic review and meta-analysis.* Int J Tuberc Lung Dis, 2012. **16**(4): p. 447-54.

123. Wasserman, S., G. Meintjes, and G. Maartens, *Linezolid in the treatment of drug-resistant tuberculosis: the challenge of its narrow therapeutic index.* Expert Rev Anti Infect Ther, 2016. **14**(10): p. 901-15.

124. Lee, M., et al., *Linezolid for treatment of chronic extensively drug-resistant tuberculosis.* N Engl J Med, 2012. **367**(16): p. 1508-18.

125. Mehta, S., et al., *Linezolid-Associated Optic Neuropathy in Drug-Resistant Tuberculosis Patients in Mumbai, India.* PLoS One, 2016. **11**(9): p. e0162138.

126. Carroll, M.W., et al., *Rhabdomyolysis in a patient treated with linezolid for extensively drug-resistant tuberculosis.* Clin Infect Dis, 2012. **54**(11): p. 1624-7.

127. De Lorenzo, S., et al., *Efficacy and safety of meropenem-clavulanate added to linezolid-containing regimens in the treatment of MDR-/XDR-TB.* Eur Respir J, 2013. **41**(6): p. 1386-92.

128. Ryan, N.J. and J.H. Lo, *Delamanid: first global approval.* Drugs, 2014. **74**(9): p. 1041-5.

129. Gler, M.T., et al., *Delamanid for multidrug-resistant pulmonary tuberculosis.* N Engl J Med, 2012. **366**(23): p. 2151-60.

130. Skripconoka, V., et al., *Delamanid improves outcomes and reduces mortality in multidrug-resistant tuberculosis.* Eur Respir J, 2013. **41**(6): p. 1393-400.

131. Thakare, R., et al., *Delamanid for the treatment of pulmonary multidrug-resistant tuberculosis.* Drugs Today (Barc), 2015. **51**(2): p. 117-23.

132. Wells, C.D., et al., *Long-term mortality assessment of multidrug-resistant tuberculosis patients treated with delamanid.* Eur Respir J, 2015. **45**(5): p. 1498-501.

133. Diacon, A.H., et al., *Randomized pilot trial of eight weeks of bedaquiline (TMC207) treatment for multidrug-resistant tuberculosis: long-term outcome, tolerability, and effect on emergence of drug resistance.* Antimicrob Agents Chemother, 2012. **56**(6): p. 3271-6.

134. Diacon, A.H., et al., *Multidrug-resistant tuberculosis and culture conversion with bedaquiline.* N Engl J Med, 2014. **371**(8): p. 723-32.

135. Diacon, A.H., et al., *The diarylquinoline TMC207 for multidrug-resistant tuberculosis.* N Engl J Med, 2009. **360**(23): p. 2397-405.

136. Koul, A., et al., *The challenge of new drug discovery for tuberculosis.* Nature, 2011. **469**(7331): p. 483-90.

137. Mdluli, K., T. Kaneko, and A. Upton, *The tuberculosis drug discovery and development pipeline and emerging drug targets.* Cold Spring Harb Perspect Med, 2015. **5**(6).

138. Katsuno, K., et al., *Hit and lead criteria in drug discovery for infectious diseases of the developing world.* Nat Rev Drug Discov, 2015. **14**(11): p. 751-8.

139. Dartois, V. and C.E. Barry, 3rd, *A medicinal chemists' guide to the unique difficulties of lead optimization for tuberculosis.* Bioorg Med Chem Lett, 2013. **23**(17): p. 4741-50.

140. Dartois, V., *The path of anti-tuberculosis drugs: from blood to lesions to mycobacterial cells.* Nat Rev Microbiol, 2014. **12**(3): p. 159-67.

141. Nielsen, E.I. and L.E. Friberg, *Pharmacokinetic-pharmacodynamic modeling of antibacterial drugs.* Pharmacol Rev, 2013. **65**(3): p. 1053-90.

142. Egelund, E.F., A.B. Barth, and C.A. Peloquin, *Population pharmacokinetics and its role in anti-tuberculosis drug development and optimization of treatment.* Curr Pharm Des, 2011. **17**(27): p. 2889-99.

143. Zumla, A., P. Nahid, and S.T. Cole, *Advances in the development of new tuberculosis drugs and treatment regimens.* Nat Rev Drug Discov, 2013. **12**(5): p. 388-404.

144. Sassetti, C.M. and E.J. Rubin, *Genetic requirements for mycobacterial survival during infection.* Proc Natl Acad Sci U S A, 2003. **100**(22): p. 12989-94.

145. Rohde, K.H., et al., *Linking the Transcriptional Profiles and the Physiological States of Mycobacterium tuberculosis during an Extended Intracellular Infection.* Plos Pathogens, 2012. **8**(6).

146. Payne, D.J., et al., *Drugs for bad bugs: confronting the challenges of antibacterial discovery.* Nat Rev Drug Discov, 2007. **6**(1): p. 29-40.

147. Szumowski, J.D., et al., *Antimicrobial efflux pumps and Mycobacterium tuberculosis drug tolerance: evolutionary considerations.* Curr Top Microbiol Immunol, 2013. **374**: p. 81-108.

148. Vetting, M.W., et al., *Aminoglycoside 2'-N-acetyltransferase from Mycobacterium tuberculosis in complex with coenzyme A and aminoglycoside substrates.* Nat Struct Biol, 2002. **9**(9): p. 653-8.

149. Vetting, M.W., et al., *Mechanistic and structural analysis of aminoglycoside N-acetyltransferase AAC(6 ')-Ib and its bifunctional, fluoroquinolone-active AAC(6 ')-Ib-cr variant.* Biochemistry, 2008. **47**(37): p. 9825-9835.

150. Andries, K., et al., *A diarylquinoline drug active on the ATP synthase of Mycobacterium tuberculosis.* Science, 2005. **307**(5707): p. 223-7.

151. Makarov, V., et al., *Benzothiazinones kill Mycobacterium tuberculosis by blocking arabinan synthesis.* Science, 2009. **324**(5928): p. 801-4.

152. Chaturvedi, V., et al., *Evaluation of Mycobacterium smegmatis as a possible surrogate screen for selecting molecules active against multi-*

drug resistant Mycobacterium tuberculosis. J Gen Appl Microbiol, 2007. **53**(6): p. 333-7.

153. Dick, T., B.H. Lee, and B. Murugasu-Oei, *Oxygen depletion induced dormancy in Mycobacterium smegmatis.* FEMS Microbiol Lett, 1998. **163**(2): p. 159-64.

154. Mayuri, et al., *Molecular analysis of the dormancy response in Mycobacterium smegmatis: expression analysis of genes encoding the DevR-DevS two-component system, Rv3134c and chaperone alpha-crystallin homologues.* FEMS Microbiol Lett, 2002. **211**(2): p. 231-7.

155. Jordao, L., et al., *On the killing of mycobacteria by macrophages.* Cell Microbiol, 2008. **10**(2): p. 529-48.

156. Bange, F.C., F.M. Collins, and W.R. Jacobs, Jr., *Survival of mice infected with Mycobacterium smegmatis containing large DNA fragments from Mycobacterium tuberculosis.* Tuber Lung Dis, 1999. **79**(3): p. 171-80.

157. Altaf, M., et al., *Evaluation of the Mycobacterium smegmatis and BCG models for the discovery of Mycobacterium tuberculosis inhibitors.* Tuberculosis (Edinb), 2010. **90**(6): p. 333-7.

158. Bueno, C., et al., *The excited-state interaction of resazurin and resorufin with amines in aqueous solutions. Photophysics and photochemical reactions.* Photochem Photobiol, 2002. **76**(4): p. 385-90.

159. Katawera, V., M. Siedner, and Y. Boum, 2nd, *Evaluation of the modified colorimetric resazurin microtiter plate-based antibacterial assay for rapid and reliable tuberculosis drug susceptibility testing.* BMC Microbiol, 2014. **14**: p. 259.

160. O'Neill, T.E., et al., *Optimisation of the microplate resazurin assay for screening and bioassay-guided fractionation of phytochemical extracts against Mycobacterium tuberculosis.* Phytochem Anal, 2014. **25**(5): p. 461-7.

161. Palomino, J.C., et al., *Resazurin microtiter assay plate: simple and inexpensive method for detection of drug resistance in Mycobacterium tuberculosis.* Antimicrob Agents Chemother, 2002. **46**(8): p. 2720-2.

162. Taneja, N.K. and J.S. Tyagi, *Resazurin reduction assays for screening of anti-tubercular compounds against dormant and actively growing Mycobacterium tuberculosis, Mycobacterium bovis BCG and Mycobacterium smegmatis.* J Antimicrob Chemother, 2007. **60**(2): p. 288-93.

163. Changsen, C., S.G. Franzblau, and P. Palittapongarnpim, *Improved green fluorescent protein reporter gene-based microplate screening for*

antituberculosis compounds by utilizing an acetamidase promoter. Antimicrob Agents Chemother, 2003. **47**(12): p. 3682-7.

164. Collins, L.A., M.N. Torrero, and S.G. Franzblau, *Green fluorescent protein reporter microplate assay for high-throughput screening of compounds against Mycobacterium tuberculosis.* Antimicrob Agents Chemother, 1998. **42**(2): p. 344-7.

165. Kremer, L., et al., *Green fluorescent protein as a new expression marker in mycobacteria.* Mol Microbiol, 1995. **17**(5): p. 913-22.

166. Carroll, P., et al., *Sensitive detection of gene expression in mycobacteria under replicating and non-replicating conditions using optimized far-red reporters.* PLoS One, 2010. **5**(3): p. e9823.

167. Andreu, N., et al., *Optimisation of bioluminescent reporters for use with mycobacteria.* PLoS One, 2010. **5**(5): p. e10777.

168. Andreu, N., et al., *Rapid measurement of antituberculosis drug activity in vitro and in macrophages using bioluminescence.* J Antimicrob Chemother, 2012. **67**(2): p. 404-14.

169. Larsson, M.C., et al., *A luciferase-based assay for rapid assessment of drug activity against Mycobacterium tuberculosis including monitoring of macrophage viability.* J Microbiol Methods, 2014. **106**: p. 146-50.

170. Sharma, S., et al., *Simple and rapid method to determine antimycobacterial potency of compounds by using autoluminescent Mycobacterium tuberculosis.* Antimicrob Agents Chemother, 2014. **58**(10): p. 5801-8.

171. Vocat, A., et al., *Bioluminescence for assessing drug potency against nonreplicating Mycobacterium tuberculosis.* Antimicrob Agents Chemother, 2015. **59**(7): p. 4012-9.

172. Pethe, K., et al., *Discovery of Q203, a potent clinical candidate for the treatment of tuberculosis.* Nat Med, 2013. **19**(9): p. 1157-60.

173. Queval, C.J., et al., *A microscopic phenotypic assay for the quantification of intracellular mycobacteria adapted for high-throughput/high-content screening.* J Vis Exp, 2014(83): p. e51114.

174. Sorrentino, F., et al., *Development of an Intracellular Screen for New Compounds Able To Inhibit Mycobacterium tuberculosis Growth in Human Macrophages.* Antimicrob Agents Chemother, 2015. **60**(1): p. 640-5.

175. VanderVen, B.C., et al., *Novel inhibitors of cholesterol degradation in Mycobacterium tuberculosis reveal how the bacterium's metabolism is constrained by the intracellular environment.* PLoS Pathog, 2015. **11**(2): p. e1004679.

176. Hudson, S.A., et al., *Mycobacterium tuberculosis cytochrome P450 enzymes: a cohort of novel TB drug targets.* Biochem Soc Trans, 2012. **40**(3): p. 573-9.

177. Frank, D.J., et al., *Cholesterol Analogs with Degradation-resistant Alkyl Side Chains Are Effective Mycobacterium tuberculosis Growth Inhibitors.* J Biol Chem, 2016. **291**(14): p. 7325-33.

178. Stanley, S.A., et al., *Identification of host-targeted small molecules that restrict intracellular Mycobacterium tuberculosis growth.* PLoS Pathog, 2014. **10**(2): p. e1003946.

179. Nathan, C., *Fresh approaches to anti-infective therapies.* Sci Transl Med, 2012. **4**(140): p. 140sr2.

180. Grant, S.S., et al., *Identification of novel inhibitors of nonreplicating Mycobacterium tuberculosis using a carbon starvation model.* ACS Chem Biol, 2013. **8**(10): p. 2224-34.

181. Bassett, I.M., et al., *Detection of inhibitors of phenotypically drug-tolerant Mycobacterium tuberculosis using an in vitro bactericidal screen.* J Microbiol, 2013. **51**(5): p. 651-8.

182. Cho, S.H., et al., *Low-oxygen-recovery assay for high-throughput screening of compounds against nonreplicating Mycobacterium tuberculosis.* Antimicrob Agents Chemother, 2007. **51**(4): p. 1380-5.

183. Mak, P.A., et al., *A high-throughput screen to identify inhibitors of ATP homeostasis in non-replicating Mycobacterium tuberculosis.* ACS Chem Biol, 2012. **7**(7): p. 1190-7.

184. Gold, B., et al., *Novel Cephalosporins Selectively Active on Nonreplicating Mycobacterium tuberculosis.* J Med Chem, 2016. **59**(13): p. 6027-44.

185. Warrier, T., et al., *Identification of Novel Anti-mycobacterial Compounds by Screening a Pharmaceutical Small-Molecule Library against Nonreplicating Mycobacterium tuberculosis.* ACS Infect Dis, 2015. **1**(12): p. 580-5.

186. Zheng, P., et al., *Synthetic calanolides with bactericidal activity against replicating and nonreplicating Mycobacterium tuberculosis.* J Med Chem, 2014. **57**(9): p. 3755-72.

187. Gold, B., T. Warrier, and C. Nathan, *A multi-stress model for high throughput screening against non-replicating Mycobacterium tuberculosis.* Methods Mol Biol, 2015. **1285**: p. 293-315.

188. Gold, B., et al., *Rapid, Semiquantitative Assay To Discriminate among Compounds with Activity against Replicating or Nonreplicating Mycobacterium tuberculosis.* Antimicrob Agents Chemother, 2015. **59**(10): p. 6521-38.

189. Sala, C., et al., *Simple model for testing drugs against nonreplicating Mycobacterium tuberculosis.* Antimicrob Agents Chemother, 2010. **54**(10): p. 4150-8.

190. O'Shea, R. and H.E. Moser, *Physicochemical properties of antibacterial compounds: implications for drug discovery.* J Med Chem, 2008. **51**(10): p. 2871-8.

191. Harvey, A.L., R. Edrada-Ebel, and R.J. Quinn, *The re-emergence of natural products for drug discovery in the genomics era.* Nat Rev Drug Discov, 2015. **14**(2): p. 111-29.

192. Montaser, R. and H. Luesch, *Marine natural products: a new wave of drugs?* Future Med Chem, 2011. **3**(12): p. 1475-89.

193. Ortholand, J.Y. and A. Ganesan, *Natural products and combinatorial chemistry: back to the future.* Curr Opin Chem Biol, 2004. **8**(3): p. 271-80.

194. Newman, D.J. and G.M. Cragg, *Natural products as sources of new drugs over the 30 years from 1981 to 2010.* J Nat Prod, 2012. **75**(3): p. 311-35.

195. Copp, B.R., *Antimycobacterial natural products.* Nat Prod Rep, 2003. **20**(6): p. 535-57.

196. Farah, S.I., et al., *Opportunities and Challenges for Natural Products as Novel Antituberculosis Agents.* Assay Drug Dev Technol, 2016. **14**(1): p. 29-38.

197. Camacho-Corona Mdel, R., et al., *Activity against drug resistant-tuberculosis strains of plants used in Mexican traditional medicine to treat tuberculosis and other respiratory diseases.* Phytother Res, 2008. **22**(1): p. 82-5.

198. Sureram, S., et al., *Antimycobacterial activity of bisbenzylisoquinoline alkaloids from Tiliacora triandra against multidrug-resistant isolates of Mycobacterium tuberculosis.* Bioorg Med Chem Lett, 2012. **22**(8): p. 2902-5.

199. Guzman, J.D., et al., *Anti-tubercular screening of natural products from Colombian plants: 3-methoxynordomesticine, an inhibitor of MurE ligase of Mycobacterium tuberculosis.* J Antimicrob Chemother, 2010. **65**(10): p. 2101-7.

200. Hughes, C.C. and W. Fenical, *Antibacterials from the sea.* Chemistry, 2010. **16**(42): p. 12512-25.

201. Kong, D.X., Y.Y. Jiang, and H.Y. Zhang, *Marine natural products as sources of novel scaffolds: achievement and concern.* Drug Discov Today, 2010. **15**(21-22): p. 884-6.

202. El Sayed, K.A.B., P.; Shen, X.; Perry, T.L.; Zjawiony, J.K.; Hamann, M.T., *Marine Natural Products as Antituberculosis Agents.* Tetrahedron, 2000. **56**: p. 5.

203. Daletos, G., et al., *Antimycobacterial Metabolites from Marine Invertebrates.* Arch Pharm (Weinheim), 2016. **349**(10): p. 763-773.

204. Liu, X., et al., *Exploring anti-TB leads from natural products library originated from marine microbes and medicinal plants.* Antonie Van Leeuwenhoek, 2012. **102**(3): p. 447-61.

205. de Oliveira, M.F., et al., *Antimycobacterial brominated metabolites from two species of marine sponges.* Planta Med, 2006. **72**(5): p. 437-41.

206. Wei, X., et al., *Synthesis and in vitro biological evaluation of ring B abeo-sterols as novel inhibitors of Mycobacterium tuberculosis.* Bioorg Med Chem Lett, 2008. **18**(20): p. 5448-50.

207. Arai, M., et al., *Halicyclamine A, a marine spongean alkaloid as a lead for anti-tuberculosis agent.* Bioorg Med Chem, 2008. **16**(14): p. 6732-6.

208. Arai, M., et al., *Anti-dormant mycobacterial activity and target molecule of melophlins, tetramic acid derivatives isolated from a marine sponge of Melophlus sp.* J Nat Med, 2016. **70**(3): p. 467-75.

209. Muller, D., et al., *Brunsvicamides A-C: sponge-related cyanobacterial peptides with Mycobacterium tuberculosis protein tyrosine phosphatase inhibitory activity.* J Med Chem, 2006. **49**(16): p. 4871-8.

210. Pruksakorn, P., et al., *Trichoderins, novel aminolipopeptides from a marine sponge-derived Trichoderma sp., are active against dormant mycobacteria.* Bioorg Med Chem Lett, 2010. **20**(12): p. 3658-63.

211. Wilson, M.C., et al., *An environmental bacterial taxon with a large and distinct metabolic repertoire.* Nature, 2014. **506**(7486): p. 58-62.

212. Smanski, M.J., et al., *Synthetic biology to access and expand nature's chemical diversity.* Nat Rev Microbiol, 2016. **14**(3): p. 135-49.

213. Koeberle, A. and O. Werz, *Multi-target approach for natural products in inflammation.* Drug Discov Today, 2014. **19**(12): p. 1871-82.

214. Burgos-Moron, E., et al., *The dark side of curcumin.* Int J Cancer, 2010. **126**(7): p. 1771-5.

215. Cimermancic, P., et al., *Insights into secondary metabolism from a global analysis of prokaryotic biosynthetic gene clusters.* Cell, 2014. **158**(2): p. 412-21.

216. Medema, M.H., et al., *A systematic computational analysis of biosynthetic gene cluster evolution: lessons for engineering biosynthesis.* PLoS Comput Biol, 2014. **10**(12): p. e1004016.

217. Donia, M.S., et al., *A systematic analysis of biosynthetic gene clusters in the human microbiome reveals a common family of antibiotics.* Cell, 2014. **158**(6): p. 1402-14.

218. Watve, M.G., et al., *How many antibiotics are produced by the genus Streptomyces?* Arch Microbiol, 2001. **176**(5): p. 386-90.

219. Doroghazi, J.R., et al., *A roadmap for natural product discovery based on large-scale genomics and metabolomics.* Nat Chem Biol, 2014. **10**(11): p. 963-8.

220. Luo, Y., et al., *Engineered biosynthesis of natural products in heterologous hosts.* Chem Soc Rev, 2015. **44**(15): p. 5265-90.

221. Fischbach, M. and C.A. Voigt, *Prokaryotic gene clusters: a rich toolbox for synthetic biology.* Biotechnol J, 2010. **5**(12): p. 1277-96.

222. Chan, L.Y., S. Kosuri, and D. Endy, *Refactoring bacteriophage T7.* Mol Syst Biol, 2005. **1**: p. 2005 0018.

223. Temme, K., D. Zhao, and C.A. Voigt, *Refactoring the nitrogen fixation gene cluster from Klebsiella oxytoca.* Proc Natl Acad Sci U S A, 2012. **109**(18): p. 7085-90.

224. Yamanaka, K., et al., *Direct cloning and refactoring of a silent lipopeptide biosynthetic gene cluster yields the antibiotic taromycin A.* Proc Natl Acad Sci U S A, 2014. **111**(5): p. 1957-62.

225. Chang, F.Y., et al., *Discovery and synthetic refactoring of tryptophan dimer gene clusters from the environment.* J Am Chem Soc, 2013. **135**(47): p. 17906-12.

226. Shao, Z., et al., *Refactoring the silent spectinabilin gene cluster using a plug-and-play scaffold.* ACS Synth Biol, 2013. **2**(11): p. 662-9.

227. Luo, Y., et al., *Activation and characterization of a cryptic polycyclic tetramate macrolactam biosynthetic gene cluster.* Nat Commun, 2013. **4**: p. 2894.

228. Qi, L.S., et al., *Repurposing CRISPR as an RNA-guided platform for sequence-specific control of gene expression.* Cell, 2013. **152**(5): p. 1173-83.

229. Gilbert, L.A., et al., *CRISPR-mediated modular RNA-guided regulation of transcription in eukaryotes.* Cell, 2013. **154**(2): p. 442-51.

230. Tong, Y., et al., *CRISPR-Cas9 Based Engineering of Actinomycetal Genomes.* ACS Synth Biol, 2015. **4**(9): p. 1020-9.

231. Piatek, A., et al., *RNA-guided transcriptional regulation in planta via synthetic dCas9-based transcription factors.* Plant Biotechnol J, 2015. **13**(4): p. 578-89.

232. Zalatan, J.G., et al., *Engineering complex synthetic transcriptional programs with CRISPR RNA scaffolds.* Cell, 2015. **160**(1-2): p. 339-50.

233. Nguyen, K.T., et al., *Combinatorial biosynthesis of novel antibiotics related to daptomycin.* Proc Natl Acad Sci U S A, 2006. **103**(46): p. 17462-7.

234. Menzella, H.G., et al., *Combinatorial polyketide biosynthesis by de novo design and rearrangement of modular polyketide synthase genes.* Nat Biotechnol, 2005. **23**(9): p. 1171-6.

235. Kakule, T.B., Z. Lin, and E.W. Schmidt, *Combinatorialization of fungal polyketide synthase-peptide synthetase hybrid proteins.* J Am Chem Soc, 2014. **136**(51): p. 17882-90.

236. van Dijk, E.L., et al., *Ten years of next-generation sequencing technology.* Trends Genet, 2014. **30**(9): p. 418-26.

237. Tahlan, K., et al., *SQ109 targets MmpL3, a membrane transporter of trehalose monomycolate involved in mycolic acid donation to the cell wall core of Mycobacterium tuberculosis.* Antimicrob Agents Chemother, 2012. **56**(4): p. 1797-809.

238. Ioerger, T.R., et al., *Identification of new drug targets and resistance mechanisms in Mycobacterium tuberculosis.* PLoS One, 2013. **8**(9): p. e75245.

239. van Kessel, J.C. and G.F. Hatfull, *Recombineering in Mycobacterium tuberculosis.* Nat Methods, 2007. **4**(2): p. 147-52.

240. Islam, M.M., et al., *Drug resistance mechanisms and novel drug targets for tuberculosis therapy.* J Genet Genomics, 2017. **44**(1): p. 21-37.

241. Njire, M., et al., *Pyrazinamide resistance in Mycobacterium tuberculosis: Review and update.* Adv Med Sci, 2016. **61**(1): p. 63-71.

242. Ling, L.L., et al., *A new antibiotic kills pathogens without detectable resistance.* Nature, 2015. **517**(7535): p. 455-9.

243. Gardete, S. and A. Tomasz, *Mechanisms of vancomycin resistance in Staphylococcus aureus.* J Clin Invest, 2014. **124**(7): p. 2836-40.

244. Lu, J., et al., *Mechanisms of fluoroquinolone monoresistance in Mycobacterium tuberculosis.* FEMS Microbiol Lett, 2014. **353**(1): p. 40-8.

245. Boshoff, H.I., et al., *The transcriptional responses of Mycobacterium tuberculosis to inhibitors of metabolism: novel insights into drug mechanisms of action.* J Biol Chem, 2004. **279**(38): p. 40174-84.

246. Murima, P., et al., *Exploring the mode of action of bioactive compounds by microfluidic transcriptional profiling in mycobacteria.* PLoS One, 2013. **8**(7): p. e69191.

247. Protopopova, M., et al., *Identification of a new antitubercular drug candidate, SQ109, from a combinatorial library of 1,2-ethylenediamines.* J Antimicrob Chemother, 2005. **56**(5): p. 968-74.

248. Jia, L., et al., *Pharmacoproteomic effects of isoniazid, ethambutol, and N-geranyl-N'-(2-adamantyl)ethane-1,2-diamine (SQ109) on Mycobacterium tuberculosis H37Rv.* J Pharmacol Exp Ther, 2005. **315**(2): p. 905-11.

249. Shell, S.S., et al., *Leaderless Transcripts and Small Proteins Are Common Features of the Mycobacterial Translational Landscape.* PLoS Genet, 2015. **11**(11): p. e1005641.

250. Lin, W., et al., *Transcriptional Profiling of Mycobacterium tuberculosis Exposed to In Vitro Lysosomal Stress.* Infect Immun, 2016. **84**(9): p. 2505-23.

251. Skvortsov, T.A., et al., *Mycobacterium tuberculosis Transcriptome Profiling in Mice with Genetically Different Susceptibility to Tuberculosis.* Acta Naturae, 2013. **5**(2): p. 62-9.

252. Namouchi, A., et al., *The Mycobacterium tuberculosis transcriptional landscape under genotoxic stress.* BMC Genomics, 2016. **17**(1): p. 791.

253. Naran, K., et al., *Bioluminescent Reporters for Rapid Mechanism of Action Assessment in Tuberculosis Drug Discovery.* Antimicrob Agents Chemother, 2016. **60**(11): p. 6748-6757.

254. Szardenings, K., et al., *Fishing for targets: novel approaches using small molecule baits.* Drug Discov Today Technol, 2004. **1**(1): p. 9-15.

255. Wolfe, L.M., et al., *A chemical proteomics approach to profiling the ATP-binding proteome of Mycobacterium tuberculosis.* Mol Cell Proteomics, 2013. **12**(6): p. 1644-60.

256. Paquet, T., et al., *Antimalarial efficacy of MMV390048, an inhibitor of Plasmodium phosphatidylinositol 4-kinase.* Sci Transl Med, 2017. **9**(387).

257. Bantscheff, M., et al., *Proteomics-based strategies in kinase drug discovery.* Ernst Schering Found Symp Proc, 2007(3): p. 1-28.

258. Bantscheff, M., et al., *Quantitative chemical proteomics reveals mechanisms of action of clinical ABL kinase inhibitors.* Nat Biotechnol, 2007. **25**(9): p. 1035-44.

259. Baell, J.B. and G.A. Holloway, *New substructure filters for removal of pan assay interference compounds (PAINS) from screening libraries and for their exclusion in bioassays.* J Med Chem, 2010. **53**(7): p. 2719-40.

260. Baell, J. and M.A. Walters, *Chemistry: Chemical con artists foil drug discovery.* Nature, 2014. **513**(7519): p. 481-3.

261. McGovern, S.L., et al., *A common mechanism underlying promiscuous inhibitors from virtual and high-throughput screening.* J Med Chem, 2002. **45**(8): p. 1712-22.

262. Veber, D.F., et al., *Molecular properties that influence the oral bioavailability of drug candidates.* J Med Chem, 2002. **45**(12): p. 2615-23.

263. Leeson, P.D. and A.M. Davis, *Time-related differences in the physical property profiles of oral drugs.* J Med Chem, 2004. **47**(25): p. 6338-48.

264. van de Waterbeemd, H., *The fundamental variables of the biopharmaceutics classification system (BCS): a commentary.* Eur J Pharm Sci, 1998. **7**(1): p. 1-3.

265. van De Waterbeemd, H., et al., *Property-based design: optimization of drug absorption and pharmacokinetics.* J Med Chem, 2001. **44**(9): p. 1313-33.

266. Leeson, P., *Drug discovery: Chemical beauty contest.* Nature, 2012. **481**(7382): p. 455-6.

267. Lipinski, C.A., Lombardo, F., Dominy, B.W., Feeney, P.J., *Experimental and computational approaches to estimate solubility and permeability in drug discovery and development settings.* Advanced Drug Delivery Reviews, 1997. **23**(1-3): p. 22.

268. Nettleton, D.O. and H.J. Einolf, *Assessment of cytochrome p450 enzyme inhibition and inactivation in drug discovery and development.* Curr Top Med Chem, 2011. **11**(4): p. 382-403.

269. Staudacher, I., et al., *hERG: protein trafficking and potential for therapy and drug side effects.* Curr Opin Drug Discov Devel, 2010. **13**(1): p. 23-30.

270. Hughes, D. and A. Karlen, *Discovery and preclinical development of new antibiotics.* Ups J Med Sci, 2014. **119**(2): p. 162-9.

271. Mueller, M., A. de la Pena, and H. Derendorf, *Issues in pharmacokinetics and pharmacodynamics of anti-infective agents: kill curves versus MIC.* Antimicrob Agents Chemother, 2004. **48**(2): p. 369-77.

272. Bax, H.I., et al., *The role of the time-kill kinetics assay as part of a preclinical modeling framework for assessing the activity of anti-tuberculosis drugs.* Tuberculosis (Edinb), 2017. **105**: p. 80-85.

273. Wallis, R.S., et al., *Tuberculosis--advances in development of new drugs, treatment regimens, host-directed therapies, and biomarkers.* Lancet Infect Dis, 2016. **16**(4): p. e34-46.

274. Wallis, R.S., et al., *Biomarkers and diagnostics for tuberculosis: progress, needs, and translation into practice.* Lancet, 2010. **375**(9729): p. 1920-37.

275. Donald, P.R. and A.H. Diacon, *The early bactericidal activity of anti-tuberculosis drugs: a literature review.* Tuberculosis (Edinb), 2008. **88 Suppl 1**: p. S75-83.

276. Rustomjee, R., et al., *Early bactericidal activity and pharmacokinetics of the diarylquinoline TMC207 in treatment of pulmonary tuberculosis.* Antimicrob Agents Chemother, 2008. **52**(8): p. 2831-5.

277. Diacon, A.H., et al., *14-day bactericidal activity of PA-824, bedaquiline, pyrazinamide, and moxifloxacin combinations: a randomised trial.* Lancet, 2012. **380**(9846): p. 986-93.

278. Dawson, R., et al., *Efficiency and safety of the combination of moxifloxacin, pretomanid (PA-824), and pyrazinamide during the first 8 weeks of antituberculosis treatment: a phase 2b, open-label, partly randomised trial in patients with drug-susceptible or drug-resistant pulmonary tuberculosis.* Lancet, 2015. **385**(9979): p. 1738-47.

279. Pym, A.S., et al., *Bedaquiline in the treatment of multidrug- and extensively drug-resistant tuberculosis.* Eur Respir J, 2016. **47**(2): p. 564-74.

280. Jindani, A., et al., *High-dose rifapentine with moxifloxacin for pulmonary tuberculosis.* N Engl J Med, 2014. **371**(17): p. 1599-608.

281. Skoura, E., A. Zumla, and J. Bomanji, *Imaging in tuberculosis.* Int J Infect Dis, 2015. **32**: p. 87-93.

282. Berry, M.P., et al., *An interferon-inducible neutrophil-driven blood transcriptional signature in human tuberculosis.* Nature, 2010. **466**(7309): p. 973-7.

283. Lee, M.R., et al., *Mycobacterium abscessus Complex Infections in Humans.* Emerg Infect Dis, 2015. **21**(9): p. 1638-46.

284. Ferro, B.E., et al., *Failure of the Amikacin, Cefoxitin, and Clarithromycin Combination Regimen for Treating Pulmonary Mycobacterium abscessus Infection.* Antimicrob Agents Chemother, 2016. **60**(10): p. 6374-6.

285. Nessar, R., et al., *Mycobacterium abscessus: a new antibiotic nightmare.* J Antimicrob Chemother, 2012. **67**(4): p. 810-8.

286. Morris, R.P., et al., *Ancestral antibiotic resistance in Mycobacterium tuberculosis.* Proc Natl Acad Sci U S A, 2005. **102**(34): p. 12200-5.

287. Pryjma, M., et al., *Antagonism between front line antibiotics clarithromycin and amikacin used for the treatment of Mycobacterium abscessus infections is mediated by the whiB7 gene.* Antimicrob Agents Chemother, 2017.

288. Hurst-Hess, K., P. Rudra, and P. Ghosh, *Mycobacterium abscessus WhiB7 regulates a species -specific repertoire of genes to confer extreme antibiotic resistance.* Antimicrob Agents Chemother, 2017.

289. Lenaerts, A., C.E. Barry, 3rd, and V. Dartois, *Heterogeneity in tuberculosis pathology, microenvironments and therapeutic responses.* Immunol Rev, 2015. **264**(1): p. 288-307.

290. Nathan, C. and C.E. Barry, 3rd, *TB drug development: immunology at the table.* Immunol Rev, 2015. **264**(1): p. 308-18.

291. Liu, Y., et al., *Immune activation of the host cell induces drug tolerance in Mycobacterium tuberculosis both in vitro and in vivo.* J Exp Med, 2016. **213**(5): p. 809-25.

292. Newman, D.J. and G.M. Cragg, *Natural Products as Sources of New Drugs from 1981 to 2014.* J Nat Prod, 2016. **79**(3): p. 629-61.

293. Li, C.K., et al., *FastCloning: a highly simplified, purification-free, sequence- and ligation-independent PCR cloning method.* Bmc Biotechnology, 2011. **11**.

294. Lee, W., et al., *Intracellular Mycobacterium tuberculosis exploits host-derived fatty acids to limit metabolic stress.* J Biol Chem, 2013. **288**(10): p. 6788-800.

295. O'Brien, J., et al., *Investigation of the Alamar Blue (resazurin) fluorescent dye for the assessment of mammalian cell cytotoxicity.* Eur J Biochem, 2000. **267**(17): p. 5421-6.

296. Lambert, R.J. and J. Pearson, *Susceptibility testing: accurate and reproducible minimum inhibitory concentration (MIC) and non-inhibitory concentration (NIC) values.* J Appl Microbiol, 2000. **88**(5): p. 784-90.

297. Bergguist, P.R.C., S.C., *Family Petrosiidae Van Soest 1980*, in *Systema Porifera: A guide to the classification of sponges*, R.V.S. JNA Hooper, Editor. 2002, Kluwer Academic/Plenum Publisher: New York. p. 1082-1085.

298. Rogers, E.W., et al., *Stereochemical heterogeneity in Verongid sponge metabolites. Absolute stereochemistry of (+)-fistularin-3 and (+)-11-epi-fistularin-3 by microscale LCMS-Marfey's analysis.* J. Nat. Prod., 2005. **68**(Copyright (C) 2017 American Chemical Society (ACS). All Rights Reserved.): p. 891-896.

299. Zheng, C.J., et al., *Methyl-branched fatty acids, inhibitors of enoyl-ACP reductase with antibacterial activity from Streptomyces sp. A251.* J Microbiol Biotechnol, 2010. **20**(5): p. 875-80.

300. Alcolado, P.M., *Nueva especie de porifero (genero Strongylophora) encontrada en Cuba [New species of Porifera (genus Strongylophora) from Cuba].* Poeyana, 1979. **196**: p. 1-5.

301. Van Soest, R.W.M., *Marine sponges from Curaçao and other Caribbean localities. Part II. Haplosclerida.* Studies on the Fauna of Curaçao and other Caribbean Islands 1980. **62**(191): p. 1-173.

302. Van Soest, R.W.M.S., N. , *Barbados Deep-Water Sponges.* Studies on the Fauna of Curaçao andother Caribbean Islands. , 1988. **70**(215): p. 1-175.

303. Van Soest, R.W.M., *Sponges of the Guyana Shelf.* Zootaxa, 2017. **4217**(1): p. 1-225.

304. Desqueyroux-Faundez, V.C., *Family Aplysinidae Carter 1875*, in *Systema Porifera : A Guide to the Classification of Sponges* R.V.S. JNA Hooper, Editor. 2002, Kluwer Academic/Plenum Publishers: New York. p. 906-917.

305. Bourguet-Kondracki, M.-L., F. Lacombe, and M. Guyot, *Methanol adduct of puupehenone, a biologically active derivative from the marine sponge Hyrtios species.* J. Nat. Prod., 1999. **62**(Copyright (C) 2017 American Chemical Society (ACS). All Rights Reserved.): p. 1304-1305.

306. Hamann, M.T., P.J. Scheuer, and M. Kelly-Borges, *Biogenetically diverse, bioactive constituents of a sponge, order Verongida: bromotyramines and sesquiterpene-shikimate derived metabolites.* J. Org. Chem., 1993. **58**(Copyright (C) 2017 American Chemical Society (ACS). All Rights Reserved.): p. 6565-9.

307. Rogers, E.W., et al., *Stereochemical heterogeneity in verongid sponge metabolites. Absolute stereochemistry of (+)-fistularin-3 and (+)-11-epi-fistularin-3 by microscale LCMS-Marfey's analysis.* Journal of Natural Products, 2005. **68**(6): p. 891-896.

308. Gopichand, Y.S., F.J., *Marine Natural Products: Fistularin-1, -2 and -3 from the Sponge Aplysina fistularis forma fulva.* Tetrahedron Letters, 1979. **20**(41): p. 4.

309. Heilbron, I.M., Owen, W.M., *The unsaponifiable matter from the oils of elsamobranch fish. Part IV. The establishment of the structure of selachyl and batyl as monoglyceryl ethers.* J. Chem. Soc. London, 1928: p. 942-947.

310. Magnusson, C.D. and G.G. Haraldsson, *Ether lipids.* Chem Phys Lipids, 2011. **164**(5): p. 315-40.

311. Bourguet-Kondracki, M.L., F. Lacombe, and M. Guyot, *Methanol adduct of puupehenone, a biologically active derivative from the marine sponge Hyrtios species.* J Nat Prod, 1999. **62**(9): p. 1304-5.

312. Kanda, R., et al., *Factors Affecting Time to Sputum Culture Conversion in Adults with Pulmonary Tuberculosis: A Historical Cohort Study without Censored Cases.* PLoS One, 2015. **10**(11): p. e0142607.

313. Whitfield, M.G., et al., *A Global Perspective on Pyrazinamide Resistance: Systematic Review and Meta-Analysis.* PLoS One, 2015. **10**(7): p. e0133869.

314. Dhar, N., J. McKinney, and G. Manina, *Phenotypic Heterogeneity in Mycobacterium tuberculosis.* Microbiol Spectr, 2016. **4**(6).

315. Siricilla, S., et al., *Discovery of a capuramycin analog that kills nonreplicating Mycobacterium tuberculosis and its synergistic effects with translocase I inhibitors.* J Antibiot (Tokyo), 2015. **68**(4): p. 271-8.

316. Gordaliza, M., *Cytotoxic terpene quinones from marine sponges.* Mar Drugs, 2010. **8**(12): p. 2849-70.

317. Kraus, G.A.N., T.; Bae, J.; Hostetter, J.; Steadham, E., *Synthesis and antitubercular activity of tricyclic analogs of puupehenone.* Tetrahedron, 2004. **60**: p. 3.

318. Xu, W.H., et al., *Puupehanol, a sesquiterpene-dihydroquinone derivative from the marine sponge Hyrtios sp.* Bioorg Med Chem Lett, 2009. **19**(21): p. 6140-3.

319. Hagiwara, K., et al., *Puupehenol, a potent antioxidant antimicrobial meroterpenoid from a Hawaiian deep-water Dactylospongia sp. sponge.* J Nat Prod, 2015. **78**(2): p. 325-9.

320. Ciavatta, M.L.G., M.P.L.; Gavagnin, M.; Romero, V.; Melck, D.; Manzo, E.; Guo, Y.W.; van Soest, R.; Cimino, G., *Studies on puupehenone metabolites of a Dysdea sp.: structure and biology activity.* Tetrahedron, 2007. **63**: p. 5.

321. Robinson, S.J., et al., *Using enzyme assays to evaluate the structure and bioactivity of sponge-derived meroterpenes.* J Nat Prod, 2009. **72**(10): p. 1857-63.

322. Weinstein, E.A., et al., *Inhibitors of type IINADH :-menaquinone oxidoreductase represent a class of antitubercular drugs.* Proceedings of the National Academy of Sciences of the United States of America, 2005. **102**(12): p. 4548-4553.

323. Quideau, S., M. Lebon, and A.M. Lamidey, *Enantiospecific synthesis of the antituberculosis marine sponge metabolite (+)-puupehenone. The arenol oxidative activation route.* Org Lett, 2002. **4**(22): p. 3975-8.

324. Barrero, A.F.A.-M., E.J.; Herrador, M.M.; Valdivia, M.V.; Chahnoun, R., *Synthesis of Monoterpenic Analoques of Puupehenone and Puupehedione* Tetrahedron, 1998. **39**: p. 4.

325. Harper, J., et al., *Mouse model of necrotic tuberculosis granulomas develops hypoxic lesions.* J Infect Dis, 2012. **205**(4): p. 595-602.

326. Kramnik, I., et al., *Genetic control of resistance to experimental infection with virulent Mycobacterium tuberculosis.* Proc Natl Acad Sci U S A, 2000. **97**(15): p. 8560-5.

327. Rodrigues Felix, C., et al., *Selective Killing Of Dormant Mycobacterium tuberculosis By Marine Natural Products.* Antimicrob Agents Chemother, 2017.

328. Pandey, A.K. and C.M. Sassetti, *Mycobacterial persistence requires the utilization of host cholesterol.* Proc Natl Acad Sci U S A, 2008. **105**(11): p. 4376-80.

329. Lu, Z., et al., *Plakinamine M, a steroidal alkaloid from the marine sponge Corticium sp.* J Nat Prod, 2013. **76**(11): p. 2150-2.

330. Prevots, D.R. and T.K. Marras, *Epidemiology of human pulmonary infection with nontuberculous mycobacteria: a review.* Clin Chest Med, 2015. **36**(1): p. 13-34.

331. Peddireddy, V., S.N. Doddam, and N. Ahmed, *Mycobacterial Dormancy Systems and Host Responses in Tuberculosis.* Front Immunol, 2017. **8**: p. 84.

332. Guenin-Mace, L., R. Simeone, and C. Demangel, *Lipids of pathogenic Mycobacteria: contributions to virulence and host immune suppression.* Transbound Emerg Dis, 2009. **56**(6-7): p. 255-68.

333. Bhowruth, V., et al., *Tuberculosis: a balanced diet of lipids and carbohydrates.* Biochem Soc Trans, 2008. **36**(Pt 4): p. 555-65.

334. Chua, J., et al., *A tale of two lipids: Mycobacterium tuberculosis phagosome maturation arrest.* Curr Opin Microbiol, 2004. **7**(1): p. 71-7.

335. Russell, D.G., et al., *Mycobacterium tuberculosis Wears What It Eats.* Cell Host & Microbe, 2010. **8**(1): p. 68-76.

336. Howard, S.T. and T.F. Byrd, *The rapidly growing mycobacteria: saprophytes and parasites.* Microbes Infect, 2000. **2**(15): p. 1845-53.

337. Bar-On, O., et al., *Increasing nontuberculous mycobacteria infection in cystic fibrosis.* Journal of Cystic Fibrosis, 2015. **14**(1): p. 53-62.

338. Hoagland, D.T., et al., *New agents for the treatment of drug-resistant Mycobacterium tuberculosis.* Adv Drug Deliv Rev, 2016. **102**: p. 55-72.

339. Gold, B. and C. Nathan, *Targeting Phenotypically Tolerant Mycobacterium tuberculosis.* Microbiology Spectrum, 2017. **5**(1).

340. Choi, G.E., et al., *Macrolide treatment for Mycobacterium abscessus and Mycobacterium massiliense infection and inducible resistance.* Am J Respir Crit Care Med, 2012. **186**(9): p. 917-25.

341. Maurer, F.P., et al., *Erm(41)-dependent inducible resistance to azithromycin and clarithromycin in clinical isolates of Mycobacterium abscessus.* Journal of Antimicrobial Chemotherapy, 2014. **69**(6): p. 1559-1563.

342. Koh, W.J., et al., *Pulmonary TB and NTM lung disease: comparison of characteristics in patients with AFB smear-positive sputum.* Int J Tuberc Lung Dis, 2006. **10**(9): p. 1001-7.

343. Nessar, R., et al., *Mycobacterium abscessus: a new antibiotic nightmare.* Journal of Antimicrobial Chemotherapy, 2012. **67**(4): p. 810-818.

344. Abraham, E., *ATS/IDSA statement: Diagnosis, treatment, and prevention of nontuberculous mycobacterial diseases (vol 175, pg 394, 2007).* American Journal of Respiratory and Critical Care Medicine, 2007. **175**(7): p. 744-745.

345. Berners-Price, S.J. and A. Filipovska, *Gold compounds as therapeutic agents for human diseases.* Metallomics, 2011. **3**(9): p. 863-873.

346. Kelland, L., *The resurgence of platinum-based cancer chemotherapy.* Nat Rev Cancer, 2007. **7**(8): p. 573-84.

347. Finkelstein, A.E., et al., *Auranofin - New Oral Gold Compound for Treatment of Rheumatoid-Arthritis.* Annals of the Rheumatic Diseases, 1976. **35**(3): p. 251-257.

348. Sutton, B.M., et al., *Oral Gold - Antiarthritic Properties of Alkylphosphinegold Coordination Complexes.* Journal of Medicinal Chemistry, 1972. **15**(11): p. 1095-+.

349. Li, X.N., et al., *Functional Gold Nanoparticles as Potent Antimicrobial Agents against Multi-Drug-Resistant Bacteria.* Acs Nano, 2014. **8**(10): p. 10682-10686.

350. Lima, E., et al., *Gold nanoparticles as efficient antimicrobial agents for Escherichia coli and Salmonella typhi.* Chemistry Central Journal, 2013. **7**.

351. Shamaila, S., et al., *Gold Nanoparticles: An Efficient Antimicrobial Agent against Enteric Bacterial Human Pathogen.* Nanomaterials, 2016. **6**(4).

352. Zhou, Y., et al., *Antibacterial activities of gold and silver nanoparticles against Escherichia coli and bacillus Calmette-Guerin.* Journal of Nanobiotechnology, 2012. **10**.

353. Benedek, T.G., *The history of gold therapy for tuberculosis.* J Hist Med Allied Sci, 2004. **59**(1): p. 50-89.

354. Agertt, V.A., et al., *Identification of antimicrobial activity among new sulfonamide metal complexes for combating rapidly growing mycobacteria.* Biometals, 2016. **29**(5): p. 807-816.

355. Barbosa, A.R., et al., *Potential of Casiopeinas(R) Copper Complexes and Antituberculosis Drug Combination against Mycobacterium tuberculosis.* Chemotherapy, 2016. **61**(5): p. 249-55.

356. Crabol, Y., et al., *Rifabutin: where do we stand in 2016?* Journal of Antimicrobial Chemotherapy, 2016. **71**(7): p. 1759-1771.

357. Dinah Binte Aziz, et al., *Rifabutin Is Active Against Mycobacterium abscessus Complex.* Antimicrobial agents and Chemotherapy, 2017.

358. Chopra, S., et al., *Identification of antimicrobial activity among FDA-approved drugs for combating Mycobacterium abscessus and Mycobacterium chelonae.* Journal of Antimicrobial Chemotherapy, 2011. **66**(7): p. 1533-1536.

359. Kaushik, A., et al., *Carbapenems and Rifampin Exhibit Synergy against Mycobacterium tuberculosis and Mycobacterium abscessus.* Antimicrobial Agents and Chemotherapy, 2015. **59**(10): p. 6561-6567.

360. Rangel-Vega, A., et al., *Drug repurposing as an alternative for the treatment of recalcitrant bacterial infections.* Frontiers in Microbiology, 2015. **6**: p. 282.

361. Livia, V., et al., *The Antibacterial Activity of Metal Complexes Containing 1,10- phenanthroline: Potential as Alternative Therapeutics in the Era of Antibiotic Resistance.* Current Topics in Medicinal Chemistry, 2017. **17**(11): p. 1280-1302.

362. Cruz-Muñiz, M.Y., et al., *Repurposing the anticancer drug mitomycin C for the treatment of persistent Acinetobacter baumannii infections.* International Journal of Antimicrobial Agents. **49**(1): p. 88-92.

363. Kaneko, Y., et al., *The transition metal gallium disrupts Pseudomonas aeruginosa iron metabolism and has antimicrobial and antibiofilm activity.* The Journal of clinical investigation, 2007. **117**(4): p. 877.

364. Bonchi, C., et al., *Repurposing of gallium-based drugs for antibacterial therapy.* BioFactors, 2014. **40**(3): p. 303-312.

365. Hijazi, S., P. Visca, and E. Frangipani, *Gallium-Protoporphyrin IX Inhibits Pseudomonas aeruginosa Growth by Targeting Cytochromes.* Frontiers in Cellular and Infection Microbiology, 2017. **7**(12).

366. Akerman, K.J., et al., *Gold(III) macrocycles: nucleotide-specific unconventional catalytic inhibitors of human topoisomerase I.* J Am Chem Soc, 2014. **136**(15): p. 5670-82.

367. Munro, O.Q., K.J. Akerman, and P. Akerman, *Gold complexes for use in the treatment of cancer*. 2016, US Patent 9,346,832.

368. *CrysAlis CCD and CrysAlis RED*. 2006, Oxford Diffraction: Oxford Diffraction Ltd, Abingdon, Oxfordshire, England.

369. Dolomanov, O.V., et al., *OLEX2: a complete structure solution, refinement and analysis program.* Journal of Applied Crystallography, 2009. **42**(2): p. 339-341.

370. Sheldrick, G.M., *SHELXT–Integrated space-group and crystal-structure determination.* Acta Crystallographica Section A: Foundations and Advances, 2015. **71**(1): p. 3-8.

371. Fleischmann, R.D., et al., *Whole-genome comparison of Mycobacterium tuberculosis clinical and laboratory strains.* J Bacteriol, 2002. **184**(19): p. 5479-90.

372. Homolka, S., et al., *Functional genetic diversity among Mycobacterium tuberculosis complex clinical isolates: delineation of conserved core and lineage-specific transcriptomes during intracellular survival.* PLoS Pathog, 2010. **6**(7): p. e1000988.

373. Howard, S.T., et al., *Spontaneous reversion of Mycobacterium abscessus from a smooth to a rough morphotype is associated with reduced expression of glycopeptidolipid and reacquisition of an invasive phenotype.* Microbiology, 2006. **152**(Pt 6): p. 1581-90.

374. Greendyke, R. and T.F. Byrd, *Differential antibiotic susceptibility of Mycobacterium abscessus variants in biofilms and macrophages compared to that of planktonic bacteria.* Antimicrobial Agents and Chemotherapy, 2008. **52**(6): p. 2019-2026.

375. Zhang, J.H., T.D.Y. Chung, and K.R. Oldenburg, *A simple statistical parameter for use in evaluation and validation of high throughput screening assays.* Journal of Biomolecular Screening, 1999. **4**(2): p. 67-73.

376. Lambert, R.J.W. and J. Pearson, *Susceptibility testing: accurate and reproducible minimum inhibitory concentration (MIC) and non-inhibitory concentration (NIC) values.* Journal of Applied Microbiology, 2000. **88**(5): p. 784-790.

377. Palomino, J.C., et al., *Resazurin microtiter assay plate: Simple and inexpensive method for detection of drug resistance in Mycobacterium tuberculosis.* Antimicrobial Agents and Chemotherapy, 2002. **46**(8): p. 2720-2722.

378. Andreu, N., et al., *Optimisation of Bioluminescent Reporters for Use with Mycobacteria.* Plos One, 2010. **5**(5).

379. Aldred, K.J., R.J. Kerns, and N. Osheroff, *Mechanism of quinolone action and resistance.* Biochemistry, 2014. **53**(10): p. 1565-74.

380. WHO, *Global tuberculosis report*. 2016.

381. Lemire, J.A., J.J. Harrison, and R.J. Turner, *Antimicrobial activity of metals: mechanisms, molecular targets and applications.* Nat Rev Microbiol, 2013. **11**(6): p. 371-84.

382. Ferro, B.E., et al., *Time-kill kinetics of antibiotics active against rapidly growing mycobacteria.* Journal of Antimicrobial Chemotherapy, 2015. **70**(3): p. 811-817.

383. Lerat, I., et al., *In vivo evaluation of antibiotic activity against Mycobacterium abscessus.* J Infect Dis, 2014. **209**(6): p. 905-12.

384. Forbes, M., N.A. Kuck, and E.A. Peets, *Mode of action of ethambutol.* J Bacteriol, 1962. **84**: p. 1099-103.

385. Akerman, M.P., *Structural, Physical and Biological Studies of Gold(III) Bis(Pyrrolide-Imine) Schiff Base Complexes: Potential Chemotherapeutic Agents.* PhD Thesis, University of KwaZulu-Natal, 2010.

386. Akerman, M.P., et al., *Biodistribution (as determined by the radiolabelled equivalent) of a gold (III) bis (pyrrolide-imine) Schiff base complex: a potential chemotherapeutic.* Journal of Labelled Compounds and Radiopharmaceuticals, 2013. **56**(9-10): p. 530-535.

387. Roca, J., *The mechanisms of DNA topoisomerases.* Trends Biochem Sci, 1995. **20**(4): p. 156-60.

388. Baker, N.M., R. Rajan, and A. Mondragon, *Structural studies of type I topoisomerases.* Nucleic Acids Res, 2009. **37**(3): p. 693-701.

389. Sassetti, C.M., D.H. Boyd, and E.J. Rubin, *Genes required for mycobacterial growth defined by high density mutagenesis.* Mol Microbiol, 2003. **48**(1): p. 77-84.

390. Ahmed, W., et al., *Conditional silencing of topoisomerase I gene of Mycobacterium tuberculosis validates its essentiality for cell survival.* FEMS Microbiol Lett, 2014. **353**(2): p. 116-23.

391. Ahmed, W., et al., *Reduction in DNA topoisomerase I level affects growth, phenotype and nucleoid architecture of Mycobacterium smegmatis.* Microbiology, 2015. **161**(Pt 2): p. 341-53.

392. Burman, W.J., et al., *Moxifloxacin versus ethambutol in the first 2 months of treatment for pulmonary tuberculosis.* Am J Respir Crit Care Med, 2006. **174**(3): p. 331-8.

393. Sandhaus, S., et al., *Small-Molecule Inhibitors Targeting Topoisomerase I as Novel Antituberculosis Agents.* Antimicrob Agents Chemother, 2016. **60**(7): p. 4028-36.

394. Godbole, A.A., et al., *Targeting Mycobacterium tuberculosis topoisomerase I by small-molecule inhibitors.* Antimicrob Agents Chemother, 2015. **59**(3): p. 1549-57.

395. Pommier, Y., *Drugging topoisomerases: lessons and challenges.* ACS Chem Biol, 2013. **8**(1): p. 82-95.

396. Lechartier, B. and S.T. Cole, *Mode of Action of Clofazimine and Combination Therapy with Benzothiazinones against Mycobacterium tuberculosis.* Antimicrob Agents Chemother, 2015. **59**(8): p. 4457-63.

397. Ouellet, H., J.B. Johnston, and P.R. Ortiz de Montellano, *The Mycobacterium tuberculosis cytochrome P450 system.* Arch Biochem Biophys, 2010. **493**(1): p. 82-95.

398. Johnston, J.B., H. Ouellet, and P.R. Ortiz de Montellano, *Functional redundancy of steroid C26-monooxygenase activity in Mycobacterium tuberculosis revealed by biochemical and genetic analyses.* J Biol Chem, 2010. **285**(47): p. 36352-60.

399. Pham, D.D., E. Fattal, and N. Tsapis, *Pulmonary drug delivery systems for tuberculosis treatment.* Int J Pharm, 2015. **478**(2): p. 517-29.

400. Lenaerts, A.J., M.A. Degroote, and I.M. Orme, *Preclinical testing of new drugs for tuberculosis: current challenges.* Trends Microbiol, 2008. **16**(2): p. 48-54.

401. Basaraba, R.J., *Experimental tuberculosis: the role of comparative pathology in the discovery of improved tuberculosis treatment strategies.* Tuberculosis (Edinb), 2008. **88 Suppl 1**: p. S35-47.

402. Irwin, S.M., et al., *Limited activity of clofazimine as a single drug in a mouse model of tuberculosis exhibiting caseous necrotic granulomas.* Antimicrob Agents Chemother, 2014. **58**(7): p. 4026-34.

403. Driver, E.R., et al., *Evaluation of a mouse model of necrotic granuloma formation using C3HeB/FeJ mice for testing of drugs against Mycobacterium tuberculosis.* Antimicrob Agents Chemother, 2012. **56**(6): p. 3181-95.

404. Rosenthal, I.M., et al., *Dose-ranging comparison of rifampin and rifapentine in two pathologically distinct murine models of tuberculosis.* Antimicrob Agents Chemother, 2012. **56**(8): p. 4331-40.

405. Yano, T., et al., *Reduction of clofazimine by mycobacterial type 2 NADH:quinone oxidoreductase: a pathway for the generation of*

bactericidal levels of reactive oxygen species. J Biol Chem, 2011. **286**(12): p. 10276-87.

406. Coleman, M.T., et al., *PET/CT imaging reveals a therapeutic response to oxazolidinones in macaques and humans with tuberculosis.* Sci Transl Med, 2014. **6**(265): p. 265ra167.

407. Gupta, R.K., et al., *Structure-based design of DevR inhibitor active against nonreplicating Mycobacterium tuberculosis.* J Med Chem, 2009. **52**(20): p. 6324-34.

408. Zheng, H., et al., *Inhibitors of Mycobacterium tuberculosis DosRST signaling and persistence.* Nat Chem Biol, 2017. **13**(2): p. 218-225.

409. Prideaux, B. and M. Stoeckli, *Mass spectrometry imaging for drug distribution studies.* J Proteomics, 2012. **75**(16): p. 4999-5013.

410. Prideaux, B., et al., *High-sensitivity MALDI-MRM-MS imaging of moxifloxacin distribution in tuberculosis-infected rabbit lungs and granulomatous lesions.* Anal Chem, 2011. **83**(6): p. 2112-8.

411. Kjellsson, M.C., et al., *Pharmacokinetic evaluation of the penetration of antituberculosis agents in rabbit pulmonary lesions.* Antimicrob Agents Chemother, 2012. **56**(1): p. 446-57.

412. Prideaux, B., et al., *The association between sterilizing activity and drug distribution into tuberculosis lesions.* Nat Med, 2015. **21**(10): p. 1223-7.

413. Malherbe, S.T., et al., *Persisting positron emission tomography lesion activity and Mycobacterium tuberculosis mRNA after tuberculosis cure.* Nat Med, 2016. **22**(10): p. 1094-1100.